SEPT. - DEC. 1997
Volume III Number III

ISSN 0859 144X

THE ASEAN JOURNAL OF RADIOLOGY

Published by The Radiological Society and
The Royal College of Radiologists of Thailand,
Bangkok, Thailand

Supported through an educational grant from

PICKER

FULL LINE OF DIAGNOSTIC IMAGING SYSTEMS

The next frontier in MR Imaging

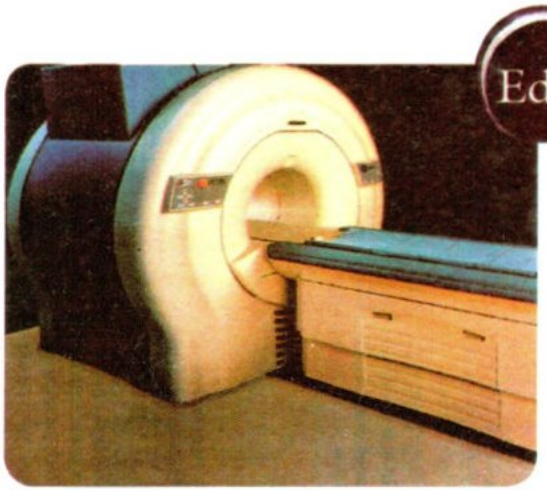

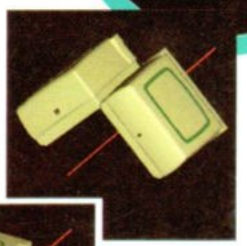

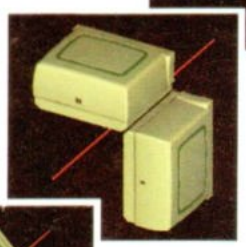

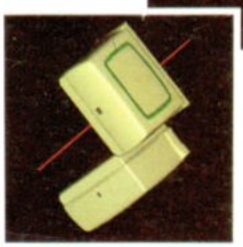

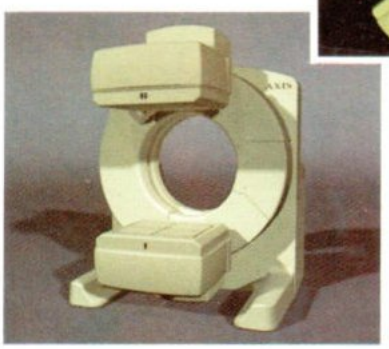

Nuclear Imaging

IRIX 3

CT Imaging

PQ 6000

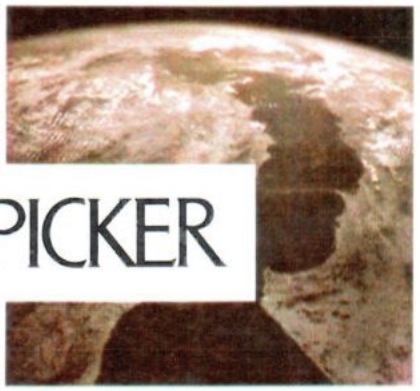

PICKER

More than Image insight

For more information , contact

Representative's office
Picker International Inc
29F ,2908 Suntowers Bldg B
123 Vibhavadi-Rangsit Rd.
Jatujuk, Bangkok, 10900
Tel: 662 6178212-4
Fax: 662 6178215.
E-mail : pickerth@loxinfo.co.th

Sole Distributor's office
United 4 Co.,Ltd.
43/1085 Raminthra 1
Raminthra Rd.
Bangkhen, Bangkok 10220
Tel: 662 9707034/35/37/39
Fax: 662 5527840
E-mail : united4@loxinfor.co.th

SEPT. - DEC. 1997
Volume III Number III

ISSN 0859 144X

THE ASEAN JOURNAL OF RADIOLOGY

Published by The Radiological Society and
The Royal College of Radiologists of Thailand,
Bangkok, Thailand

Supported through an educational grant from

BRACCO
INTERNATIONAL

ASDIR

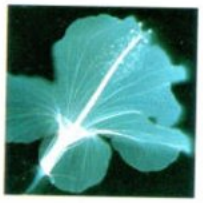

EDUCATION

Asian-Oceanian Seminars on Diagnostic and Interventional Radiology

1 9 9 8

Emergency Radiology
April 16-18
Subic, Philippines
Programme Leader:
A. Tingcungco

Imaging of the Digestive System: Current Status & Future Direction
June 6-8
Beijing, China
Programme Leaders:
G.N. Liu
J.P. Dai

Radiology in Obstetrics & Gynaecology
October 15-17
Lahore, Pakistan
Programme Leader:
M.A.J. Siddiqui

BRACCO
INTERNATIONAL

For further information please contact:
Bracco International B.V.
47 Hill Street, #06-05
S.C.C.C.I. Building
Singapore 179365
Tel: ++65-337 1880
Fax: ++65-337 7576
E-mail: singapore@braccoint.com.sg
http://www.bracco-group.com

1. The AAR Journal of Radiology publishes the papers on Radiological Sciences, such as research work, review articles, case reports, innovations in Medical Sciences related to all branches of Radiology, and letters to the editor. The aforementioned materials can be written in English only.

2. The authors have to submit 2 copies of the manuscript and a diskette: **to Prof. Dr. Kawee Tungsubutra,** 318 Kaweevej Hospital, Tarksin Road, Dhonburi, Bangkok 10600, Thailand. **or to the Associate Editors** at the Radiological Society of Malaysia, Indonesia, Philippine, Singapore and Brunei. The names and adresses of the Associate Editors in each country were published in the front page of this Journal.

3. The original copy to be submitted must be typed in a double space on one side of the page of 8.1/2"x 11.1/2" paper.

4. The format of the article must include :
   a. Title page and address of the author (s)
   b. Abstract
   c. Introduction (Background)
   d. Material and Method
   e. Results and discussion (Tables and Illustrations)
   f. Acknowledgement (if any)
   g. References (Follow the Vancouver style developed by ICMJE)

5. We will provide 25 copies of reprints for the author (s) who submit (s) an article for publication in the AAR Journal.

6. The illustrations and tables must be clearly prepared with legends in English as they are the art works to be reproduced.

7. The authors are responsible for the contents of the article as to its facts and findings.

8. Ethics.

Paper reporting studies which might be interpreted as human experimentation (e.g. controlled trials) should conform to the standards of the Declaration of Helsinki (see British Medical Journal 1964:2:177) and should indicate that, approval that such studies may proceed, has been granted by the local or hospital Ethics Committee.

When reporting experiments on animals indicate whether the institution's or the National Research Council's guide for, or any national law on, the care and use of laboratory animals was followed.

THE ASEAN JOURNAL OF RADIOLOGY

Volume III Number III SEPT.-DEC. 1997

CONTENTS

THE ASEAN JOURNAL OF RADIOLOGY

Volume III Number III SEPT.-DEC. 1997

PRENATAL DIAGNOSIS OF CONGENITAL DIAPHRAGMATIC HERNIA BY ULTRASONOGRAPHY : A CASE REPORT

Shashilekha BALACHANDRA[1,2], Somchit VIRANKABUTR[2], Pimjai SIRIWONGPAIRAT[1,2], Sawai SIRIWONGPAIRAT[3], Siriphan VONGHABSHI[2].

ABSTRACT

A case of congenital diaphragmatic hernia diagnosed sonographically in utero at 20 weeks gestation is described. In previous reports, this diagnosis has been made as early as 15 weeks gestation[1]. Recognition of this severe abnormality in the second trimester is beneficial. The parents can interrupt the pregnancy. Or, prompt operative treatment after delivery of an infant with this disorder may minimize the development of hypoxemia and acidosis commonly occur in these cases. In addition, appropriate parental counseling may be started.

CASE REPORT

A 34 year-old gravida 2, para 1 underwent ultrasound study at 20 weeks of pregnancy at the Bangkok Christian Hospital to confirm her dates. A right diaphragmatic hernia in the fetus was diagnosed at that time; loops of bowel were in the right hemithorax, displacing the heart to the left. (Fig.1-3). This was confirmed at 24 weeks gastation, and there was no evidence of poly hydramnios. Amniocentesis for karyotype analysis was done and revealed a 46 XY normal male karyotype. The patient chose to continue the pregnancy despite the poor prognosis. She delivered her baby by cesarian section without any complication. There was no associated anomalies. Chest X-ray of the infant after birth confirmed the pre-natal diagnosis of a right diaphragmatic hernia showing multiple loops of bowel in right side of the chest. The lungs were compressed and hypoplastic. The infant received prompt operative treatment and survived.

DISCUSSION

Congenital diaphragmatic hernia is known to occur in approximately one in 2,200-5,000 births[2]. It is also part of schisis association[3]. Congenital postero-lateral diaphragmatic hernia occur as an isolated defect about 60% of the time.[4] Because of the mass effect produced in the fetal thorax for many months in utero, the fetal lungs remain hypoplastic, and the prognosis for the newborn is poor despite immediate post natal surgery. With optimal conventional therapy, most fetuses with detectable congenital diaphragmatic hernia will die in the neonatal period (80% mortality). The defect is present by week 10 of fetal development; therefore, even subtle signs of a mass effect in the fetal thorax in the second trimester[5] may be significant for early diagnosis. The bowel was forced through the lumbo-costal triangle as a result of the inverted position of the fetus[6]. Polyhydramnios is both a common prenatal marker for congenital diaphragmatic hernia (present in 76% of the fetuses) and a predictor for

[1] Department of Radiology, Ramathibodi Hospital, Rama 6 Road, Bangkok 10400, Thailand.
[2] Department of Radiology, Bangkok Christian Hospital, 124 Silom Road, Bangkok, Thailand.
[3] Department of OB-Gyn, Bangkok Christian Hospital

poor clinical outcome, only 11% survived. Fetal congenital diaphragmatic hernia is a dynamic process. Non survivors have larger defects and may have more viscera displaced into the chest at an earlier stage of development[7]. It is important that prenatal diagnosis of congenital diaphragmatic hernia not only be accurate but also predict clinical outcome. Amniocentesis for karyotype analysis may also be indicated, since among the series of 94 cases reported by Adzick NS et al., there were 4 cases of trisomy.

In our patient, the major sonographic finding when the diagnosis was made at 20 and 24 weeks was cystic structures in the right hemithorax and displacement of the heart in the fetal chest owing to mass effect. Displacement of the fetal mediastinum is a non specific sign that can be seen in cases of dextrocardia, various intra-thoracic masses and congenital diaphragmatic hernia. The differential diagnoses include congenital cystic adenomatoid mal-formation of the lung, pulmonary sequestration and bronchogenic cyst.

1.A,B.

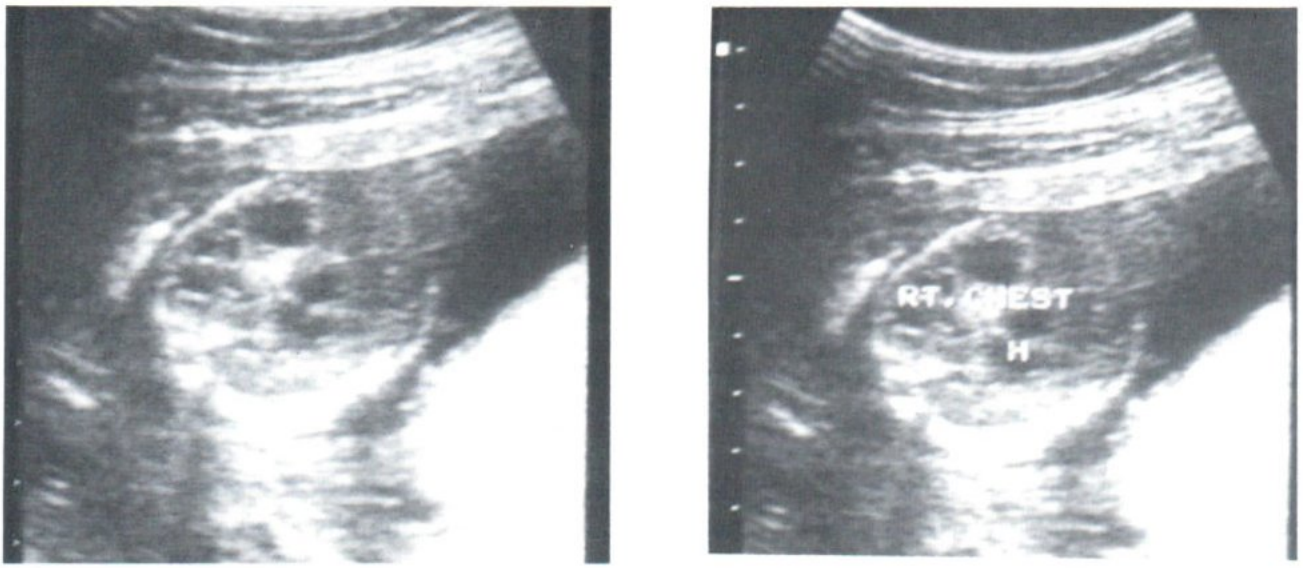

2.A,B.

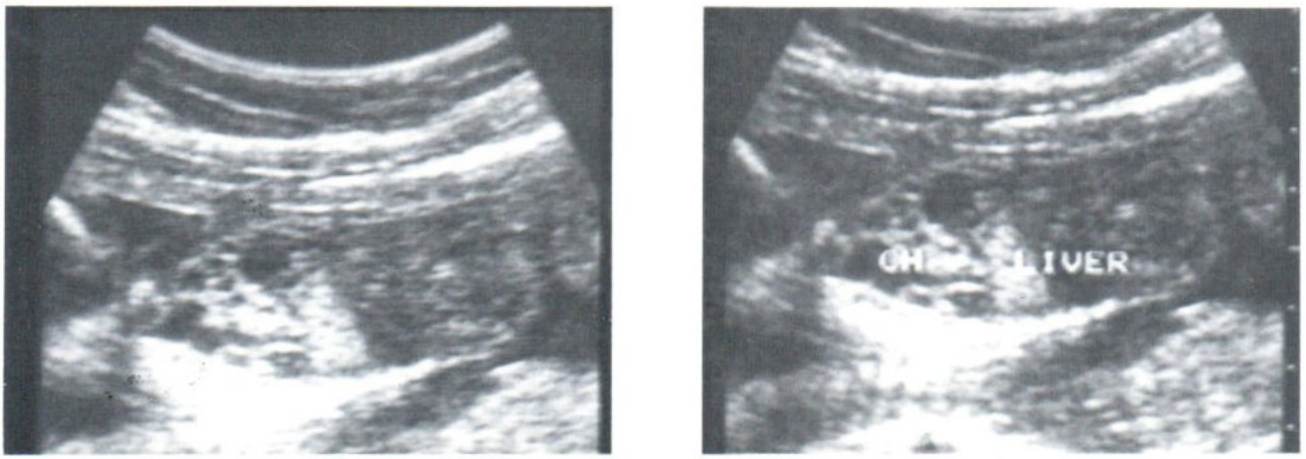

Fig. 1,2 A,B Cross sectional and longitudinal scans of fetal thorax and abdomen shows fluid filled loops of bowel in the right chest displacing the heart to the left side. The loops of bowel were seen above the liver on longitudinal scan.

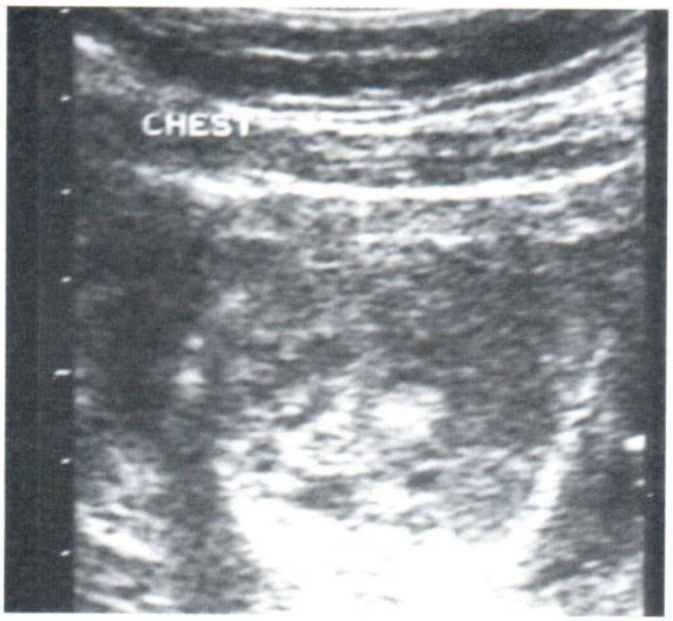

3A.

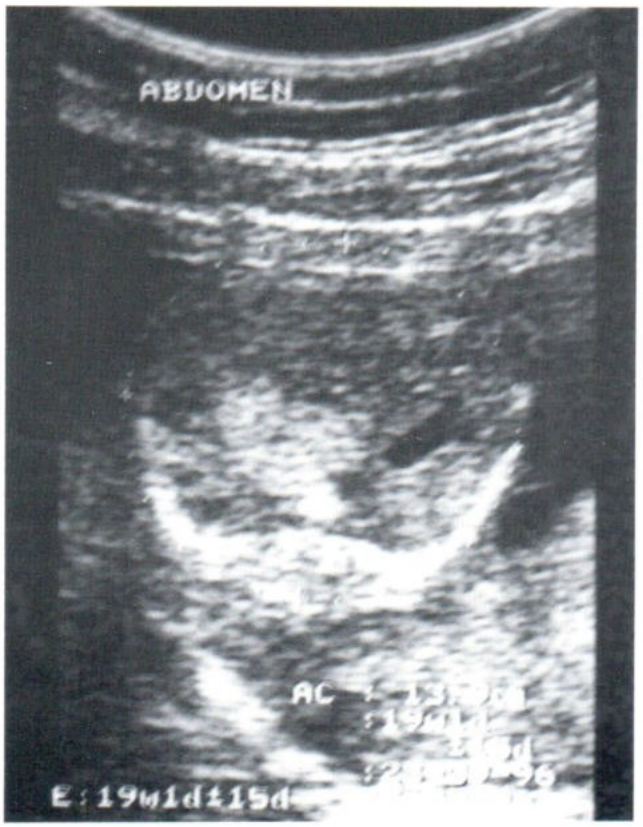

3B.

Fig. 3 A,B Cross sectional scans of the chest and abdomen shows loops of bowel in the right chest and at right postero - lateral part of the abdomen. Findings suggest herniation of loops of bowel through the right foramen of Bochdalek.

REFERENCES:

1. Benacerraf BR. and Adzick NS. Fetal diaphragmatic hernia: ultrasound diagnosis and clinical outcome in 19 cases. Obstet Gynecol 1987;156:573-6.
2. Harrison MR, De lorimier AA. Congenital diaphragmatic hernia. Surg Clin North Am 1981;61:1023-35.
3. Czeizel A: Schisis-association. Am J Med Genet 1981;10:25-35.
4. Benjamin DR, Juul S. and Siebert JR. Congenital postero-lateral diaphragmatic hernia: associated malformations. J of Ped Surg 1988;23:899-903.
5. Stiller RJ, Roberts NS, Weiner S, et al. Congenital diaphragmatic hernia antenatal diagnosis and obstetrical management. J Clin Ultrasound 1985;13:212-5.
6. Cullen ML, Klein MD and Philippart AI. Congenital diaphragmatic hernia . Surg Clin of North Am 1985;65:1115-37.
7. Adzick NS, Harrison MR, Glick PL. et al. Diaphragmatic hernia in the fetuses: prenatal diagnosis and outcome in 94 cases. J of Ped Surg 1985;20:357-61.

CT OF RETROPERITONEAL MYXOID LIPOSARCOMA IN A CHILD

Pannee VISRUTARATNA, Chusak SIRIVANICHAI, Sukanya REUNGRONGRAT.

ABSTRACT

Abdominal CT scans of a 2-year-3-month-old boy with retroperitoneal myxoid liposarcoma are presented which show a well-demarcated soft tissue mass with near-water density and intermingled septa.

INTRODUCTION

Abdominal masses in pediatric patients are a common problem encountered by radiologists. Neuroblastomas and Wilms tumors are common abdominal tumors in this age group. We present a case of retroperitoneal myxoid liposarcoma, a rare cause of abdominal masses in children.

CASE REPORT

A 2-year-3-month-old boy appeared with a large abdomen, which he had had for a few months. Physical examination revealed a large abdominal mass on the left side fixed to underlying tissue with firm consistency and a smooth surface. There was no tenderness on palpation. A complete blood count and urine analysis were normal. CT scans of the abdomen showed a large well-demarcated mass on the left side of retroperitoneum (Figs. 1 and 2), which was of near-water density and had intermingled septa. There were no calcifications in the mass. The left kidney was displaced posteriorly. The remainder of the abdomen was normal. A chest radiograph and bone scan were normal. A sample from fine needle aspiration biopsy of the mass was myxoid. On exploratory laparotomy, a mass measuring 11X12X14 cm and weighing 2000 gm was found arising from the soft tissue of the retroperitoneum and was removed completely. Pathological examination showed myxoid liposarcoma. The patient has remained well 10 months after surgery.

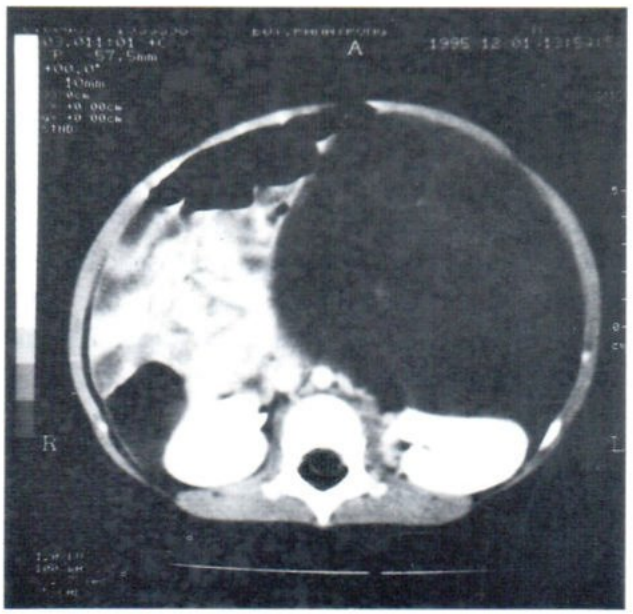

Fig 1. CT scan at the level of the renal hila shows a well-demarcated mass with near -water density containing intermingled septa. The mass has pushed the left kidney posteriorly.

Department of Radiology, Faculty of Medicine, Chiang Mai University, Chiang Mai 50200, THAILAND

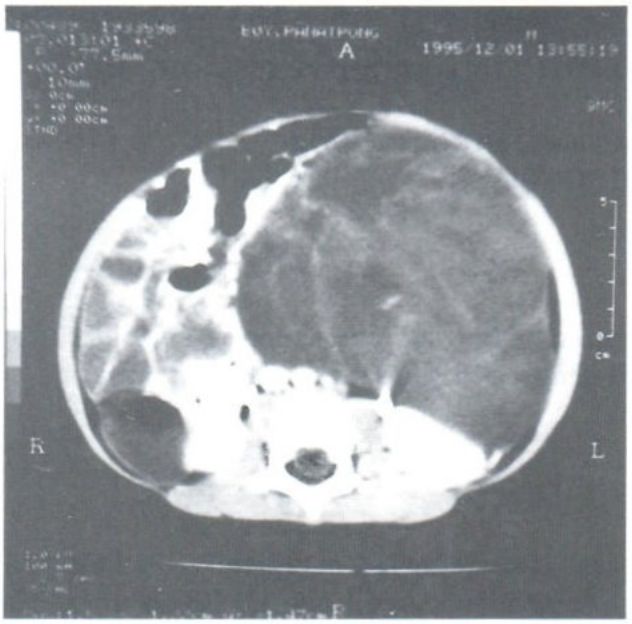

Fig 2. CT scan at the level of the lower pole of the kidneys. Note that the mass does not encase the aorta and inferior vena cava.

DISCUSSION

Liposarcoma is one of the most common soft tissue sarcomas in adults. It is usually located in the deep soft tissues of extremities (especially the thigh) and the retroperitoneum. It is currently classified into well-differentiated, myxoid, round cell and pleomorphic types.[1]

Liposarcoma is rare in children. Childhood liposarcoma tends to occur in infancy and early adolescence. It occurs primarily in the extremities. In one review article,[2] retroperitoneal liposarcoma was found in 10.8% of cases of childhood liposarcomas. The most common type in this age group is myxoid, which has a better prognosis overall than it does in adults.

The density of a myxoid liposarcoma on CT scans is greater than that of normal fat. Usually it has a homogeneous soft tissue appearance on a CT scan, but well-differentiated portions can be radiolucent and poorly-differentiated portions can be more radiodense.[3] Waligore et al.[4] reviewed the CT appearance of 11 myxoid liposarcomas and found that the dominant densities of these tumors varied considerably. At the lower end of densities the tumors had densities near that of water, and at the higher end densities similar to that of muscle. Most of the tumors were sharply defined. Focal calcifications were seen in two of the tumors. Only three of the tumors contained components of the same density as normal fat. In the present case, the mass was well-demarcated and displaced the retroperitoneal structures, which is different from neuroblastoma, the more common retroperitoneal tumor in childhood. Neuroblastoma has a poorly-defined margin, and it usually encases the aorta and its major branches. The density of the mass in our case was also different from that of neuroblastoma.

Regarding the treatment, complete surgical resection is crucial for survival in young patients with liposarcoma. External beam radiation therapy may be effective against residual tissue.[5]

REFERENCES:

1. Smith TA, Easley KA, Goldblum JR. Myxoid/round cell liposarcoma of the extremities. Am J Surg Pathol 1996;20(2):171-180.
2. Castleberry RP, Kelly DR, Wilson ER, Cain WS, Salter MR. Childhood liposarcoma: report of a case and review of the literature. Cancer 1984;54:579-584.
3. Mikkilineni RS, Bhat S, Cheng AW, Prevosti LG. Liposarcoma of the posterior mediastinum in a child. Chest 1994;106:-1288-89.
4. Waligore MP, Stephens DH, Soule EH, McLeod RA. Lipomatous tumors of the abdominal cavity: CT appearance and pathologic correlation. AJR 1981;137:539-545.
5. La Quaglia MP, Spiro SA, Ghavimi F, Hadju SI, Meyers P, Exelby PR. Liposarcoma in patients younger than or equal to 22 years of age. Cancer 1993;72:3114-9.

ULTRASONOGRAPHY OF EXTRAPULMONARY NOCARDIOSIS IN PATIENTS WITH HUMAN IMMUNODEFICIENCY VIRUS

Pannee VISRUTARATNA, MD, Suwalee POJCHAMARNWIPUTH, MD.

ABSTRACT

We report ultrasonographic findings of three patients with human immunodeficiency virus (HIV) and extrapulmonary nocardial abscesses. The first patient had a hypoechoic mass anterior to the thyroid gland. The second had a hypoechoic mass in the right liver lobe. The third patient had two hypoechoic masses in the liver (one in the right liver lobe, the other one in the left liver lobe) and a hypoechoic mass in the lower pole of left kidney. The chest radiographs of the first two patients with pulmonary nocardiosis showed patchy infiltrates with cavities. The combination of ultrasonographic findings of hypoechoic mass in various organs and chest radiographs of patchy infiltrates with cavities in patients with HIV suggests nocardiosis.

INTRODUCTION

Nocardia species are gram-positive, aerobic, filamentous bacteria found in the soil worldwide. *N. asteroides* is the species most frequently isolated from clinical specimens.[1] Infection most often occurs in immunocompromised hosts, particularly in patients who have deficiencies in cellular immunity. Afflicted patients may either be on immunosuppressive therapy, such as corticosteroids; or antineoplastic chemotherapy; or be organ transplant recipients; or have underlying immunosuppressive disorders such as chronic granulomatous disease, diabetes, alcoholism, or HIV/AIDS.

The incidence of nocardiosis varies geographically. In an autopsy study[2], the incidence in HIV-positive patients was 4% (10 in 247 HIV-positive adult cadavers). In another clinical review[3], the incidence was 1.8% (30 in 1,655 AIDS patients). In the reported cases of HIV/AIDS patients, the lung is the predominant site of the disease.[1,2] The infection can cause abscesses in the brain, kidney, liver, or soft tissues. It can also cause lymphadenitis and pericarditis.

Since 1987 when the first case of AIDS was seen at the Chiang Mai University Hospital, we have seen many cases of pulmonary nocardiosis, a few cases of nocardial brain abscesses, and three cases of nocardial abscesses in other organs in HIV-infected patients. We describe here ultrasonographic findings of the three patients with extrapulmonary nocardial abscesses.

CASE REPORTS

The clinical data of the three HIV-infected patients with extrapulmonary nocardiosis are in (Table 1). The first patient had an abscess anterior to the thyroid gland. The second patient had a liver abscess. The sputum cultures and pus cultures of the first two patients grew *N. asteroides*. The third patient had two concurrent infections, nocardiosis and penicilliosis marneffei. A pus culture from the liver abscesses of the third patient grew *N. asteroides*. A culture from the papules grew *P. marneffei*. However, a sputum culture grew nothing.

Department of Radiology, Faculty of Medicine, Chiang Mai University, Chiang Mai 50200, THAILAND.

Ultrasonography showed the abscesses in the three patients to be hypoechoic. The abscess in the first patient was anterior to both right and left lobes of the thyroid gland and to the trachea (Fig 1A). The second patient had an abscess in the right liver lobe (Fig 2A). The third patient had an abscess in the right liver lobe (Fig 3A), one in the left liver lobe, and one in the lower pole of the left kidney (Fig 3B).

The chest radiographs of the three patients are in Fig 1B, Fig 2B and Fig 3C, respectively.

All three patients responded to trimethoprim-sulfamethoxazole.

TABLE 1. Clinical data, US and CXR findings of the patien

Patient No.	History	Ultrasonography	Chest X-ray
1 34y/M	Fever for 20 days and neck mass.	Hypoechoic mass, 4X4X2 cm, anterior to thyroid gland.	Patchy infiltrate with cavities in left upper lobe.
2 31y/M	Intermittent fever for 3 weeks.	3 cm hypoechoic mass in right liver lobe.	Patchy infiltrate with cavities in right middle lobe. Reticulonodular infiltrate in both upper lobes.
3 31y/M	Fever and papules on face for 1 week. week. Treated for Penicilliosis marneffei and *S. enteritidis* septicemia 7 months prior.	Two hypoechoic masses, one 2.8 cm in right liver lobe, other 3.2 cm in left liver lobe. 4 cm hypoechoic mass in lower pole of left kidney.	Patchy infiltrate with cavities in left upper lobe.

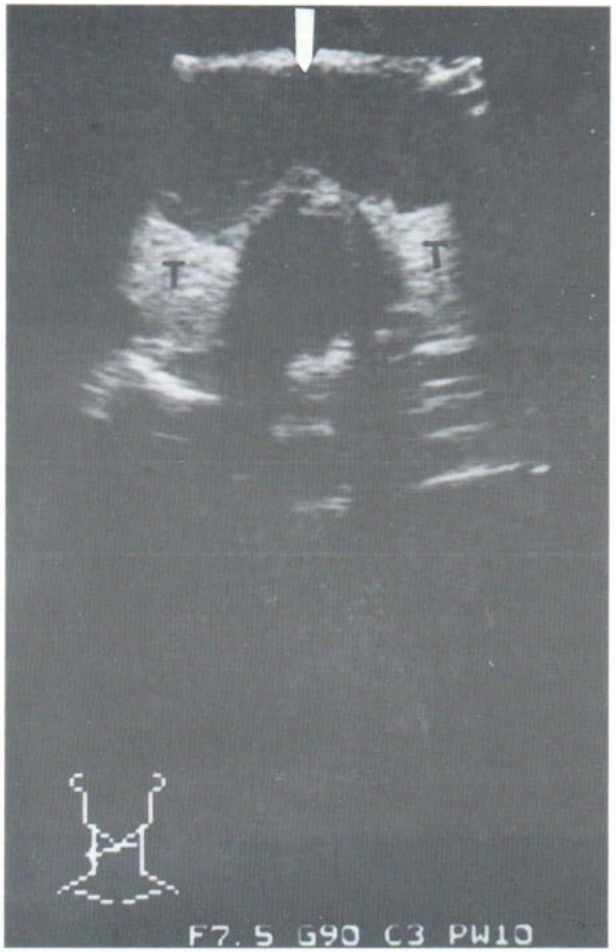

Fig 1A. Transverse ultrasound image of the neck shows an abscess (arrow) anterior to both lobes of the thyroid gland (T).

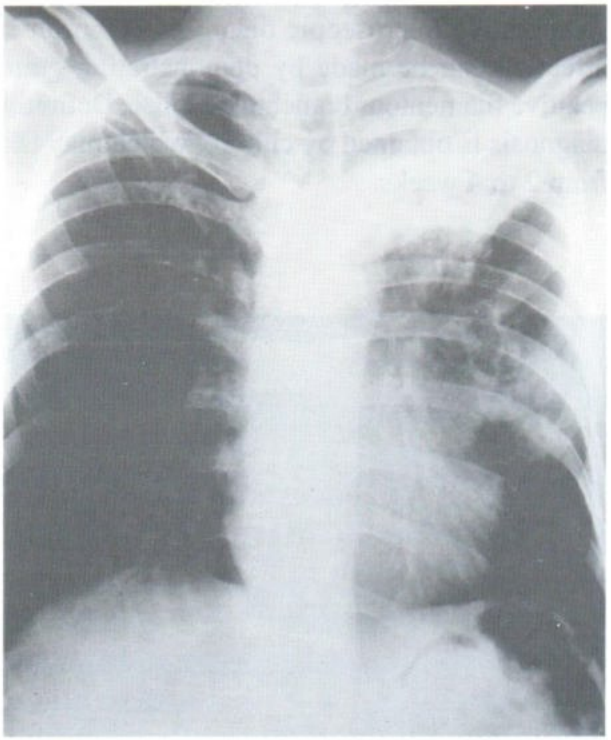

Fig 1B. Chest radiograph shows patchy infiltrate with cavities in the left upper lobe.

DISCUSSION

Nocardiosis is an uncommon opportunistic infection complicating HIV infection. It is not included in the definition for AIDS of the Centers for Disease Control[4]; hence, the total number of cases is unknown. Symptoms of nocardial infection in HIV-infected patients are usually nonspecific. Most patients have advanced immunodeficiency (CD4 cell counts less than 0.2 X 10^9/L) with fever, night sweats, malaise, cough, and weight loss[1]. Although nocardiosis is frequently disseminated in HIV infection, the lung is the most common site of involvement.[1,2] This is consistent with the mode of infection, which is most often by inhalation. When Uttamchandani et al.[3] studied chest radiographs of 21 patients with pulmonary nocardiosis and HIV, they found alveolar infiltrates in 14 patients, reticulonodular infiltrates in 2, mixed alveolar and reticulonodular patterns in 6, cavitation in 4, and pleural effusion in 3. However, in our experience, the most common radiographic abnormality of pulmonary nocardiosis is inhomogeneous consolidation with multiple cavities.[5]

Besides lung diseases, *Nocardia* can cause brain abscesses[6], meningitis[6], septic arthritis[7], pericarditis[1], soft-tissue abscesses[1], renal abscesses[1], and lymphadenitis.[3]

Nocardia is a bacterium and thus should be responsive to antibiotic therapy. The sulfa drugs, including trimethoprim-sulfamethoxazole, are the treatment of choice. Early recognition of this disease is crucial as it is potentially treatable, but treatment must begin as soon as possible. A presumptive microscopic diagnosis of nocardial infection can be made by demonstrating gram-positive filamentous branching hyphae. Definitive diagnosis is obtained by culture, which may take from 2 to 4 weeks.

The ultrasonographic findings of extrapulmonary nocardial abscesses are nonspecific. They cannot be differentiated from abscesses caused by other organisms. An associated pulmonary infiltrate with cavities can provide a clue to the diagnosis. With the numbers of HIV-infected individuals rising steadily, the frequency of all opportunistic infections, including Nocardia, may be expected to increase. Increased awareness of this unusual infection is crucial to its early diagnosis.

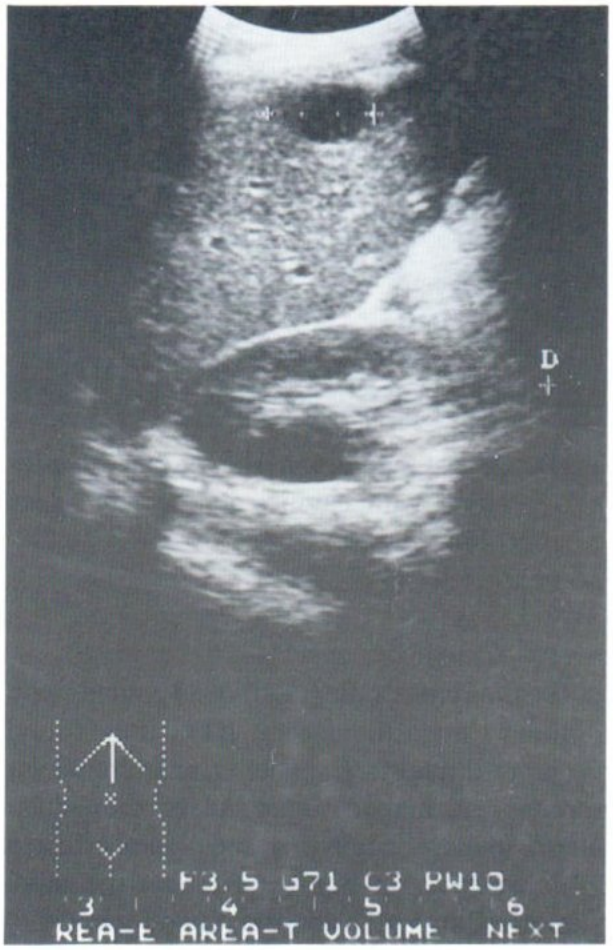

Fig 2A. Longitudinal ultrasound image of the liver shows a hypoechoic mass (+...+) in the right liver lobe.

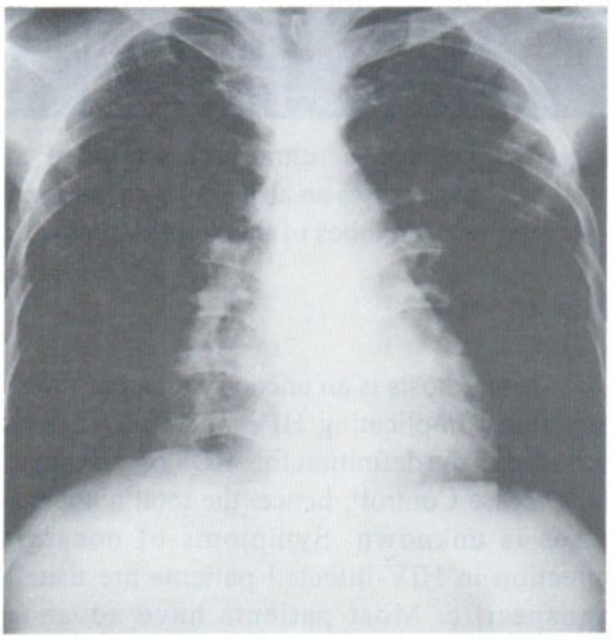

Fig 2B. Chest radiograph shows patchy infiltrate with cavities in right middle lobe and reticulonodular infiltrate in both upper lobes.

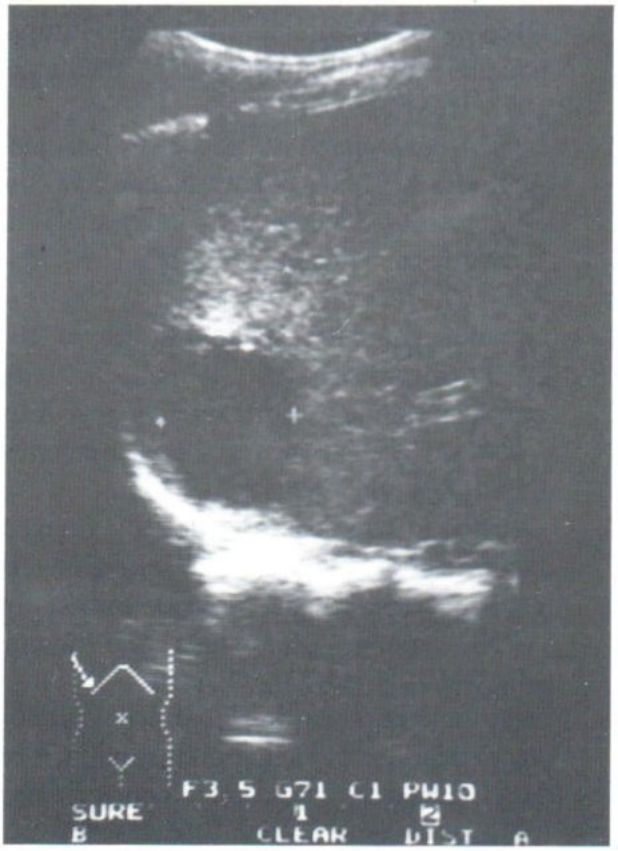

Fig 3A. Oblique ultrasound image of the liver shows a hypoechoic mass (+...+) in the right liver lobe.

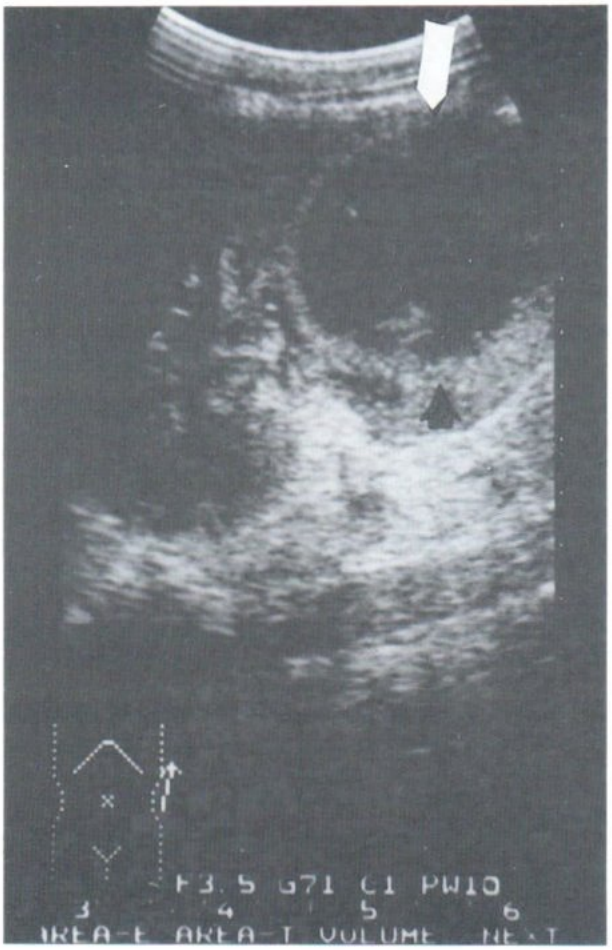

Fig 3B. Longitudinal ultrasound image of the left kidney shows a hypoechoic mass in the lower pole of the left kidney.

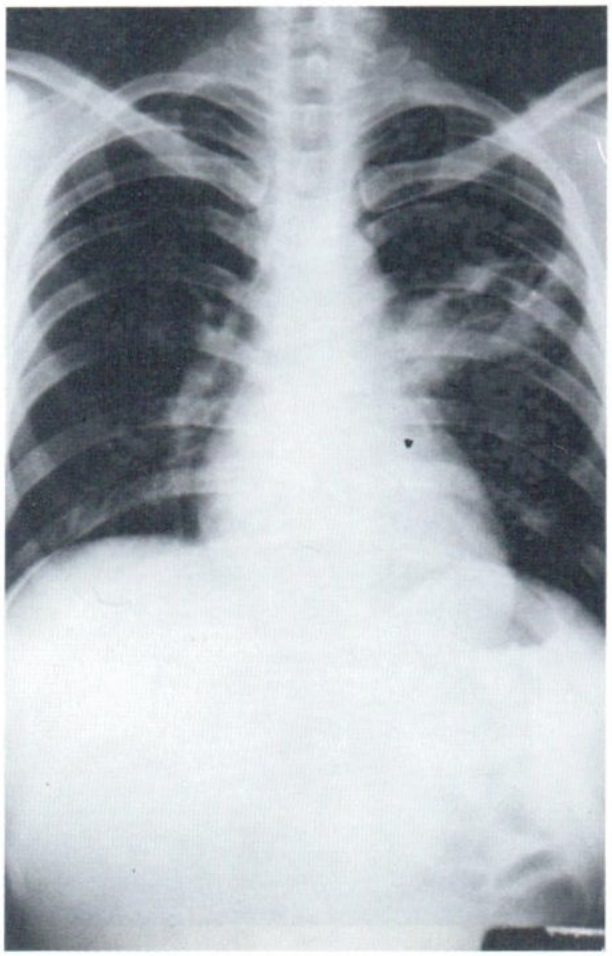

Fig 3C. Chest radiograph shows patchy infiltrate with cavities in left upper lobe.

REFERENCES

1. Javaly K, Horowitz HW, Wormser GP. Nocardiosis in patients with human immunodeficiency virus infection. Medicine 1992;71(3):128-138.
2. Lucas SB, Hounnou A, Peacock C, Beaumel A, Kadio A, De Cock KM. Nocardiosis in HIV-positive patients: an autopsy study in West Africa. Tubercle Lung Dis 1994;75:-301-307.
3. Uttamchandani RB, Daikos GL, Reyes RR, et al. Nocardiosis in 30 patients with advanced human immunodeficiency virus infection: clinical features and outcome. Clin Infect Dis 1994;18:348-353.
4. Centers for Disease Control. 1993 revised classification system for HIV infection and expanded surveillance case definition for AIDS among adolescents and adults. MMWR 1992;41(RR-17):1-19.
5. Vivitmongkornchai K, Simaruk S. Pulmonary nocardiosis: radiographic findings in HIV infection and other compromised statuses. Asean J Radiol 1995;1(3):87-95.
6. LeBlang SD, Whiteman MLH, Post MJD, Uttamchandani RB, Bell MD, Smirnitopolous JG. CNS Nocardia in AIDS patients: CT and MRI with pathologic correlation. J Comput Assist Tomogr 1995;19(1):15-22.
7. Ray TD, Nimityongskul P, Ramsey KM. Disseminated Nocardia asteroides infection presenting as septic arthritis in a patients with AIDS. Clin Infect Dis 1994;18:256-257.

CT OF FACE AND NECK MASSES IN CHILDREN

Pannee VISRUTARATNA[1], MD., Piyadara KHONGPIBOONKIJ[1], MD., Jesada SINGHAVEJSAKUL[2], MD., Aumnart YOUSUKH[3], MD.

ABSTRACT

CT scans of 16 patients with face and/or neck masses were reviewed. These patients were diagnosed by histopathology or clinical follow up as having cystic hygromas (6 cases), hemangiomas (5 cases), benign lymphoepithelial parotid cysts (2 cases), plunging ranula (1 case), non-Hodgkin lymphoma (1 case), and plexiform neurofibromatosis (1 case). Cystic hygromas were seen as uniloculated or multiloculated cystic masses with septa of variable thicknesses. The masses were usually not discrete. Hemangiomas were characterized by intense enhancement. Children with human immunodeficiency virus and benign lymphoepithelial cysts had bilateral diffuse enlarged parotid glands with multiple small cysts. The plunging ranula appeared as a well-defined homogeneous cystic lesion extending from the sublingual to the submandibular region. The location, extent and internal characteristics of face and/or neck masses were determined by CT.

INTRODUCTION

Face and neck masses are uncommon in children. They can be evaluated by ultrasonography (US), computed tomography (CT), or magnetic resonance (MR) imaging. CT and MR imaging are better than US for demonstrating the extent of the masses, the presence or absence of bone erosion, vascular encasement, and airway compromise.[1]

MATERIALS AND METHODS

We reviewed CT scans performed from April 1995 to January 1997 of 16 children ranging in age from 15 days to 15 years with face and/or neck masses. There were 8 females and 8 males. Both pre- and post-contrast enhanced CT scans were done using contiguous axial cuts 5 mm thick through the region with face and/or neck masses. Sometimes contiguous coronal CT scans with 5 mm thick sections were also done. The diagnoses were cystic hygromas (6 cases), hemangiomas (5 cases), benign lymphoepithelial parotid cysts (2 cases), plunging ranula (1 case), non-Hodgkin lymphoma (1 case), and plexiform neurofibromatosis (1 case). The diagnoses of 5 of the 6 patients with cystic hygroma were proved by histopathology, and of 1 by needle aspiration. For the patients with hemangiomas the diagnoses were verified by regression of the masses with corticosteroid therapy in 4 cases. Fine needle aspiration of the fifth patient with hemangioma of the left masseter muscle revealed unclotted blood, which was confirmed by MR imaging showing a hyperintense mass with serpentine signal voids on T2-weighted images. The two patients with benign lymphoepithelial parotid cysts were diagnosed by their positive anti-HIV antibody and their clinical history. The diagnoses

[1] Department of Radiology,
[2] Department of Surgery,
[3] Department of Pathology, Faculty of Medicine, Chiang Mai University, Chiang Mai 50200, Thailand.

of the patient with plunging ranula and the patient with non-Hodgkin lymphoma were proved by histopathology. The last patient with plexiform neurofibromatosis was diagnosed using her clinical history.

RESULTS

Cystic hygromas CT scans of 4 of the 6 patients with cystic hygromas showed multiloculated cystic masses (Fig. 1); CT scans of the other two patients showed uniloculated cystic masses (Fig. 2). The smaller lesions tended to be well demarcated, while the larger lesions tended to be poorly demarcated. The masses were confined to the parotid spaces in 2 cases, and invaded the parotid glands as part of extensive cervical masses in 2. In one patient the cystic hygroma was in the posterior triangle of neck. The last patient had cystic hygroma at the right submandibular triangle of the neck, which had similar CT findings to those of simple ranula. However a needle aspiration revealed fluid consistent with cystic hygroma. The density of fluid in the cystic hygromas varied from 10.7 HU to 19.4 HU. The CT scans showed displacement of the trachea and esophagus in 2 patients.

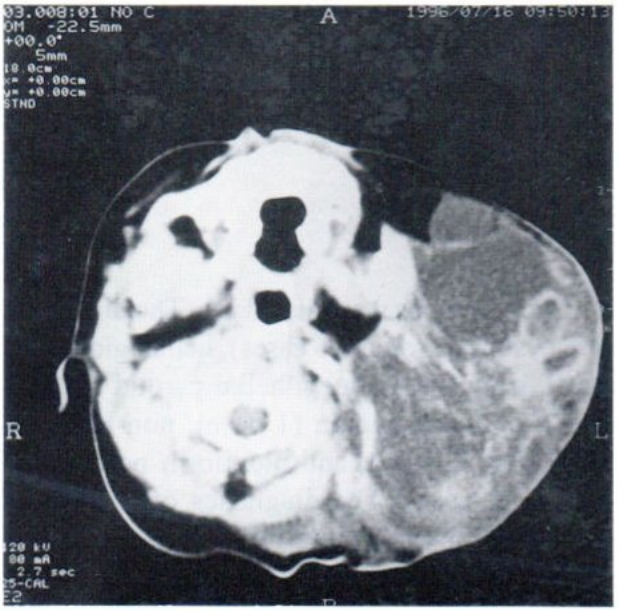

Fig.1 A 23-day-old boy with cystic hygroma of the left parotid gland. Contrast CT scan shows a multiloculated cystic mass in the left parotid region.

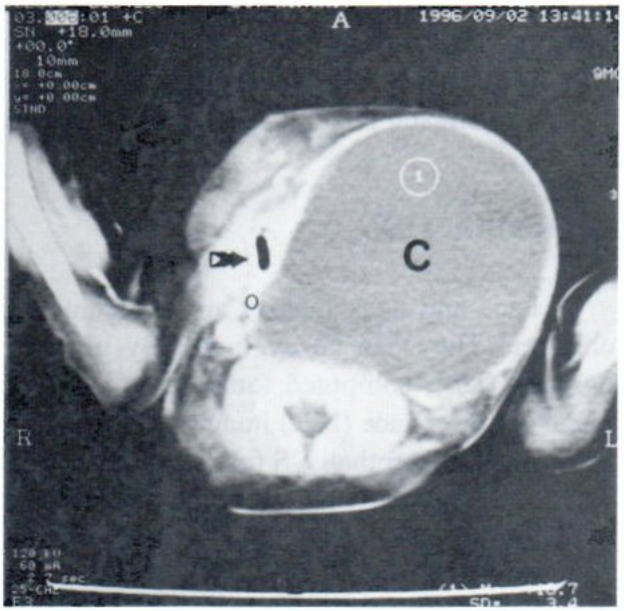

Fig.2 A 15-day-old boy with cystic hygroma of the left neck. Contrast CT scan shows a well-defined uniloculated cystic mass (c) with displacement of the endotracheal tube (arrow) and orogastric tube (o) to the right.

Hemangiomas The CT findings of the 5 patients with hemangiomas showed intense enhancement of the tumors. Three of them had hemangiomas of the right parotid glands; one had a hemangioma of the left parotid gland. The last patient had a hemangioma of the left masseter muscle. On pre-contrast CT scans the hemangiomas were slightly hypodense compared to the muscles (Fig. 3A). Post-contrast CT scans greatly enhanced the mass (Fig. 3B). In one patient a few small areas of hyperdensity were seen in the mass, consistent with focal areas of hemorrhage (Fig. 4). One of the hemangiomas compressed the trachea. Pre-contrast CT scans of the single patient with hemangioma of the left masseter muscle showed enlargement of this muscle with a hypodense mass. Post-contrast CT scans enhanced the center of the mass giving it a tortuous appearance (Fig. 5). T1-weighted MR imaging showed enlarged left masseter muscle with slight hyperintensity. T2-weighted MR imaging showed hyperintensity with serpentine signal voids. None of the five patients had phlebolith.

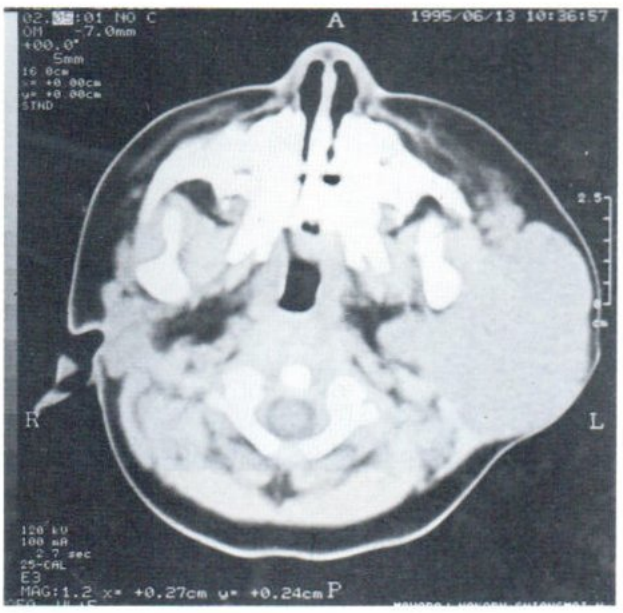

Fig.3 A 2-month-old girl with hemangioma of the left parotid gland.

Fig.3A Noncontrast CT scan shows enlarged left parotid gland with slight hypodensity compared to the muscles.

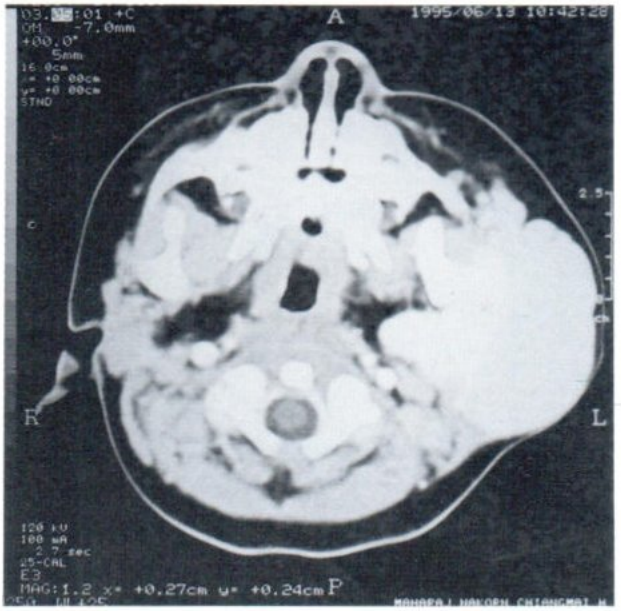

Fig.3B Contrast CT scan shows intense enhancement of the mass.

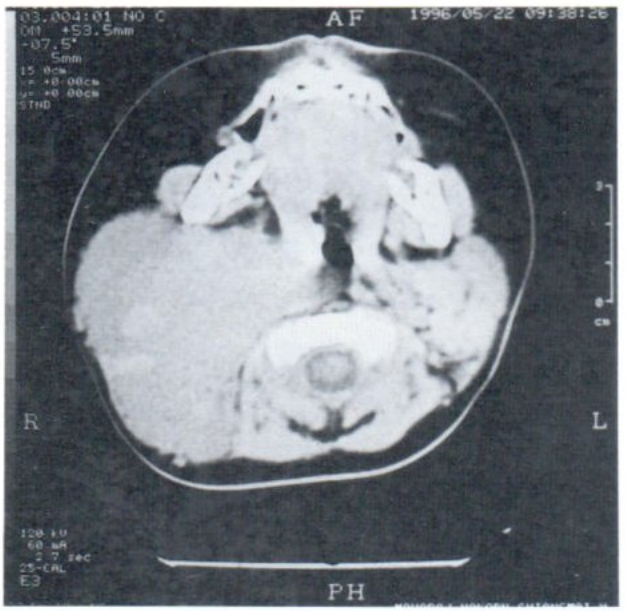

Fig.4 A 7-month-old girl with hemangioma of the right parotid gland.

Fig.4A Noncontrast CT scan shows enlarged right parotid gland with a few areas of hyperdensity consistent with hemorrhage.

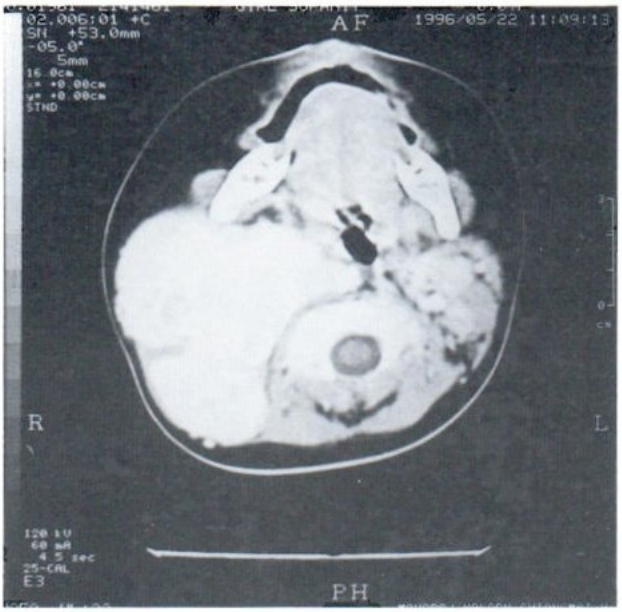

Fig.4B Contrast CT scan shows intense enhancement of the mass.

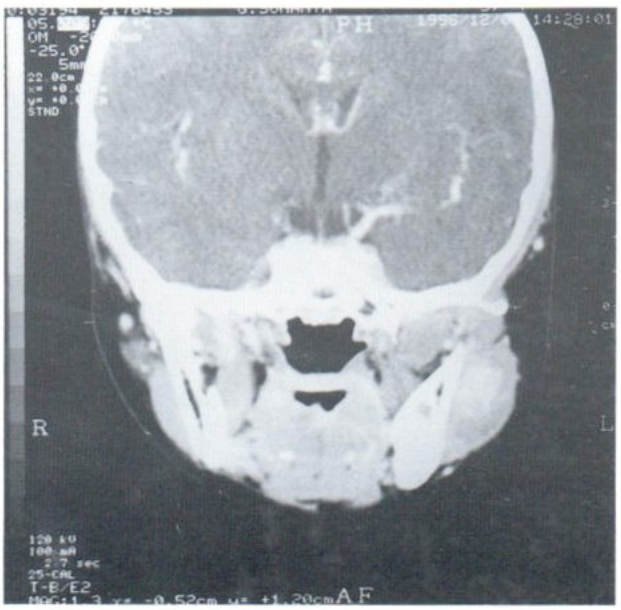

Fig.5 A 3-year-old girl with hemangioma of the left masseter muscle.

Fig.5A Contrast CT scan shows enlarged left masseter muscle with a hypodense mass and tortuous enhancement at the center.

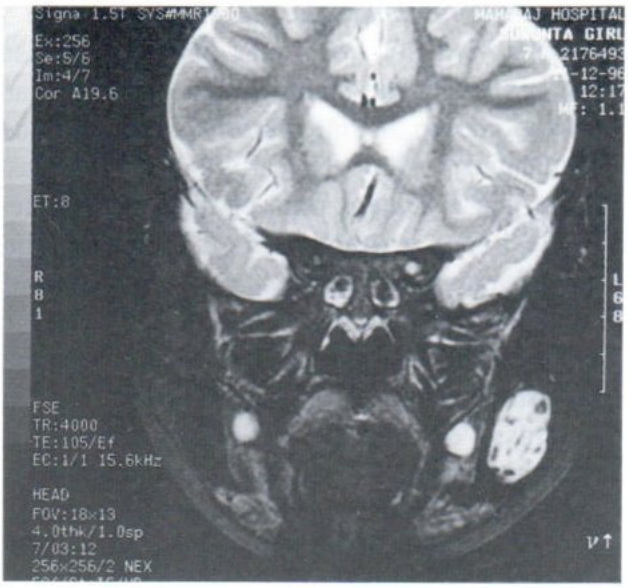

Fig.5B Coronal MR image (FSE 4000/105) shows hyperintense mass with serpentine signal voids in the left masseter muscle.

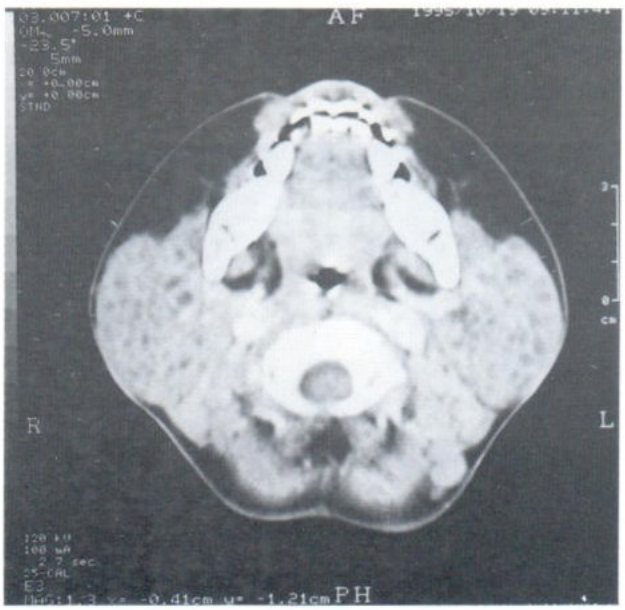

Fig.6 A 1-year-old boy with benign lymphoepithelial cysts. Contrast CT scan shows enlarged bilateral parotid glands with multiple small cysts. The parotid parenchyma is also denser than normal. Bilateral enlarged posterior cervical lymph nodes are also seen.

Benign lymphoepithelial parotid cysts The two patients with acquired immunodeficiency syndrome (AIDS) had enlarged bilateral parotid glands with multiple small cysts (Fig. 6). The parotid parenchyma was denser than normal. Multiple enlarged lymph nodes were seen in the posterior cervical region.

Ranula CT scans of the single patient with plunging ranula showed a well-defined cystic mass at the left side of the floor of the mouth with extension to the left submandibular region (Fig. 7).

Non-Hodgkin lymphoma CT scans of the patient with non-Hodgkin lymphoma showed soft tissue masses in the nasopharynx (Fig. 8) and oropharynx, which compressed the airway. Multiple enlarged cervical lymph nodes were also seen.

Plexiform neurofibromatosis Dysplasia of the left sphenoid wing, exophthalmos of the left orbit, thickening of the sclera of the left orbit and fusiform masses in the left temporalis muscle were seen on the CT scans of the patient with plexiform neurofibromatosis (Fig. 9).

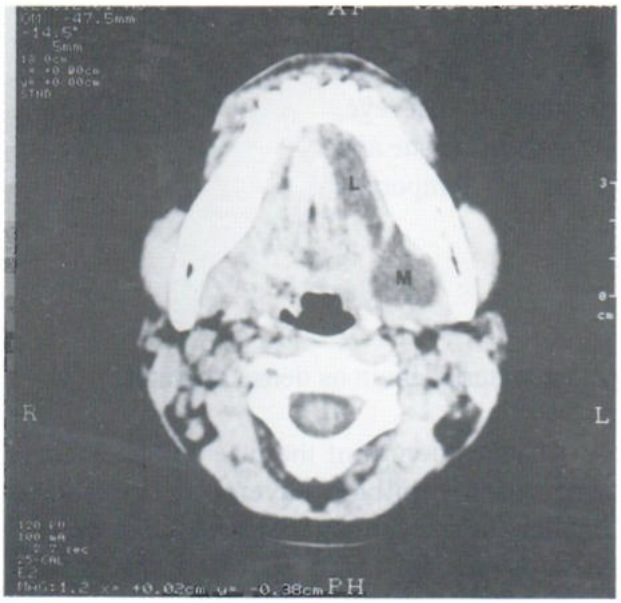

Fig.7 A 7-year-old girl with plunging ranula. Noncontrast CT scan shows a cystic mass in the left sublingual region (L) extending to the left submandibular region (M).

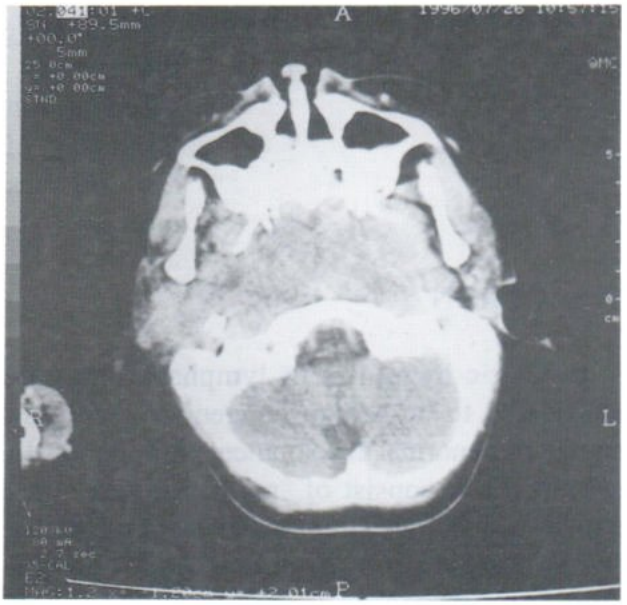

Fig.8 A 8-year-old boy with non-Hodgkin lymphoma. Contrast CT scan shows inhomogeneous mass in the nasopharynx with obliteration of the airway.

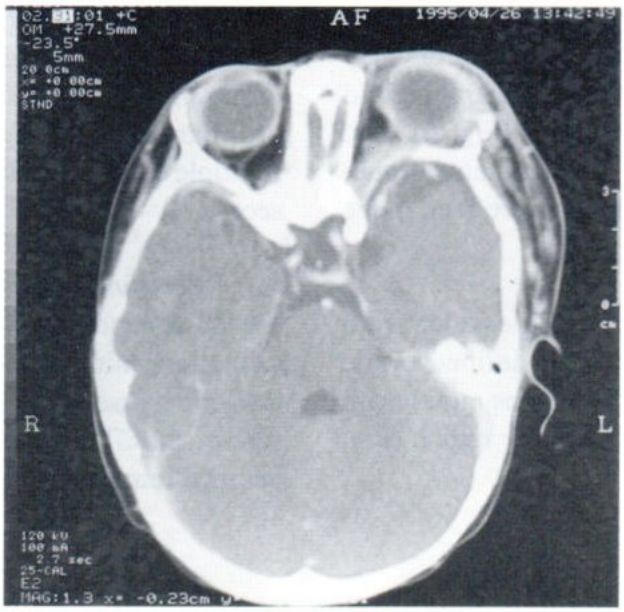

Fig.9 A 2-year-old girl with p lexiform neurofibromatosis. Note dysplasia of the left sphenoid wing, proptosis of left eye, thickening of periorbital soft tissue and fusiform masses in the left temporalis muscle.

DISCUSSION

Cystic hygromas or lymphangiomas are considered to be benign congenital neoplasms caused by abnormal development of the lymphatic system. They consist of multiloculated cystic masses with individual cysts that vary in size.[2] The mass is usually not discrete. Most hygroma patients are diagnosed by the age of 2. The neck is the most common site, especially the posterior triangle, but the face, tongue, and floor of the mouth are also occasional sites.[3] Complications of untreated cystic hygromas come from the pressure that the mass can exert on structures such as the trachea or esophagus. Although cystic hygromas of the parotid gland are rare[4], we found two patients in our review. It is more common for cystic hygromas to occur as large cervical masses which can extend to the parotid gland.[5] On CT scans they are thin-walled, uniloculated or multiloculated, non-enhanced cystic masses filled with a material about as dense as water.

Hemangiomas of the face and neck are of three types: capillary, cavernous, and mixed. Capillary hemangiomas are usually discovered at birth or during infancy; the frequency of spontaneous regression is high.[1] They are the most common parotid gland tumors in the first year of life. Usually discovered shortly after birth, they are unilateral, compressible, nonencapsulated, lobulated, soft, and more common in girls. There also may be associated hemangiomas in the overlying skin. On CT these tumors show intense enhancement; they are often lobular. They may extend to the overlying skin, or may have phleboliths within the tumor tissue.

Intramuscular hemangiomas are uncommon tumors in the head and neck region. The masseter

muscle is the most frequent site of involvement there. Masseter hemangiomas occur almost exclusively in the pediatric patients.[6] CT usually shows an enhanced, well-circumscribed intramuscular mass.

Bilateral parotid enlargement in an acquired immunodeficiency syndrome (AIDS) patient is usually due to benign lymphoepithelial cysts[7,8], which have a very similar image to cysts in Sjögren's syndrome. Both kinds of cysts are seen in large parotid glands with either inhomogeneous density or multiple cysts.[9] The parotid parenchyma is also denser than normal.

Ranulas, also termed mucoceles or mucous retention cysts of the floor of mouth, are of two varieties. The simple variety is usually due to obstruction of one of the minor salivary glands or obstruction of the sublingual gland. The plunging variety results from rupture of wall of a simple ranula. It may appear as a mass either in the submental or submandibular region. On CT scans it is usually a thin-walled, unilocular, well-defined, nonenhanced, cystic-appearing lesion.[10]

Lymphoma of the head and neck most frequently involves the cervical lymph node chain, the Waldeyer ring, and lymphoid tissue at the base of the tongue. Such lymphoma is most often non-Hodgkin[1].

The orbital-facial disfigurement and proptosis that occur with neurofibromatosis may be due to either one or a combination of disease processes that include orbital neoplasms, plexiform neurofibromatosis, orbital osseous dysplasia, and congenital glaucoma. CT is able to differentiate between these four entities and to demonstrate their full extent[11]. Plexiform neurofibromatosis appear as multiple masses or fusiform enlargements along the courses of the peripheral nerves.[12]

CONCLUSION

A diagnosis can often be made based on the appearance and location of these masses on CT. The vascular nature of a face and/or neck mass is shown on contrast CT by intense enhancement or the tubular appearance.

REFERENCES

1. Vazquez E, Enriquez G, Castellote A, et al. US, CT and MR Imaging of neck lesions in children. RadioGraphics 1995;15:105-122.
2. Goshen S, Ophir D. Cystic hygroma of the parotid gland. J Laryngol Otol 1993;107:-855-857.
3. Ricciardelli EJ, Richardson MA. Cervicofacial cystic hygroma: patterns of recurrence and management of the difficult case. Arch Otolaryngol Head Neck Surg 1991;117:546-553.
4. Stenson KM, Mischell J, Toriumi DM. Cystic hygroma of the parotid gland. Ann Otol Rhinol Laryngol 1991;100:518-520.
5. Mantravadi J, Roth LM, Kafrawy AH. Vascular neoplasms of the parotid gland. Oral Surg Oral Med Oral Pathol 1993;75:70-75.
6. Rossiter JL, Hendrix RA, Tom LWC, Potsic WP. Intramuscular hemangioma of the head and neck. Otolaryngol Head Neck Surg 1993;108:18-26.
7. Holliday RA, Cohen WA, Schinella RA, et al. Benign lymphoepithelial parotid cysts and hyperplastic cervical adenopathy in AIDS-risk patients: a new CT appearance. Radiology 1988;165:439-441.
8. Soberman N, Leonidas JC, Berdon WE, et al. Parotid enlargement in children seropositive for human immunodeficiency virus: imaging findings. AJR 1991;157:553-556.
9. Pollei SR, Harnsberger HR. The radiologic evaluation of the parotid space. Semin US CT MR 1990;11(6):486-503.

10. Som PM. Salivary glands. In: Som PM, Bergeron RT, eds. Head and Neck Imaging. 2nd ed. St. Louis: Mosby, 1991: 318-319.
11. Zimmerman RA, Bilaniuk LT, Metzger RA, Grossman RI, Schut L, Bruce DA. Computed tomography of orbital-facial neurofibromatosis. Radiology 1983;146:-113-116.
12. Bourgouin PM, Shepard JAO, Moore EH, McLoud TC. Plexiform neurofibromatosis of the mediastinum: CT appearance. AJR 1988;151:461-463.

US AND CT OF CAROLI DISEASE: REPORT OF TWO CASES

Pannee VISRUTARATNA[1], MD., Sukanya REUNGRONGRAT[1], MD., Lumdaun WONGSAWASDI[2], MD., Aumnart YOUSUKH[3], MD.

ABSTRACT

Caroli disease is a rare congenital disorder with multiple cystic dilatation of the intrahepatic bile ducts. We report two pediatric patients with cystic dilatation of intrahepatic bile ducts accompanying congenital hepatic fibrosis. CT scans of the liver showed tiny dots with strong contrast enhancement inside dilated intrahepatic bile ducts ("central dot signs"). These dot signs in CT scans corresponded to intraluminal portal veins in sonograms. Ultrasonography and CT scans are very effective noninvasive methods to diagnose this disease.

INTRODUCTION

Caroli disease is a disease of segmental nonobstructive dilatation of the intrahepatic bile ducts. It is a rare congenital abnormality, in which there can be many malformations of the hepatobiliary system. These range from isolated cystic dilatation alone of the intrahepatic bile ducts to hepatic fibrosis with cystic dilatation of the intrahepatic bile ducts.[1] We describe two children with the latter.

CASE REPORTS

Case 1.- A 10-month-old girl had fever, anemia, and a distended abdomen. Her temperature was 39°C. On palpation, the liver was enlarged. Laboratory studies showed a hemoglobin concentration of 9.3 g/dL, a white blood cell count of 11,900, and an alkaline phosphatase of 386 IU/L (normal 23-98). Creatinine was normal. Abdominal ultrasonograms showed hepatomegaly and saccular dilatation of the intrahepatic bile ducts (Fig. 1A). Increased echogenicity of the renal parenchyma of both kidneys was also noted. Abdominal CT scans showed hepatomegaly. Saccular dilatation of intrahepatic bile ducts, more severe in the right hepatic lobe, was seen. Central dot signs and bridge formation across the dilated lumina of bile ducts were seen (Fig. 1B). A slightly increased density of the renal medullas in noncontrast CT scans and striation of the renal medullas in contrast CT scans were seen (Fig. 1C). Due to persistent cholangitis, the patient underwent hepatectomy of the right lobe, after which the fever subsided. The pathological specimen showed saccular dilatation of intrahepatic bile ducts consistent with Caroli disease, active cholangitis, and congenital hepatic fibrosis. A microscopic study showed portal radicles surrounded by dilated bile ducts (Fig. 1D).

Case 2.- A 6-year-old boy had had a distended abdomen for 5 years. Physical examination revealed hepatomegaly, ascites, and dilatation of the superficial veins of the abdomen. Laboratory studies showed a hemoglobin concentration of 5.6 g/dL, a white blood cell count

[1] Department of Radiology,
[2] Department of Pediatrics,
[3] Department of Pathology, Faculty of Medicine, Chiang Mai University, Chiang Mai 50200, Thailand.

of 9,000, and an alkaline phosphatase of 188 IU/L (normal 23-98). Creatinine was normal. Abdominal ultrasonograms showed hepatomegaly, saccular dilatation of the intrahepatic bile ducts, intraluminal portal vein (Fig. 2A), increased echogenicity of the renal parenchyma of both kidneys, and splenomegaly. Abdominal CT scans showed hepatosplenomegaly and saccular dilatation of intrahepatic bile ducts, more severe in the right lobe (Fig. 2B). Central dot signs and bridge formation across the dilated lumina of bile ducts were seen. A slightly increased density of the renal medullas in noncontrast CT scans and striation of the renal medullas in contrast CT scans were seen (Fig. 2C). This patient did not undergo surgery, because he did not have persistent cholangitis or any other complications, except for portal hypertension.

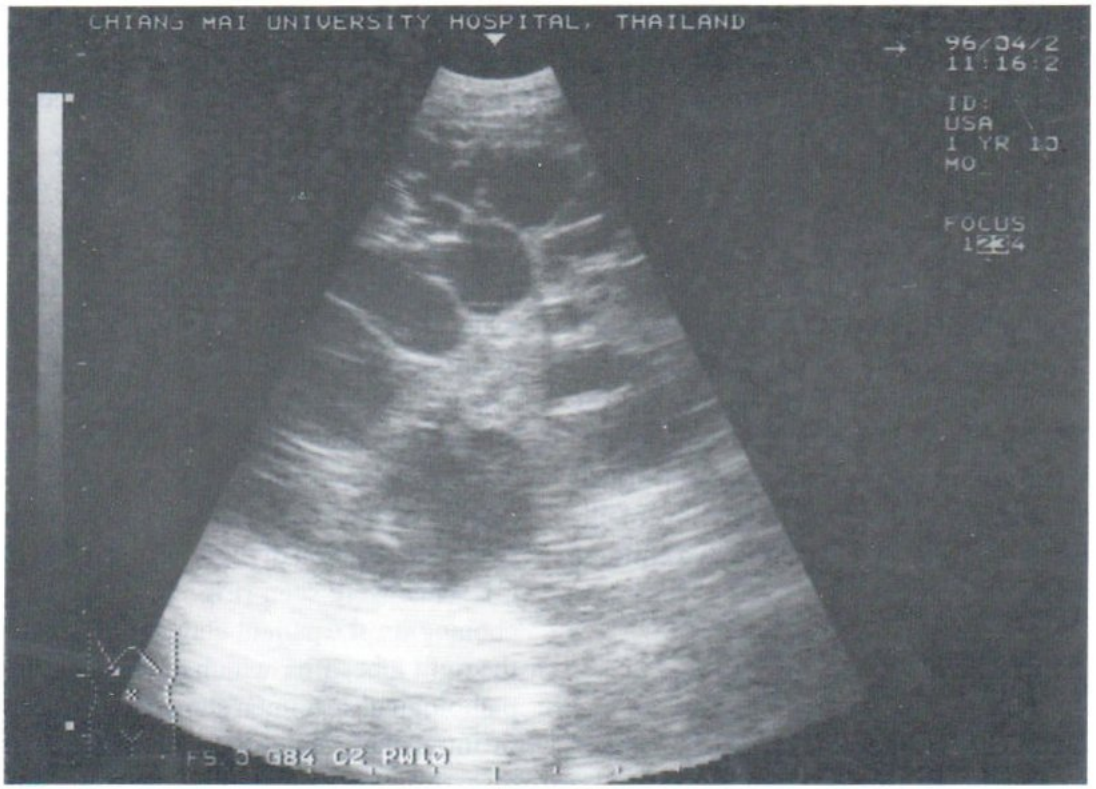

Fig. 1 Case 1
Fig. 1A Oblique sonogram of the liver shows saccular dilatations of the intrahepatic bile ducts.

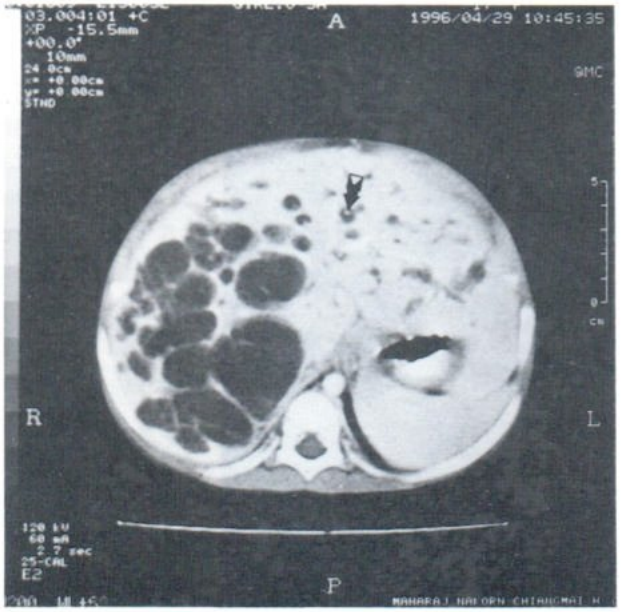

Fig. 1B Contrast CT scan shows saccular dilatation of the intrahepatic bile ducts. Several tiny dots are seen in dilated bile ducts (arrow). Bridge formation (multiple septa) across the dilated bile ducts are seen in right hepatic lobe.

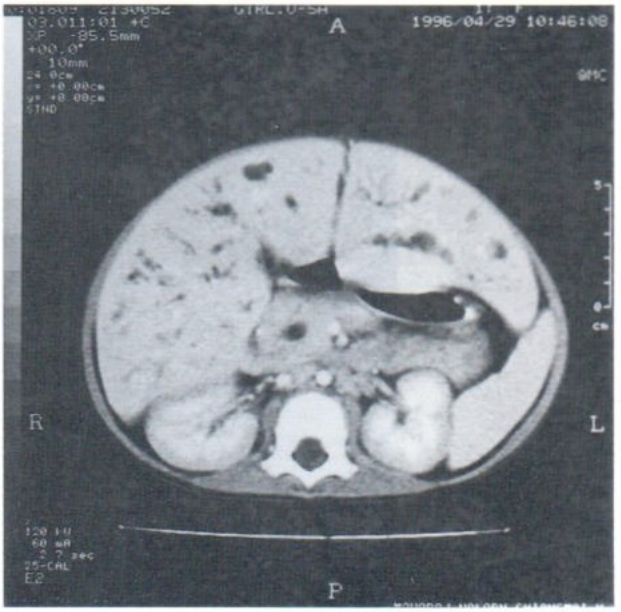

Fig. 1C Contrast CT scan shows striation of the renal medullas in both kidneys, hepatomegaly, saccular dilatation of intrahepatic ducts, and mild dilatation of the common bile duct.

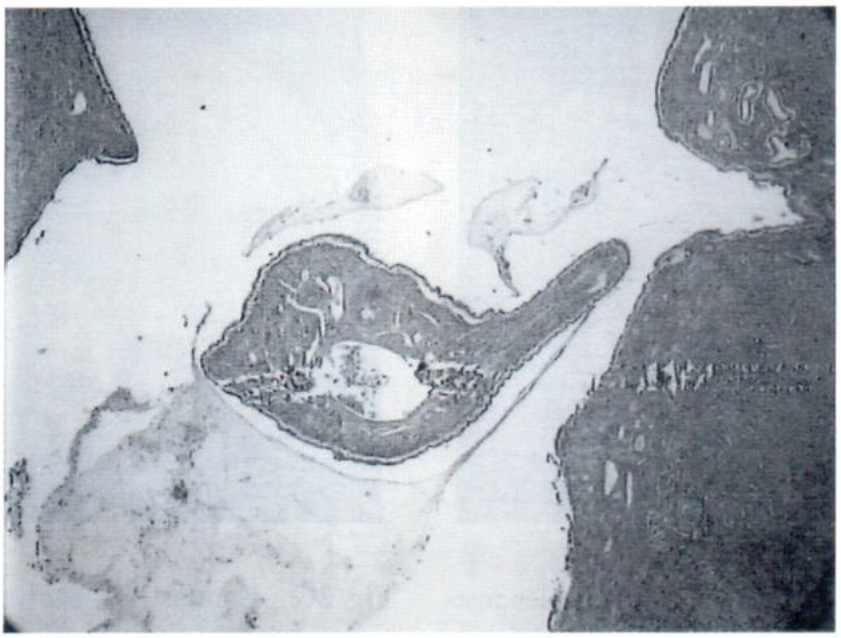

Fig. 1D Microscopic study (X40) of the liver shows dilated bile ducts surrounding a portal radicle.

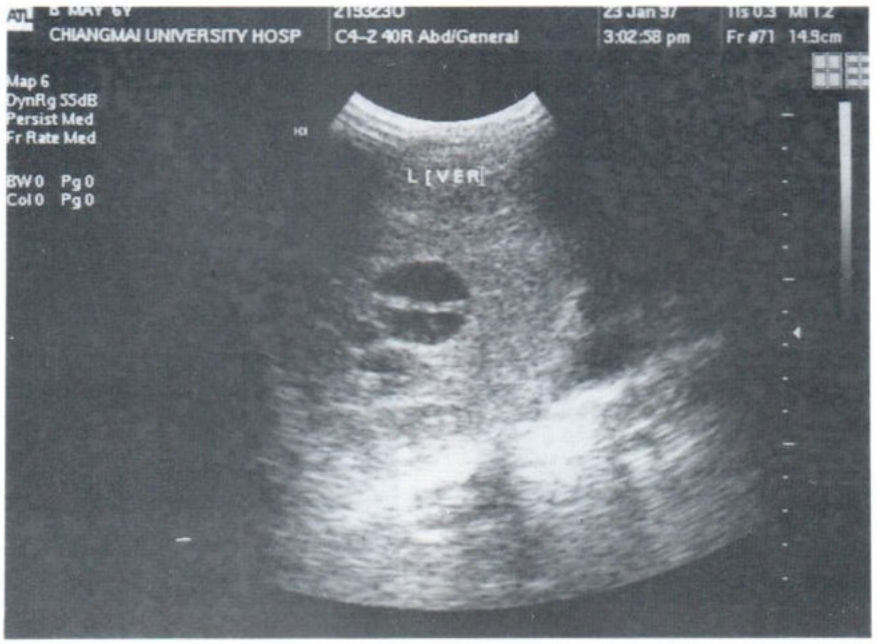

Fig. 2 Case 2

Fig. 2A Transverse sonogram of the liver shows intraluminal portal vein.

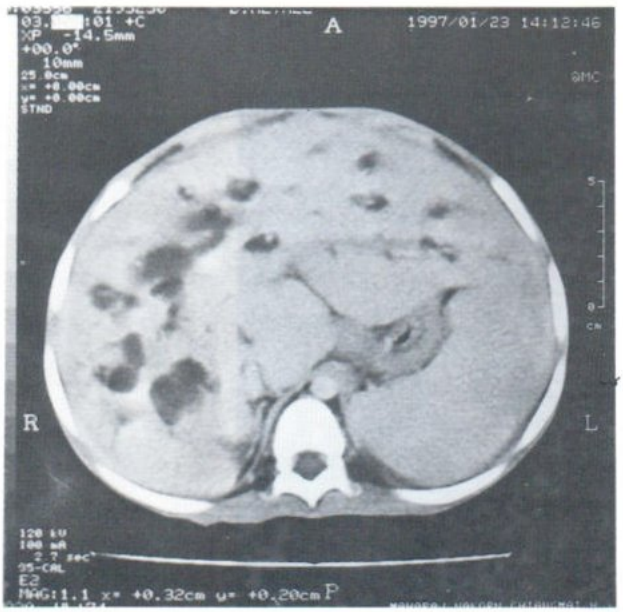

Fig. 2B Contrast CT shows hepatosplenomegaly and saccular dilatation of the intrahepatic bile ducts.

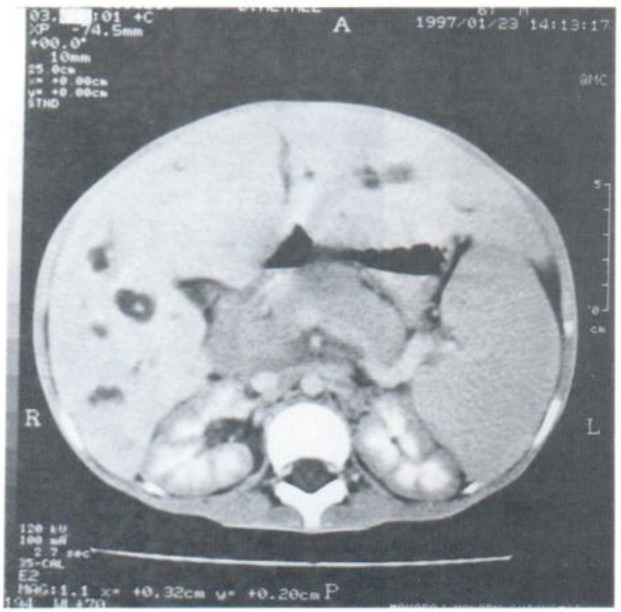

Fig. 2C Contrast CT shows hepatosplenomegaly, saccular dilatation of the intrahepatic bile ducts, central dot sign, and striation of renal medullas of both kidneys.

DISCUSSION

In Caroli disease there are congenital bile duct cysts classified as type V in Todani's system.[2] Although this disease is present from birth, most patients usually seek medical assistance for chronic recurrent upper abdominal pain or recurrent cholangitis as children or young adults. Caroli disease is associated with intrahepatic biliary calculi, hepatic abscesses, cholangiocarcinoma, hepatic fibrosis or cirrhosis.[3] There is also an association with benign renal tubular ectasia and renal cysts.[4] Patients with associated hepatic fibrosis may develop portal hypertension, while those with no hepatic fibrosis do not. Our first patient did not have portal hypertension but did have hepatic fibrosis, which was confirmed by histopathological examination. The second one had splenomegaly and dilatation of abdominal superficial veins consistent with portal hypertension. This is consistent with hepatic fibrosis although this could not be confirmed since there was no surgery. Both had evidence of tubular ectasia of the kidneys on US and CT, but the patients did not have renal biopsies. Both had normal creatinine levels.

Noninvasive imaging methods for Caroli disease are ultrasonography (US), computed tomography (CT), and nuclear scintigraphy. Invasive imaging methods for Caroli disease are endoscopic retrograde cholangiopancreatography (ERCP) and percutaneous transhepatic cholangiography (PTC). Nuclear scintigraphy, ERCP, and PTC cannot demonstrate associated abnormalities outside the biliary tract such as renal abnormalities, while US and CT can.

US and CT have been shown to be useful in detecting segmental dilatation of intrahepatic bile ducts. Marchal et al.[5] described sonographic features of Caroli disease in three patients. Besides the well-known characteristic of nonobstructive segmental dilatation of the bile ducts, they also observed portal radicles that were partially or completely surrounded by dilated bile ducts. There were similar findings in the histopathological examination of the liver of our first case and in the ultrasonogram of our second case.

Choi et al.[6] reported two adults with Caroli disease with CT scans having portal radicles surrounded by dilated intrahepatic bile ducts (the central dot sign). There were tiny dots in dilated intrahepatic bile ducts in CT scans, which enhanced strongly. These dots were not in the dependent portion of the dilated bile ducts. These intraluminal dots in CT scans corresponded to intraluminal portal veins in sonograms, which indicated that the portal radicles were surrounded by dilated bile ducts. The portal radicles were so completely enveloped by abnormal bile ducts that they appeared to lie within the lumina of the bile ducts. Bridge formation across dilated intrahepatic ducts resembling internal septa in intrahepatic ducts was also seen. This is consistent with walls of insufficiently resorbed, malformed ductal plates that surround the portal radicles.

The central dot sign was also reported in a patient with periductal cysts;[7] however the cysts did not communicate with the dilated ducts, which excluded Caroli disease.

CONCLUSION

Our cases demonstrate that US and CT scans are good noninvasive imaging methods for revealing the abnormalities of the hepatobiliary system and other organs in patients with Caroli disease. The abnormalities seen in both methods correlated well with the pathological specimens.

REFERENCES

1. Barros JL, Polo JR, Sanabia J, Garcia-Sabrido L, Gomez-Lorenzo FJ. Congenital cystic dilatation of the intrahepatic bile ducts (Caroli's disease): report of a case and review of the literature. Surgery 1979;85-(5):589-592.

2. Todani T, Watanabe Y, Narusue M, Tabuchi K, Okajima K. Congenital bile duct cysts: classification, operative procedures, and review of thirty-seven cases including cancer arising from choledochal cyst. Am J Surg 1977;134:263-269.
3. Rizzo RJ, Szucs RA, Turner MA. Congenital abnormalities of the pancreas and biliary tree in adults. RadioGraphics 1995;-15:49-68.
4. Mall JC. Ghahremani GG, Boyer JL. Caroli's disease associated with congenital hepatic fibrosis and renal tubular ectasia. Gastroenterology 1974;66:1029-1035.
5. Marchal GJ, Desmet VJ, Proesmans WC, et al. Caroli Disease: high-frequency US and pathologic findings. Radiology 1986;158:-507-511.
6. Choi BI, Yeon KM, Kim SH, Han MC. Caroli disease: central dot sign in CT. Radiology 1990;174:161-163.
7. Herman TE, Siegel MJ. Central dot sign on CT of liver cysts. J Comput Assist Tomogr 1990;14(6):1019-1021.

HEPATIC PSEUDOTUMOURS IN A PATIENT WITH IVEMARK SYNDROME - A CASE REPORT

ABU BAKAR, ABDULLAH BJJ, KUMAR G

ABSTRACT

Cardiac failure secondary to hepatic venous congestion is the predominant cause of mortality as cases of asplenia associated with cyanotic heart disease may present with hepatomegaly. C.T. imaging; may give, the appearance of 'Pseudotumours' secondary to hepatic venous congestion. We presents case of Ivemark syndrome with multiple hypodense areas in the liver as a recognised case of pseudotumour secondary to hepatic venous congestion. This entity should be recognised to avoid pitfall in the diagnosis of this condition and to avoid unnecessary cost and morbidity.

INTRODUCTION

Computed tomography (CT) has a remarkable capacity for evaluating the liver. It is clinically a valuable tool and is useful imaging modality in determining presence and the extent of mass lesions in the liver. CT has a high degree of specificity in the diagnosis of hepatic masses,[2] however there remains a variety of conditions which may mimic neoplastic changes and present as 'pseudotumour' appearance on contrasted CT scan imaging of the liver and if these condition is not recognised, it may caused a pitfall in the diagnosis of liver masses. We would like to illustrate a case of Ivemark Syndrome as one of the recognised cause of hepatomegaly resulting in hepatic pseudotumour, and emphasised the importance of recognising this condition to avoid an unnecessary mismanagement in the diagnosis of liver masses.

CASE REPORT

A 2 year child with known complex cyanotic heart disease with dextrocardia, primary atrio-septal defect, double outlet right ventricle, single atrio-ventricular valve and pulmonary stenosis presented with facial puffiness following an upper respiratory tract infection. On examination the child was cyanosed with facial puffiness, and also pitting oedema of the lower limbs. There was dextrocardia, cardiomegaly, hepatomegaly and ascites. A clinical diagnosis of nephrotic syndrome in child with cyanotic heart disease was made. However in view of the hepatomegaly a CT of the abdomen performed. This confirmed hepatomegaly and dextrocardia. The hepatomegaly occupied the entire right and left hypochondria and was of homogenous density pre-contrast. Post-intravenous iodinated contrast medium showed multiple low attenuation areas within both lobes of the liver (Figure 1). The spleen was absent with the stomach fundus on the right side. A diagnosis of multiple liver lesions possibly tumour deposits was made. The differential diagnosis of perfusion defects secondary to venous congestion was also considered. An ultrasound done subsequently showed a homogenous echo-pattern with no focal

Department of Radiology, University of Malaya Medical Center, 50603 Kuala Lumpur, MALAYSIA

Address correspondence to:
BJJ Abdullah, Department of Radiology, University of Malaya Medical Center, 50603 Kuala Lumpur, MALAYSIA
Tel no. 03-7502069, Fax no. 603-7581973

lesions within the liver. the hepatic veins and the intrahepatic IVC were dilated (Fig. 2) suggesting right heart failure. In the peripheral blood film Howell Jolly bodies were present. The a-foeto-protein was normal. The patient was treated with antifailure medication, steroids for the nephritis and penicillin for the asplenia. The patient responded and was discharged. On further follow up, there is no increase in size of hepatomegaly.

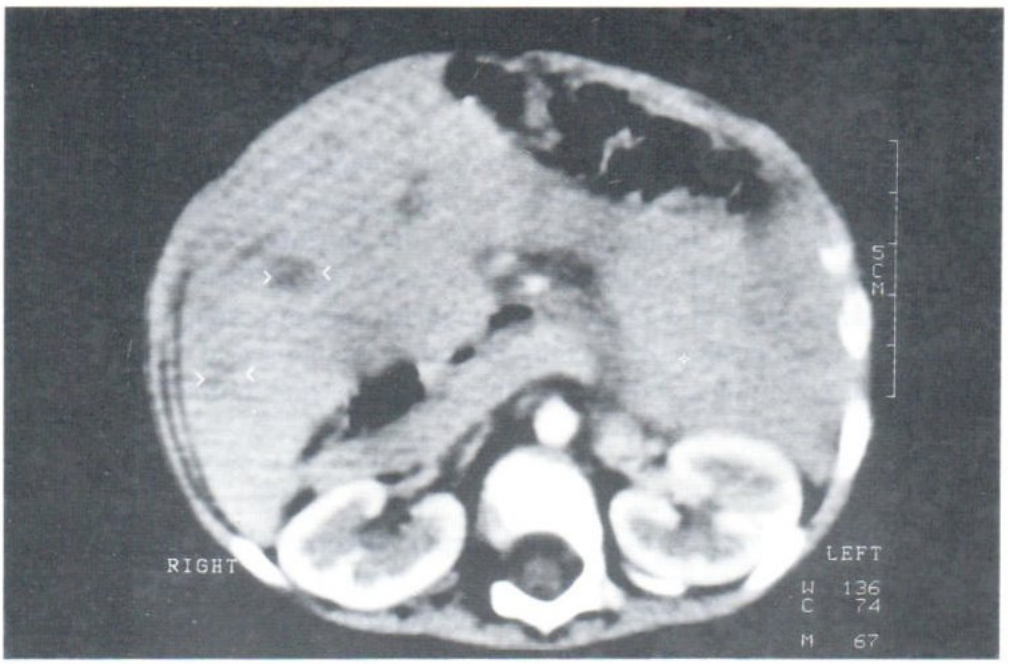

Fig 1. Axial CT scan of the abdomen after IV contrast enhancement shows hepatomegaly with multiple hypodense areas within the liver (arrowheads).

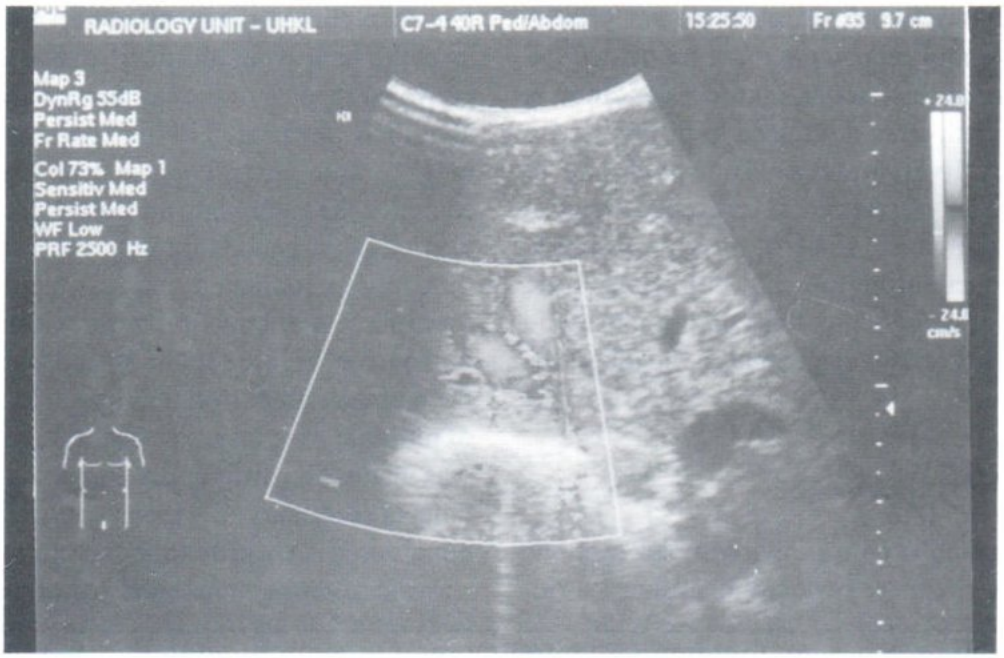

Fig 2. Doppler Ultrasound of the liver shows flow within the hepatic veins which are dilated but patent. The liver is of homogenous echogenicity.

DISCUSSION

CT is excellent at the demonstration of lesions in the liver.[2] In addition this modality is cheaper and more readily available than MRI and allows better access to the patient although the use of ionising radiation is a drawback. The diagnosis of liver masses with CT depend on the differential attenuation and enhancement pattern. The sensitivity of CT in defining the tumour is well established. There however remain several conditions that may mimic tumour giving rise to 'Pseudotumour' appearance. If these pitfalls are not recognised it may lead to an increase patient morbidity in term of unnecessary longer hospitalisation, extra investigation and even intervention such as biopsy or surgery.

Ivemark syndrome was first described in 1955[3] and is characterised by asplenia, malformation of conotruncus of the heart and abnormal lobulation of the lung. Abnormalities of the conotruncus of the heart include transposition of great artery in 72% of the cases and also pulmonary venous drainage in 72%. Death occurs in 79% of the cases in the first year of life due to cardiac failure and anoxia.[3,4,5] Cardiac failure occurring in this patient may cause a hepatic venous congestion and obstruction due to egress of blood from hepatic vein to the right heart. There is no associated increase risk of hepatic tumour in these patients. Multiple low attenuation areas within an enlarged liver in the patient presented raised the possibility of pseudotumour and the ultrasound of abdomen revealed dilated IVC and hepatic veins. In our patient although no biopsy was done to confirm the diagnosis, the clinical correlation of the clinical problem, and the correct choice of imaging modality plus the recognition of hepatic 'pseudotumour' has helped in making the correct diagnosis. In addition there was no progression of the hepatomegaly.

Recent report by Kane et al[1] illustrates multiple causes of hepatic pseudotumour appearance in children. These pseudotumours may result from chronic liver diseases such as cirrhosis and also fatty infiltration secondary to various conditions. In Tyrosinemia Type I also known as hepatorenal tyrosinemia in which there is a deficiency of fumaryl acetoacetate hydrolase. Accumulation of fumaryl and malelylacetate within the liver results in liver failure and cirrhosis which on CT gives rise to the appearance of multiple nodules with high or low density.

Other recognised causes of pseudotumour include Neimann Pick disease, Gaucher disease, Alpha I Anti Trypsin and also fatty infiltration secondary to alcoholic liver disease. In Neiman Pick disease the appearance of multiple low attenuation lesion in the liver is secondary to the accumulation of complex lipid, while in Gaucher disease it is secondary to accumulation of glucocerebroside. In alcoholic liver disease fatty in filtration may be diffuse or focal areas of low attenuation within the liver.

There have been no reported cases of hepatic venous congestion secondary to cardiac failure that have produced a pseudotumour appearance. The causes of hepatomegaly with multiple low attenuation areas include necrotic metastases, abscesses and other cystic masses.[6] In hepatic abscesses, the clinical history and pattern of rim enhancement may help in differentiating it from other cause of pseudotumour while the CT value may help in the differentiating from cystic liver disease.[7] In addition the correlation with other imaging modalities like ultrasound or MRI has help differentiate this from pseudotumour as was in the case presented. MRI with its multiplanar capability, higher soft tissue contrast resolution and pattern of enhancement is another modality that may be helpful in differentiation of various causes of focal hepatic masses and may also be able to differentiate them from pseudotumour.[8]

In summary, the presence of low attenuation lesions on the post intravenous contrast

enhancement CT scan of the liver may not always be real and that the pseudotumour has to be considered in the case presenting with congestive cardiac failure, where the clinical problem, symptoms, signs and ultrasonography have been helpful in making the correct diagnosis of a pseudotumour. This pitfall must be recognised to avoid unnecessary cost in further investigation and morbidity from inappropriate treatment.

REFERENCES.

1. Kane PA, Meili Vergani G, William R, Karani JB. Pseudotumour of hepatic imaging. Clinical Radiology 1995;51:362-365
2. Levitt RG, Sagel SS, Stanley RJ, Jost RG. Accuracy of computed tomography of the liver and biliary tract. Radiology 1977;124:-123-128.
3. Rose V, Iukawa T, Moes CAF. Syndrome of Asplenia and Polysplenia: A review of cardiac and non cardiac malformation in 60 cases with special reference to the diagnosis and prognosis. British Heart Journal 1975;-37: 840- 852
4. Winer-Muram HT, Tonkin LD. The Spectrum of heterotaxic syndrome. Cardio-pulmonary Imaging, Radiol Clin North Am1989;27:No 6
5. Swischuk L.E. Radiology of Newborn and Young Infant. 2nd Edition Cardiac Mal-formation pp 288-293.
6. Mulhern CB. Arger PH, Coleman BG, Stein GN. Nonuniform Attenuation in Computed Tomography Study in the Cirrhotic Liver. Radiology 1979;132:399-402.
7. Barnes PA, Thomas JL, Benardino ME. Pitfall in the diagnosis of Hepatic cyst by Computed Tomography. Radiology 1981;-141:129-133.
8. Ito K, Yoshimizu T, Nakanishi. T. Case Report: Pseudoglandular Hepatocellular carcinoma: Discrepancy between CT and MR findings. Clinical Radiology 1996;-51:379-381.

RADIOGRAPHIC FINDINGS IN 35 CASES OF PULMONARY INFECTION CAUSED BY RHODOCOCCUS EQUI[3]

Angsana NIMMONRAT,M.D.[1], Wittanee NA CHIANG MAI,M.D.[1], Sanan SIMARAK,M.D.[1], Thira SIRISANTHANA,M.D.[2], Malai MUTTARAK,M.D.[1]

ABSTRACT

Rhodococcus equi(Corynebacterium equi) is able to produce infections not only in animals but also in human being usually in immunosuppressed one. We report 35 cases of pulmonary infection with this organism mainly in patients infected with the human immunodeficiency virus (HIV) and this is the biggest series ever reported.

The most common pulmonary manifestations including area of opacity with cavity 48.72%, area of opacity without cavity 28.21%, other findings were mass with or without cavity, nodule and interstitial infiltration. The lesions involved the lower lobe in 55.26% while the upper lobe involvement was 42.11%. Multiple sites of involvement was noted in 11.43%. Pleural effusion encountered in 22.86%. Pericardial effusion and endobronchial lesion were noted in one and two cases respectively.

The course of the disease usually subacute with symptoms of fever, cough, chest pain and hemoptysis of various duration from 1 to12 weeks.

Rhodococcus equi infection should always be considered in the differential diagnosis of a HIV infected patient with cavitary pneumonia.

Key words: Rhodococcus equi, pulmonary infection, HIV

INTRODUCTION

Rhodococcus equi is a known cause of pulmonary infection in foals, calves and swines. It was orginally isolated as Corynebacterium equi in 1923 from foals with pneumonia and has been reclassified in the genus Rhodococcus since 1980. Microscopically,it is an aerobic,gram positive, weakly acid fast,non motile, non spore forming, pleomorphic coccobacillus. Rhodococcus equi is named for its production of red pigment.[1]

Rhodococcus equi has been a rare cause of disease in human. Golub et al[2] reported the first human case caused by this organism in 1967, but after exploding of the HIV infection, there is rising in number of disease caused by R.equi. We report the radiographic features of 35 cases of pulmonary R.equi infection.

[1] Department of Radiology,
[2] Department of Medicine, Faculty of Medicine, Chiang Mai University, Chiang Mai 50200
[3] Winning paper of bracco international award in the 9th AAR congress Singapore, 23-26 Jan. 1997.

MATERIALS AND METHODS

35 cases diagnosed at Chiang Mai University Hospital as pulmonary infection caused by R.equi during the period of April 1993 through September 1996 were reviewed for the radiographic findings. All had culture identification of R.equi from either sputum, blood, bronchial washing, pleural fluid or direct tissue tapping. Patients with concurrent pulmonary infection caused by other organisms were excluded.

RESULT

All 35 patients were immunocompromised hosts,33 were infected with HIV, one was a case of SLE on steriod treatment, another one was a late case of Hodgkin's disease. There were all male except one SLE patient. The age ranged from 20 to 69 years with the median age of 44 years. The cultures were taken from many sources,most were from sputum (80%), while others were from blood (28.6%), bronchial washing (8.6%) pleural fluid (5.7%) and direct tissue tapping (2.8%). Multiple sources were obtained in 22.85%. The common presenting symptoms were cough (90%) and fever (80%) followed by chest pain (53%) and hemoptysis (25%). The duration of symptoms range from 1 to 12 weeks.

The initial chest film findings of 39 lesions in 35 patients (table 1) were area of opacity with cavity (fig.1) 19 lesions (48.72%), area of opacity without cavity (fig.2) 11 lesions (28.21%), mass with cavity (fig.3) 5 lesions (12.82%), mass without cavity (fig.4) 2 lesions (5.13%), nodule 1 lesion (2.56%) and interstitial infiltration (fig.5) 1 lesion (2.56%).

Of 38 lesions, excluding the interstitial one, there were 18 lesions in the right lung (6 RUL,1 RML,11 RLL) and 20 lesions in the left lung (7 LUL,3 lingular,10 LLL). Bilateral simul-taneous lesions were found in 4 patients.

The associated findings were pleural effusion, 6 patients were found unilaterally (2Rt ,4 Lt) and bilaterally in 2 patients. Pericardial effusion and endobronchial lesion were noted in 1 and 2 patients respectively.

Follow up chest film were able to obtain in 24 patients ranged from few days to 6 months time and found rapid progression (change in days to weeks) 10 patients (42%),slow progression (change in months) 7 patients, no change 2 patients and improvement 5 patients which 4 patients had cystic change (fig.6).

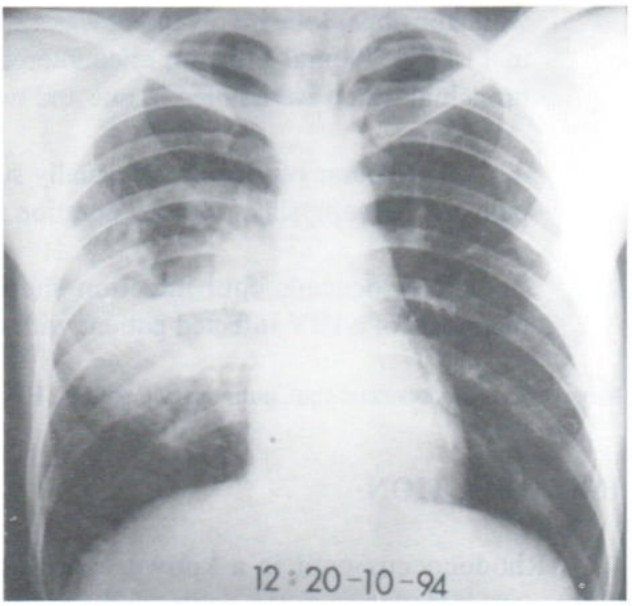

Fig 1: Chest film showing an area of opacity with cavity in the right lower lobe.

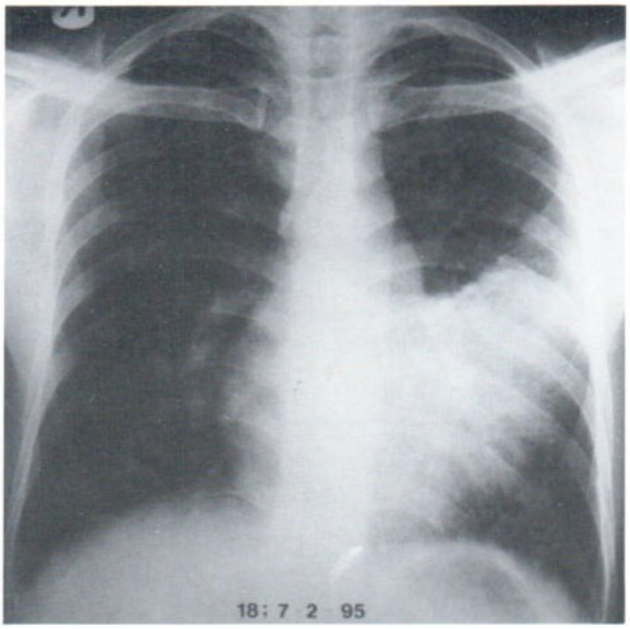

Fig 2: Chest film showing an area of opacity in lingular segment of the left upper lobe.

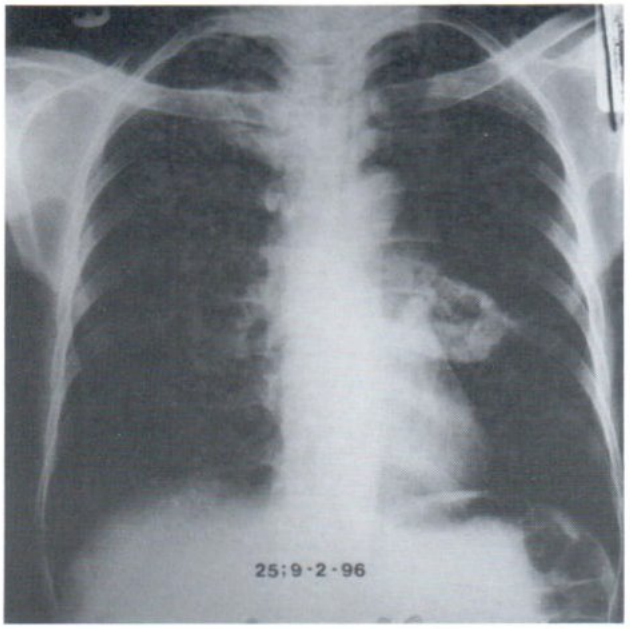

Fig 3: Single cavitary mass was noted in the left lower lobe.

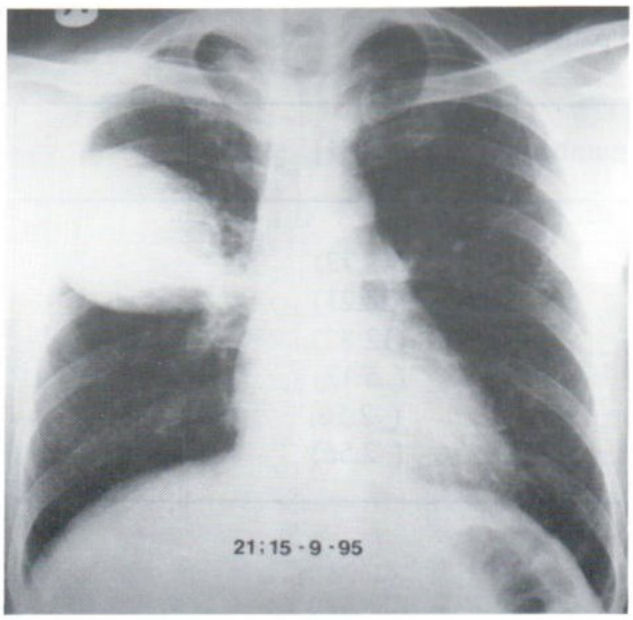

Fig 4: A big homogenous mass was noted in the right upper lobe.

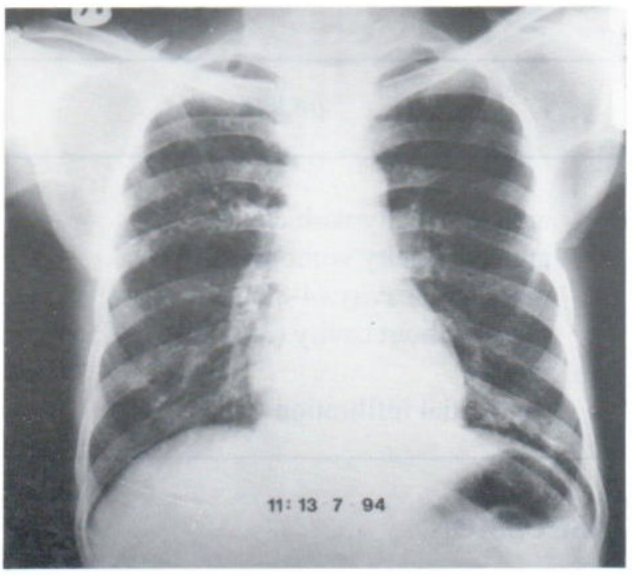

Fig 5: Chest film showing bilateral interstitial infiltration.

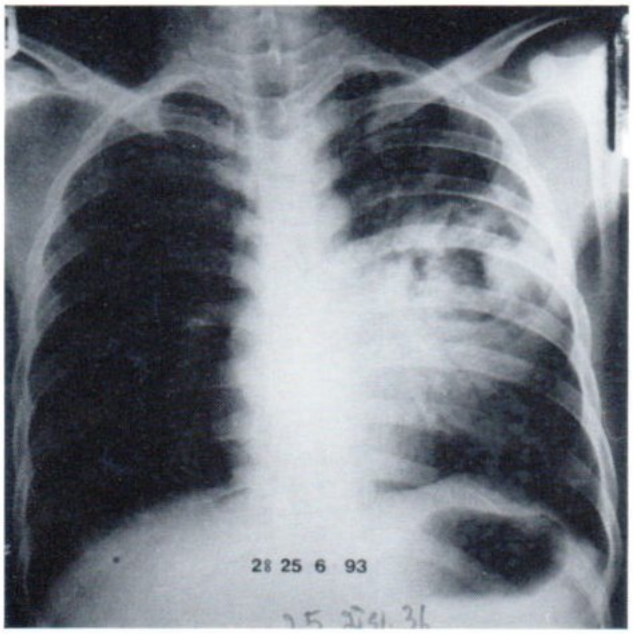

Fig 6a: The initial chest film showed an area of opacity with cavity in the left upper lobe.

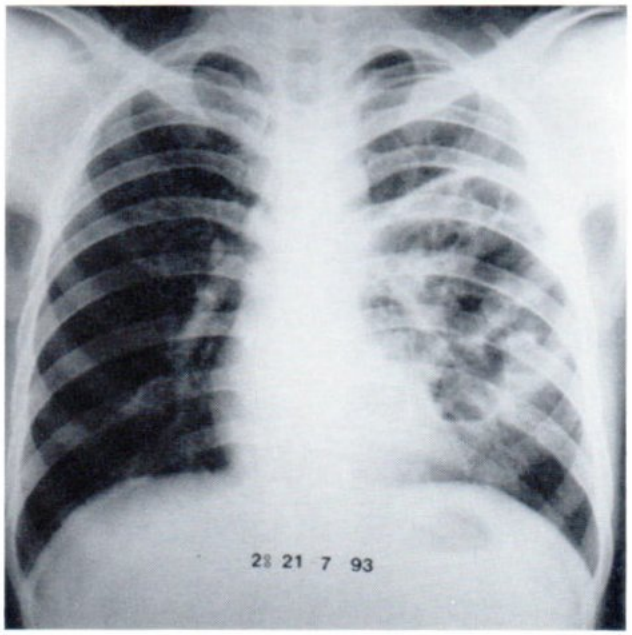

Fig 6b: The follow up film demonstrated multiple thin wall cystic replacement.

Table 1: Initial chest film findings in 39 lesions(35 patients)

pattern	number of lesion(s) [%]	
area of opacity with cavity	19	(48.72)
area of opacity without cavity	11	(28.21)
mass with cavity (4-8 cm)	5	(12.82)
mass without cavity (3-8 cm)	2	(5.13)
nodule	1	(2.56)
interstitial infiltration	1	(2.56)

DISCUSSION

Pulmonary infection is the most common form of human disease caused by Rhodococcus equi.[1] Extrapulmonary infections are rare and have been reported in central nervous system, skin, lymph nodes, bone, soft tissue and liver.[1,3,4,5] Most of the infected patients are immunocompromised host particularly in HIV infected patients,others include leukemia, lymphoma and renal transplantation.[3,6,7,8]

The typical presenting symptoms are cough,high fever, prominent fatigue, weight loss, chest pain and usually with subacute onset. Hemoptysis can also be occured.[1]

The most common radiographic finding in our study is the area of opacity with cavity which comprises about 48.72% and corresponding well to the other series that cavitary pneumonia is the most common pattern.[6,9-17] There is no predilection for the site of the lung lesion and pleural effusion is found mainly associated with the lower lobe lesion on the same side. No mediastinal lymphadenopathy is present in our series.

Rhodococcus equi is a gram positive facultative intracellular bacterium and its ability to persist in and eventually to destroy the macrophage is the basis of its pathogenicity. Clearing of this organism from lung requires functional CD4+Tcell, hence the HIV infected individual is prone to have increase incidence of severe Rhodococcus equi pneumonia.[1,18,19] Failure to clear pulmonary R.equi infection leads to development of granuloma and progressive loss of lung parenchyma to necrotizing cavitated lung.[1,19] Radiographic pictures then are shown as area of opacity or lung mass with cavity. 42% of our study had rapid progression which somehow might reflect the host immune status.

Pathologic change elicited by R.equi resembles that of other members of the Corynebacterium, Mycobacterium and Nocardia group which share lipid-rich cell wall component.[1] Thus differential diagnosis from radiographic view point should include pulmonary tuberculosis, nocardia and fungal infection.

Management requires a prolong course of antibiotics for a minimum of 2 months due to frequency of relapse following shorter courses.[1] Many reports stated its susceptibility to erythromycin, rifampin, ciprofloxacin, aminoglycosides and glycopeptides.[1,3,18,20] The most commonly used antibiotic regimen was the combination of erythromycin and rifampin.[20]

CONCLUSION

Opacity or mass with cavity is the most common radiographic feature of pulmonary R.equi infection. The associated finding of pleural effusion is mainly occurs in the ipsilateral lower lobe lesion.

We propose that in the HIV infected patient who present with a cavitary pneumonia of subacute onset, Rhodococcus equi pneumonia should be of consideration in addition to nocardia, mycobacterium and fungal infection.

REFERENCES

1. Thomas D Verville et al.Rhodococcus equi infections of human:12 cases and a review of the literature.Medicine 1994,Vol 73, No 3:119-132
2. Golub B, Falk G et al. Lung abscess due to Corynebacterium equi:Report of first human infection. Ann Intern Med 1967,66:1174-7
3. Linda L, Van Etta et al. Corynebacterium equi: A review of 12 cases of human infection. Review of Infectious Disease, Vol 5,No 6,Nov-Dec 1983:1012-1018.
4. J Fierer et al.Non-pulmonary Rhodococcus equi infection in patients with AIDS J Clin Pathol 1987;40:556-558
5. Patricia L, De Marais et al. Rhodococcus meningitis in an immunocompetent host Clinical Infectious Disease 1995;20;167-9
6. Upton D Allen, Anne Niec et al. Rhodococcus equi pneumonia in a child with leukemia. The Pediatric Infectious Disease Journal, Vol 8,No 9,Sep:656-657
7. Susan E Gardner, Ted Pearson et al. Pneumonitis due to Corynebacterium equi. CHEST;70:1,July,1976:92-94.
8. M Verginia, M Stolk-Engelaar et al. Disseminated abscess caused by Rhodococcus equi in a patient with chronic lymphocytic leukemia. Clinical infectious disease 1995;-20:478-9.
9. Bill C Frame, Alan F Petkus. Rhodococcus equi pneumonia: case report and literature review. The Annals of Pharmacotherapy, 1993,Nov,27,1340-1342

10. John H Samie, Bruce N Hathaway et al. Lung abscess due to Corynebacterium equi. The American Journal of Medicine,Vol 80, April 1986:685-688
11. Jordan S Weingartar, David Y Hung et al. Rhodococcus equi pneumonia, an unusual early manifestation of the acquired immunodeficiency syndrome (AIDS). CHEST Vol 94,No 1,July 1988:195-196
12. Janet M Shapiro et al. Rhodococcus equi endobronchial mass with lung abscess in a patient with AIDS.Thorax 1992:47:62-63
13. M Sasal J et al.Good response to antibiotic treatment of lung infection due to Rhodococcus equi in a patient infected with human immunodeficiency virus.Clinical Infectious Disease 1992:15:747-8
14. Dariln V Moyer,Arnold S Bayer.Progressive pulmonary infiltrates and positive blood culture for weakly acid-fast, gram-positive rods in a 76-old woman. CHEST;104,1,July 1993:259-261
15. Sonia Arduino, Hugo Villar et al. Combination antibiotic treatment with Clarithromycin for human immunodeficiency virus-associated Rhodococcus equi infection. Clinical Infectious Disease, 1993;17:513-514
16. Spinello Antinori et al (letter).Rhodococcus equi pneumonia in a patient with AIDS: radiographic features. AJR;161, Oct 1993:-901-2
17. Kun Y Kwon, Thomas V Colby. Rhodococcus equi pneumonia and pulmonary malakoplakia in acquired immunodeficiency syndrome. Arch Pathol Lab Med, Vol 118, July 1994:744-748
18. Margie A Scott et al.Rhodococcus equi-an incresingly recognized opportunistic pathogen, report of 12 cases and review of 65 cases in the literature. Am J Clin Pathol 1995:103:649-655
19. Suzanne T Kanaly et al.Cytikine modulation alters pulmonary clearance of Rhodococcus equi and development of granulomatous pneumonia. Infection and Immunity, Aug 1995,Vol 63,No 8:3037-3041
20. Thira Sirisanthana, Khuanchai Supparatpinyo. Pulmonary infection caused by Rhodococcus equi in patients with human immunodeficiency virus infection: report of 23 cases from Chiang Mai. J Infect Dis Antimicrob Agent 1996;13:95-9

ANKYLOSING SPONDYLITIS : VALUES OF MR IMAGING

Suphaneewan JAOVISIDHA MD[1], Pimjai SIRIWONGPAIRAT MD[1], Chathchai POOKARNJANAMORAKOT MD[2], Patchrin PEKANAN MD[1].

ABSTRACT

Two cases with ankylosing spondylitis (AS) whose MR imaging proved very helpful were reported. The first case presented with hip pain, and MR imaging was requested to clarify abnormal scintigraphic findings at femoral head-neck regions. MR imaging disclosed extensive synovitis corresponding to the known AS as well as bone marrow edema of femoral heads and necks which was an early sign of avascular necrosis (AVN). Core decompression was performed with dramatic relief of symptom . The second case had a long-standing AS, and subsequently developed colorectal carcinoma which was treated by A-P resection. He presented with back pain, abnormal spine radiographs and abnormal bone scintigram. MR imaging revealed spondylitic process and helped exclude metastasis.

INTRODUCTION

Ankylosing spondylitis (AS) is a systemic rheumatologic disorder of adults that results in disease-specific inflammation and eventual ossification at the site of ligamentous insertion . The onset of AS generally occurs between the ages of 15 and 35 years (average 26-27 years) in both men and women, although an earlier onset has been noted in some female patients.[1] Magnetic resonance (MR) imaging, due to its superior soft tissue contrast, provides important information regarding disease activity and helps differentiating AS from other disease process. We reported two cases of AS patients whose MR imaging was proved very helpful.

CASE 1

A 49-year-old single female patient, known case of AS for 10 years and receiving steroid intermittently,came to the hospital because of bilateral hip pain. She also had neck pain in the morning, but to a lesser degree. She had past history of right knee pain and straw color fluid was obtained from this joint. She had had ankle and heel pain as well. Her peripheral joints were symptom-free at the time of this presentation.

Physical examination revealed limited range of motion of back and neck. She had severe hip pain bilaterally, particularly while changing position. Her chest, abdomen, and other organs were unremarkable on physical examination.

Cervical spine radiographs revealed mild degree of degenerative change. Syndesmophyte formation was observed at the level of C2-3 and C5-6, whereas calcified or ossified posterior longitudinal ligament was seen from the level of C2 to C6 (Fig.1). Lumbar spine radiographs revealed squaring of anterior vertebral bodies,

[1] Department of Radiology, Ramathibodi hospital, Rama 6 street, Bangkok 10400, Thailand.
[2] Department of Orthopedic Surgery, Ramathibodi hospital, BKK.

hypertrophied facets at the level of L4-5 and L5-S1, syndesmophytosis, and diskal calcification. Sacroiliac joints showed bilateral, symmetrical involvement. The ligamentous portions of the SI joints were obliterated, representing ankylosis. The synovial portions of the SI joints were narrowed at their upper portions, whereas their lower portions showed erosion and sclerosis of subchondral bone (Fig.2). A radiograph of both hips revealed mild, diffuse narrowing of hip joint spaces. Extrinsic erosion was observed at lateral aspect of femoral heads-necks, involving more on the left side. Erosion and sclerosis of subchondral bone on both sides of pubic symphysis were noted with adjacent eburnation (Fig.3).

Complete blood counts were as followings: Hb 12 gm%, Hct 38%, WBC 7,940, and platelet 368,000. HLA-B27 was positive. Rheumatoid factor was negative. ESR was 92 mm. Antinuclear antigen (ANA) was homogenously positive, with titer of 1:40. The clinical impression at that time was underlying AS with arthritis.

Bone scintigraphy was subsequently performed, and revealed abnormally increased uptake at both femoral head-neck regions (Fig.4). No definite increased uptake at spinal column is noted. Magnetic resonance (MR) imaging was requested to clarify the pathology on bone scintigram.

T1-weighted coronal MR image revealed small foci of decreased signal intensity (SI) in femoral head-neck regions corresponding to scintigraphic findings, and low SI of adjacent bone marrow (Fig.5). These foci were proved to be subchondral bone cysts on sagittal gradient recalled echo (GRE) images (Fig.6). The fast multiplanar inversion recovery (FMPIR) sequence revealed diffuse bone marrow edema involving femoral heads and necks bilaterally, as well as small joint effusion (Fig.7). T1-weighted axial MR image exhibited hypertrophied synovium eroding femoral heads and necks as well as acetabuli (Fig.8). These findings explained the extrinsic erosion of femoral necks seen on plain radiograph and scintigram (Fig.3 and 4). Abnormal decreased marrow SI was also noted at pubic bones. T1-weighted fat-suppression enhanced axial images showed that the thickened synovium, the subchondral cysts, and the edematous marrow at femoral heads and necks exhibited inhomogenous enhancement, as did the pubic bone marrow (Fig.9). MR imaging findings were interpreted as 1) extensive synovitis, corresponding to the known AS, and 2) bone marrow edema of femoral heads and necks, could be an early sign of AVN or transient marrow edema.

As correlated with clinical findings, the diagnosis of an early AVN was favored, and core decompression was performed to the right hip because of more severe pain. The patient had dramatic symptom relief, and 3-months appointment was made for the treatment of the left hip.

AVN = Avascular Necrosis

CASE 2

A 60-year-old male patient has had AS for 30 years and received inadequate medical treatment . He has undergone A-P resection for the treatment of colorectal carcinoma, ten years ago. He developed back pain at lower thoracic level for 7 days. Lateral radiograph of thoracic spine revealed diskal calcification and diffuse syndesmophytosis. Nearly complete obliteration of T7-8 disk space was seen. Diskovertebral destruction at T10-11 level with compression fracture of T10 and T11 vertebral bodies were also observed (Fig.10). Bone scintigraphy showed abnormally increased uptake at lower thoracic level. MR imaging was requested to exclude metastatic process.

MR imaging revealed squaring of thoracic vertebral bodies with diffuse syndesmophytosis, and diffuse anterior longitudinal ligament ossification. The fractured T10 and T11 bodies

maintained signal of normal hyperintense fatty marrow on T1- weighted MR image, and of hypointense on T2-weighted image (Fig.11). Posterior protrusion of T11 body caused small indentation on anterior thecal sac without spinal cord compression. The T7-8 intervertebral disk showed decreased height with internal bright spot T1WI (corresponding to central type of signal change of intervertebral disk in AS patients described by Tyrrell et al),[2] and was hypointense on T2WI. The T7 and T8 bodies maintained normal fatty marrow intensity. The MR imaging findings was interpreted as diskovertebral erosion at T7-8 and spondylitic fracture at T10 and T11. Possibility of metastatic deposits was excluded.

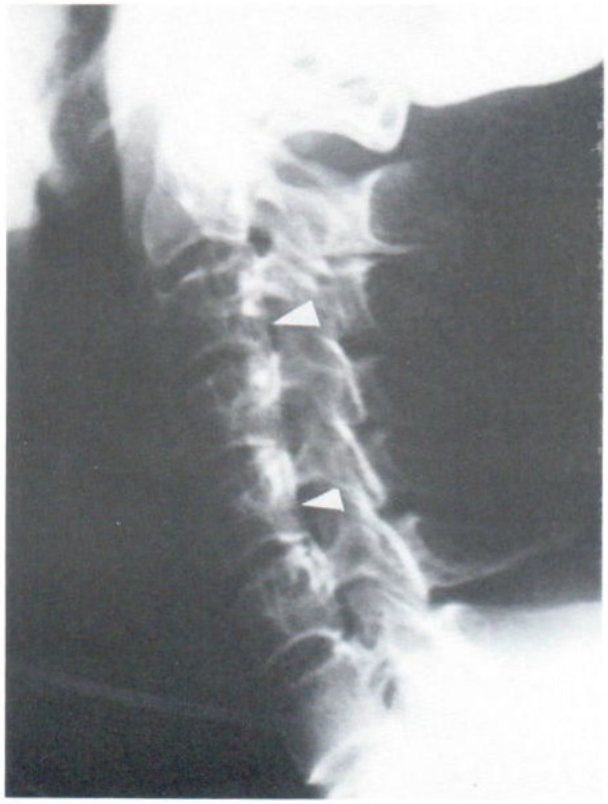

Fig. 1: Lateral cervical spine radiograph reveals posterior longitudinal ligament ossification from the level of C2 to C6 (white arrowheads). Syndesmophytes are noted at C2-3 and C5-6.

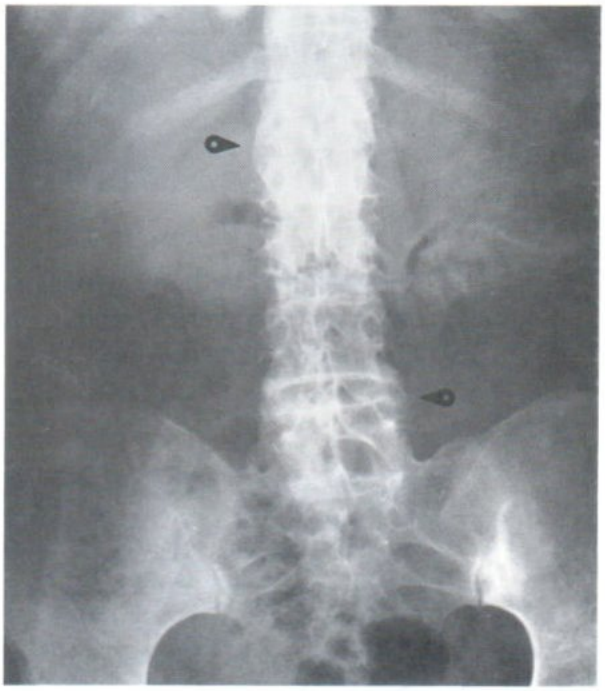

Fig. 2 : AP lumbar spine radiograph shows syndesmophytosis (round arrowheads) and hypertrophied facets. At sacroiliac joints, obliteration of the ligamentous portions is observed whereas the synovial portions show erosion and sclerosis of subchondral bones.

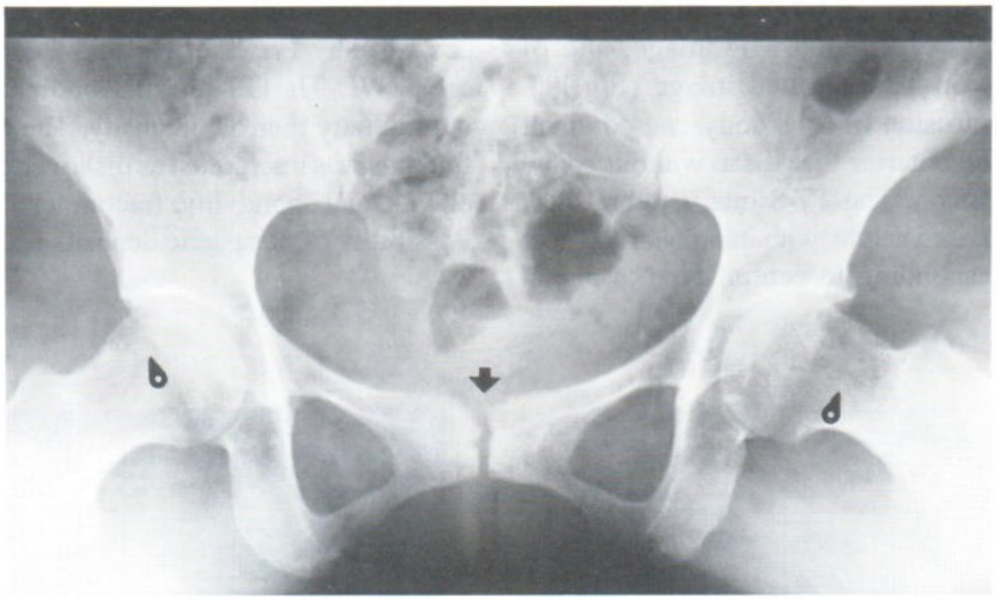

Fig. 3 : AP radiograph of both hips (frog leg view) demonstrates extrinsic erosion at femoral head-neck regions (round arrowheads). The pubic symphysis exhibits bone erosion and sclerosis of subchondral bone (arrow).

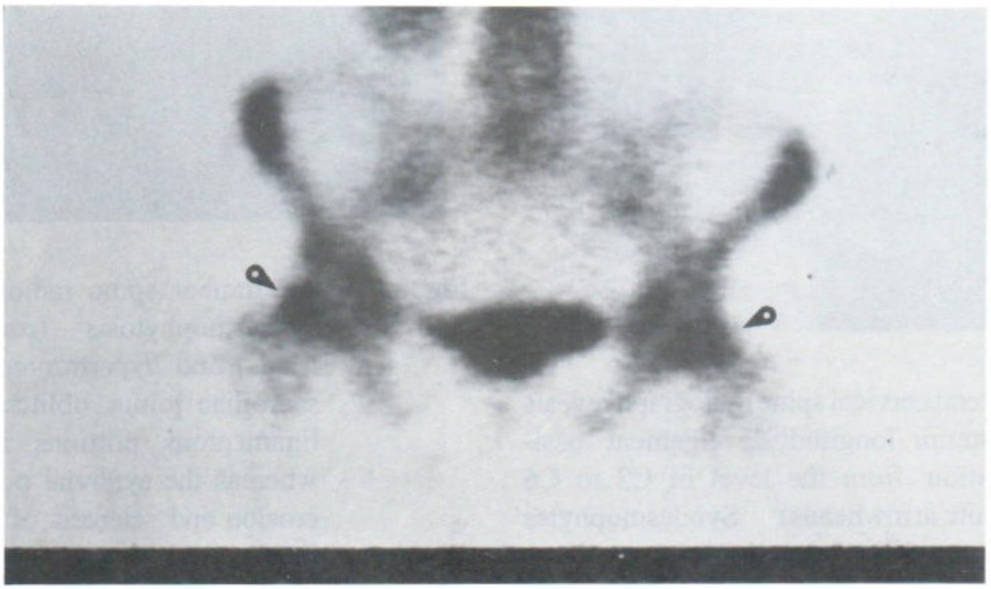

Fig. 4 : Bone scintigram reveals foci of increased radiotracer uptake at femoral head-neck regions (round arrowheads).

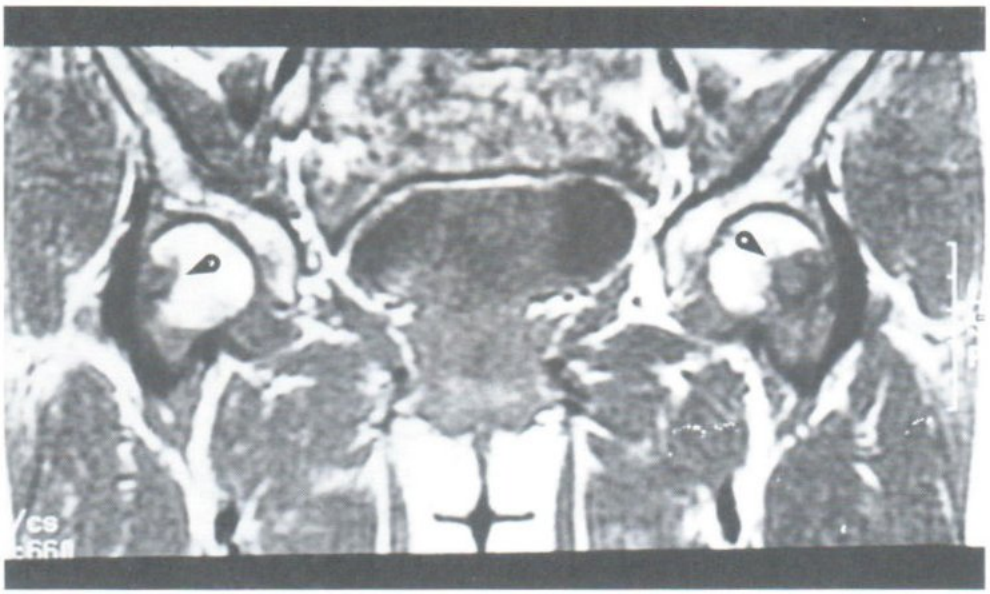

Fig. 5 : T1-weighted coronal MR image reveals that the areas of increased radionuclide uptake in bone scintigram are foci of low SI (round arrowheads)

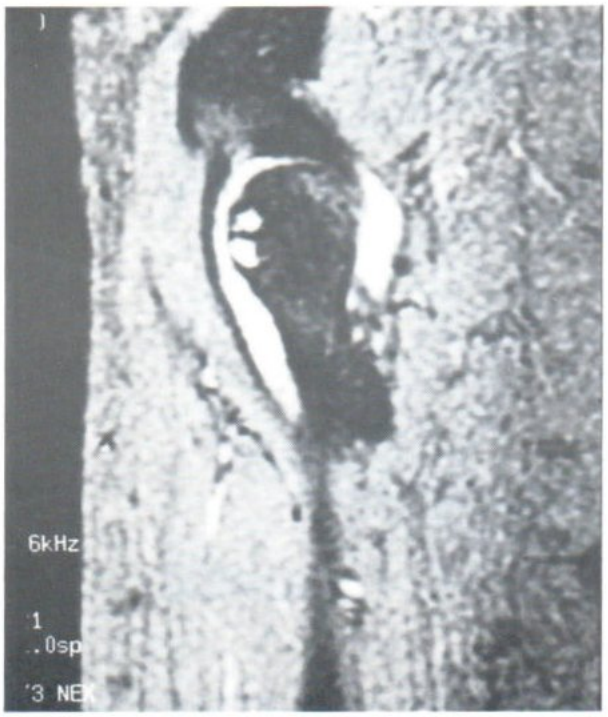

Fig. 6 A.

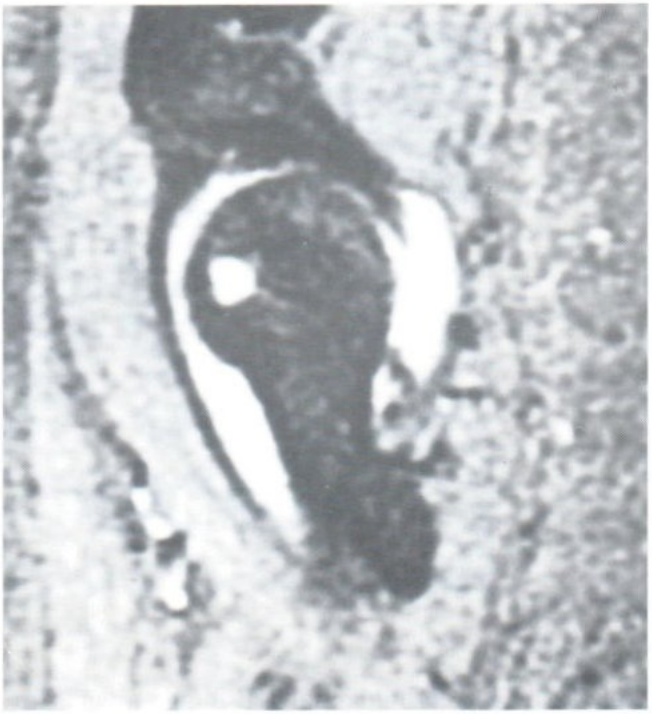

Fig. 6 B.

Fig. 6 : Gradient recalled echo sagittal MR images demonstrate that the foci of low SI in Fig. 5 are subchondral cysts on both right (Fig. 6A) and left (Fig. 6B) femoral heads.

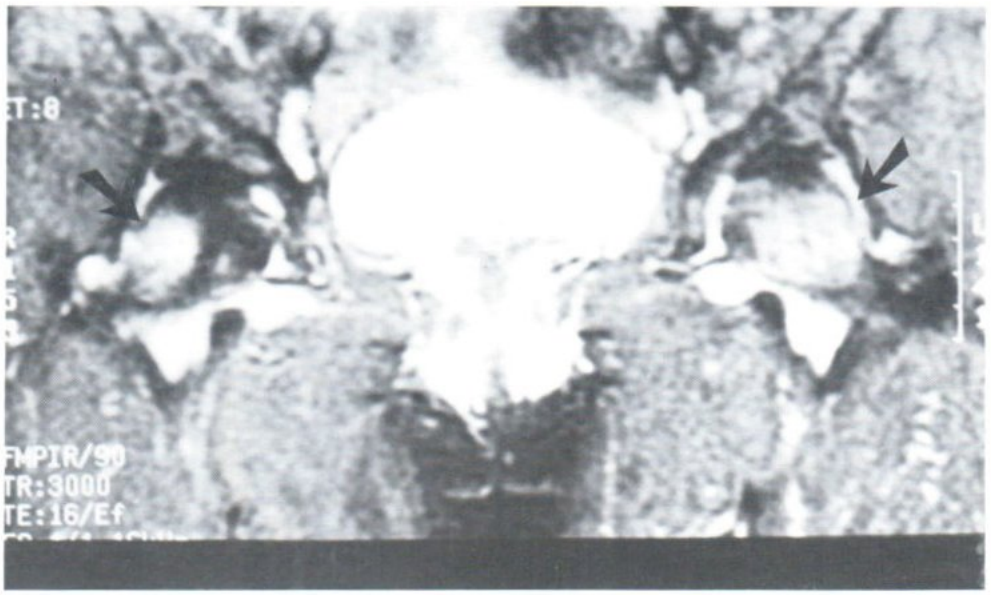

Fig. 7 : FMPIR-sequence coronal MR image demonstrates diffuse bone marrow edema involving femoral heads and necks bilaterally (arrows). Small joint effusion is observed nearby.

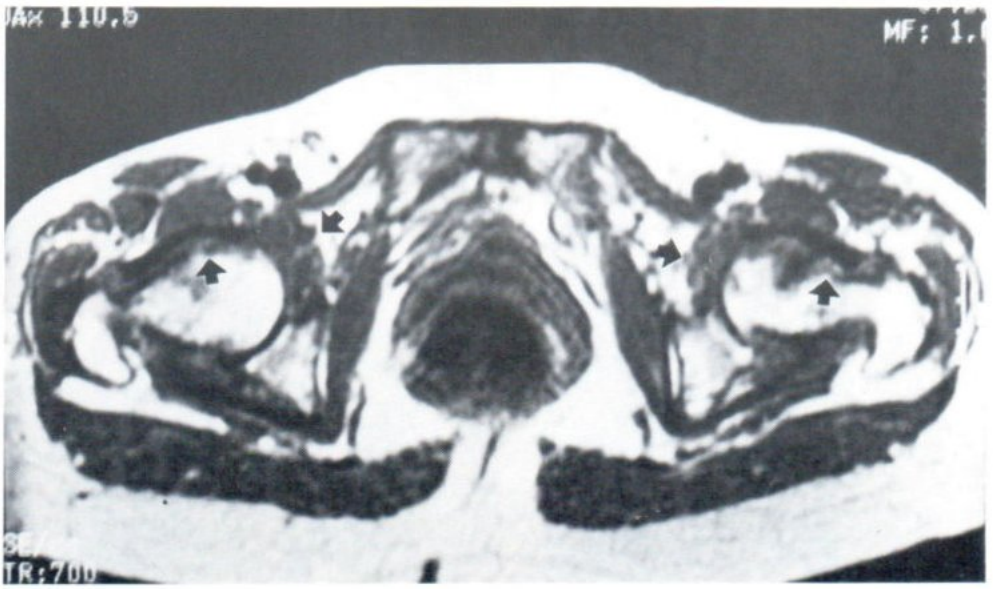

Fig. 8: T1-weighted axial MR image reveals low-SI hypertrophied synovium eroding and extending into subchondral bone both of femoral heads / necks and of acetabuli (arrows).

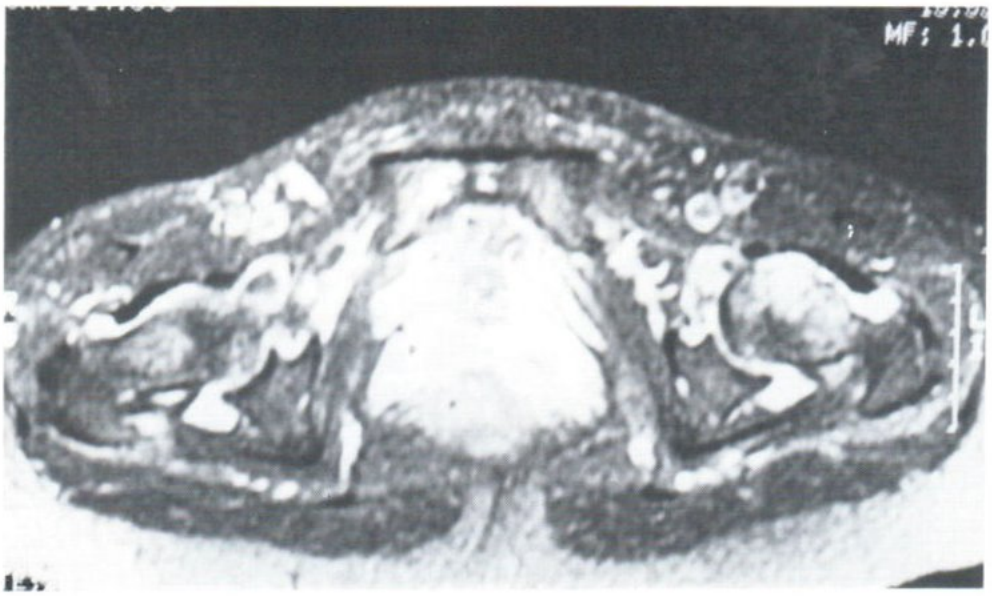

Fig. 9: T1-weighted fat-suppression enhanced axial MR image reveals that the proliferated synovium and the edematous marrow show inhomogeneous enhancement

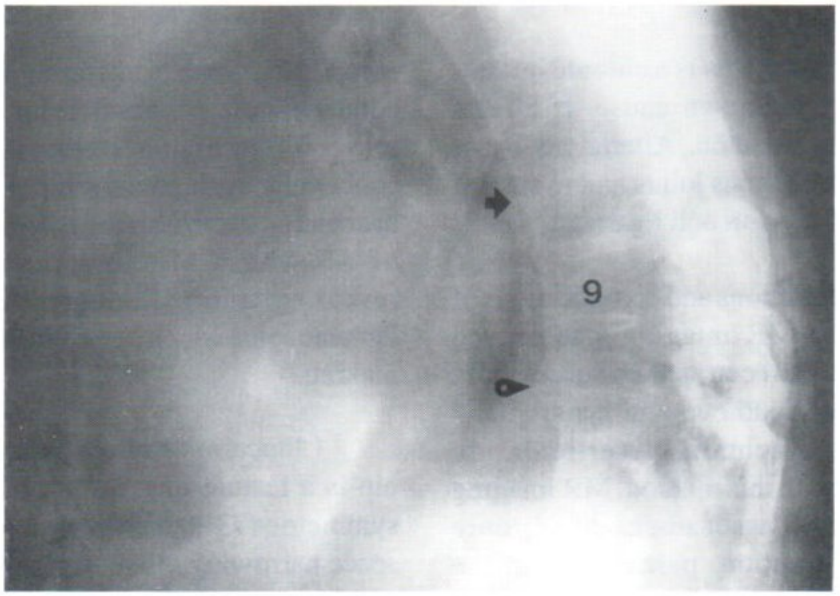

Fig. 10: Lateral thoracic spine radiograph reveals nearly complete obliteration of T7-8 disk space (arrow), with diskovertebral destruction at the level of T10-11 (round arrowheads). (Number 9 indicates level of T9)

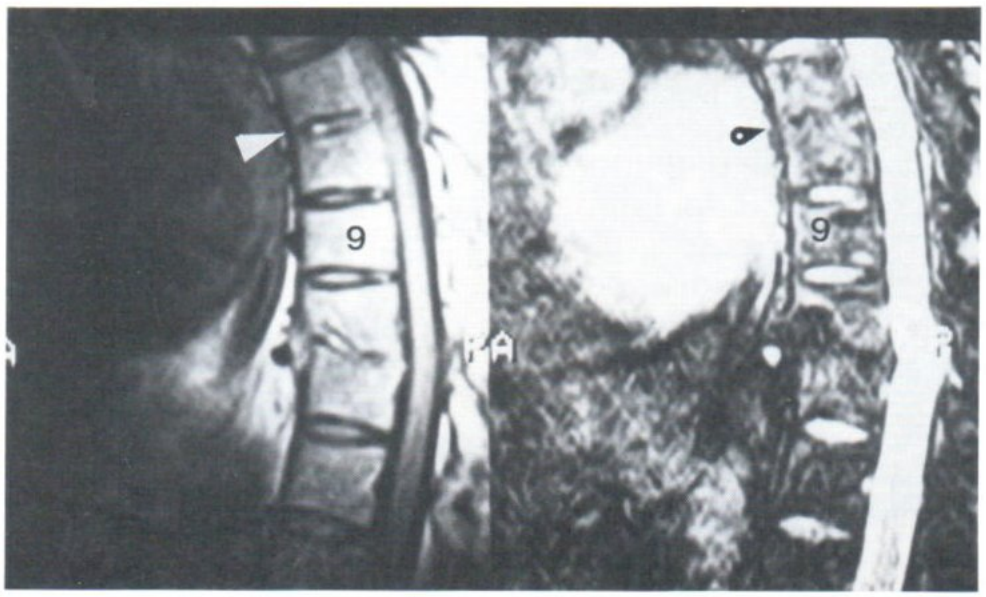

Fig. 11: T1-weighted (left) and T2-GRE (right) sagittal MR images demonstrate that the fractured T10 and T11 bodies still have normal signal of fatty marrow. The T7-8 disk shows a spot of increased SI on T1WI (white arrowhead) and decreased SI on T2GRE (round, black arrowhead).

DISCUSSION

Ankylosing spondylitis is a chronic inflammatory disorder of unknown cause. It affects principally the axial skeleton. Alterations occur in synovial and cartilaginous joints and in sites of bony attachment of tendon and ligament.[1]

Certain manifestations and complications of AS exist for which MR imaging was proved useful. MR imaging has been applied successfully in the evaluation of cauda equina syndrome.[3-6] Dorsally situated arachnoid diverticula are visualized directly with this method. MR imaging may be used in the assessment of chronic diskovertebral destruction, particularly in the differentiation of improper fracture healing, infection, and other related disorders.[1] In case 2 of this study, MR imaging is useful because of the high frequency of associated neurological symptom in AS patients. MR imaging can differentiate the various causes of cord compression and identify cord contusion.[7,8] Roles of MR imaging was to make an early diagnosis of sacroiliitis,[9] and to differentiate inflammatory edema (acute process) from fibrosis or bone sclerosis (more chronic process).[1,10] MR imaging concerning evaluation of hip pain in AS patients has seldom been described. We reported two cases of AS whose MR imaging was of value in revealing true pathologic change in hip and thoracic spine which helped in therapeutic decision making.

Clinical and radiological involvement of the hip is a feature of AS.[11] A bilateral (93%) and symmetric (73%) distribution of concentric joint space narrowing (50%) and osteophytosis (58%) are characteristic. Axial migration of the femoral head with respect to the acetabulum is a frequent feature of hip involvement in AS. It is classically related to superficial erosion of cartilage by inflammatory tissue or pannus,[12] but subchon-dral extension of inflamed synovium has also been observed.[13] Since the nutrition of mature articular cartilage is derived from the synovial surface,

subchondral infiltration does not necessarily destroy the overlying cartilage or produce cartilaginous proliferation.[1] Subchondral cysts are observed, and generally are multiple and of variable size. In case 1, MR imaging demonstrates the extensively proliferated synovium extending into subchondral and marrow compartments of acetabuli, with extrinsic erosion to the femoral head-necks anteriorly. These MR findings may explain the increased uptake on bone scintigram. Such findings could be demonstrated only by MR imaging. In addition, detection of marrow edema involving femoral heads and necks in this case was an important information because it can be an early sign of AVN.[14,15] Focal MR abnormalities subsequent to the presentation of diffuse bone marrow edema has been reported as early as 6 to 8 weeks from the time of detection.[14] Core decompression is most commonly used as the conservative or prophylactic procedure, to alleviate the elevated intraosseous pressure, and permit neovascularization.

Increased accumulation of radionuclide in the spine and at entheses can be observed in patients with AS, especially in the presence of active disease.[16-18] At any location, an abnormal scintigraphic examination is not specific, and accurate diagnosis necessitates its correlation with clinical and radiological investigation.[1] As in case 2; question arose concerning the nature of abnormalities detected by plain radiograph and bone scintigram. Malignancy induced fractures of vertebral bodies may be differentiated by MR imaging from those of benign processes.[19,20] Ninety percent of vertebral fracture caused by non-traumatic malignancy had complete tumoral replacement of the marrow, whereas 77% of benign fractures had complete preservation of normal bone marrow signal.[19] In case 2, MR imaging revealed complete preservation of normal bone marrow signal, and spondylitic process was diagnosed. Clinical improvement was obtained after medical treatment. MR imaging was proved very helpful in excluding metastasis and in suggesting appropriate treatment.

In conclusion; certain manifestations and complications of AS exist for which MR imaging was proved useful, in demonstrating disease activity, revealing early signs of critical complications, and in therapeutic decision making.

REFERENCES :

1. Resnick D, Niwayama G. Ankylosing spondylitis. In: Resnick D, ed. Diagnosis of bone and joint disorders. 3rd ed. Philadelphia, Pa: WB Saunders, 1995;1008-1074.
2. Tyrrell PNM, Davies AM, Evans N, Jubb RW. Signal changes in the intervertebral discs on MRI of the thoracolumbar spine in ankylosing spondylitis. Clin Radiol 1995; 50:377-383.
3. Ruiz A. Dural ectasia in a patient with cauda equina syndrome (CES) of AS. In: Quencer RM, ed. MRI of the spine. New York: Raven Press, 1991;61.
4. Grosman H, Gray R, St Louis EL. CT of long-standing ankylosing spondylitis with cauda equina syndrome. AJNR 1983;4:-1077-1080.
5. Abello R, Rovira M, Sanz MP, et al. MRI and CT of ankylosing spondylitis with vertebral scalloping. Neuroradiology 1988; 30:272-275.
6. Rubenstein DJ, Alvarez O, Ghelman B, Marchisello P. Cauda equina syndrome complicating ankylosing spondylitis: MR features. J Comput Assist Tomogr 1989; 13:511-513.
7. Karasick D, Schweitzer ME, Abidi NA, Cotler JM. Fractures of the vertebrae with spinal cord injuries in patients with ankylosing spondylitis: imaging findings. AJR 1995; 165:1205-1208.
8. Flanders AE, Tartaglino LM, Friedman DP, Aquilone LF. Magnetic resonance imaging in acute spinal injury. Semin Roentgenol 1992; 27:271-298.

9. Murphey MD, Wetzel LH, Bramble JM, Levine E, Simpson KM, Lindsley HB. Sacroiliitis: MR imaging findings. Radiology 1991;180:239-244.
10. Ahlstrom H, Feltelius N, Nyman R, Hallgren R. Magnetic resonance imaging in sacroiliac joint inflammation. Arthritis Rheum 1990;33:1763-1769.
11. Dwosh IL, Resnick D, Becker MA. Hip involvement in ankylosing spondylitis. Arthritis Rheum 1976;19:683-692.
12. Cruickshank B. Pathology of ankylosing spondylitis. Clin Orthop 1971; 74:43-58.
13. Pasion EG, Goodfellow JW. Pre-ankylosing spondylitis: histopathological report. Ann Rheum Dis 1975; 34:92-97.
14. Stoller DW, Matoney WJ. The hip. In: Stoller DW, ed. Magnetic resonance imaging in orthopaedics and sports medicine. Philadelphia, Pa: JB Lippincott, 1993;57-78.
15. Beltran J. Infections and avascular necrosis. In: Stark DD, Bradley WG, eds. Magnetic resonance imaging. 2nd ed. Missouri: Mosby Year Book 1992;2345-2354.
16. Weissberg DL, Resnick D, Taylor A, Becker M, Alazraki N. Rheumatoid arthritis and its variants: analysis of scintigraphic, radiographic, and clinical examinations. AJR 1978;131:665-673.
17. Esdaile J, Hawkins D, Rosenthall L. Radionuclide joint imaging in the seronegative spondyloarthropathy. Clin Orthop 1979;143:46-52.
18. Baumgarten DA, Taylor A. Enthesopathy associated with seronegative spondyloarthropathy: 99mTc-methylene diphosphonate scintigraphic findings. AJR 1993; 160:1249-1250.
19. Yuh WTC, Zachar CK, Barloon TJ, Sato Y, Sickels WJ, Hawes DR. Vertebral compression fractures: distinction between benign and malignant causes with MR imaging. Radiology 1989; 172:215-218.
20. Baker LL, Goodman SB, Perkash I, Lane B, Enzmann DR. Benign versus pathologic compression fractures of vertebral bodies: assessment with conventional spin-echo, chemical-shift, and STIR MR imaging. Radiology 1990; 174:495-502.

EVALUATION OF TECHNETIUM-LABELED RED CELLS USING Sn-kit

Nisarut RUKSAWIN M.S.

ABSTRACT

The labeling yield of ^{99m}Tc-erythrocytes by our method is higher than 97% for blood drawn from 35 patients with polycythemia vera (Hct. 50%-74%). Quality control for tagging effciency was done both in vitro and in vivo by using ionization chamber and scintillation counter respectively. All experiments were conducted with sodium petechnetate which was not the first elution from a new generator. As a results of experiments reported here, a simplified and reproducible method has been developed for the preparation of ^{99m}Tc-labeled red blood cells, it consistently produces high yield in a closed sterile system with few mechanical-steps.

INTRODUCTION

Technetium-99m-pertecnetate has been proposed as a radionuclidic label for red blood cells[1-9], however all methods were conducted with a laborious task. This paper described the preparation of an inhouse simple Sn-kit for ^{99m}Tc-labeled red blood cells in a closed sterile system with few mechanical steps. The Sn-kits have performed well after more than 12 months with 12 ml of whole blood from patients who have hematocrit higher than 50%. The labeling efficiency is higher than 97% with only 5 minute incubation time.

MATERIALS

All experiments were conducted with human blood from 35 patients with possible polycythemia referred to division of Nuclear Medicine for red cell mass measurements. The percent of ^{99m}Tc associated with red blood cells was determined by cell sedimentation. Ionization chamber was used for ^{99m}Tc assay in vitro and gamma well counter was used for ^{99m}Tc assay in vivo. Stannous freeze dried kits were prepared in our laboratory. All other chemicals were reagent grade. Surflo Int Type Wing Infusion Set with releasable injection site was used to reduce repetition of venipunctures. Methylenediphosphonic acid was purchased from Sigma Chemical Co, St.Louis, Mo. and Stannous chloride dihydrate was purchased from E-Merck, Darmstadt, Germany.

METHODS

PREPARATION OF Sn-FREEZE DRIED KITS.

Cleaned glassware and equipment were wrapped in wrapping paper, and sterilized in autoclave.

A. Dissolve $SnCl_2$ $2H_2O$ 1 g in 5 ml of concentrated HCl. Filter the solution through 0.22 μm millipore filter. Stir the filtered solution at least 30 minutes.

Department of Radiology, Faculty of Medicine, Mahidol University, Bangkok 10700

B.In a 250 ml beaker, dissolve 500 mg Methylenediphosphonic acid in 150 ml sterile distilled water.

C. To solution B add 1.3 ml of solution A containing 260 mg of stannous chloride and adjust the pH to 5.0-6.0 using 40% NaOH 2.2 ml.

D. Sterilize the solution by 0.22 μm membrane filtration into presterilized evacuated vials. Aseptically transfer 1 ml each of this solution to sterile 7 ml serum vials. Freeze dry for 24 h, seal under vacuum after freeze drying, each vial contains 1.7 mg stannous chloride and 3.25 mg methylenediphosphonic acid.

IN VITRO QUALITY CONTROL FOR ^{99m}Tc-RBC USING INHOUSE Sn-KIT.

35 adult patients suspicious of polycythemia vera with hematocrit range from 50% to 74% were studied. Erythrocytes were labeled with ^{99m}Tc using the following procedure.

1. Add 1.5 ml of normal saline to the Sn-kit, then mix the vial and withdraw the solution from the vial by using 2.5 ml syringe. Inject stannous solution to the blood circulation of the patient, after waiting for 10 minutes and withdraw12 ml of blood from the same patient, and transfer to 50 ml sterile Falcon centrifuge tube #2098 containing 2.5 ml of ACD.

2* Mix the withdrawn blood with 200 mCi of Na99mTcO4. This amount can be prepared by using Na99mTcO4 10 mCi/ml 2 drops from tuberculin syringe with needle mix and wait for 5 minutes.

3. Add 25 ml of normal saline to the sample, mix and centrifuge at 2500 rpm for 5 minutes.

4. Read the volume of the supernatant for example Y ml (Fig 1). Measure the activity of volume X (Fig 1) by using the ionization chamber.

5. Pipette 10 ml of the supernatant and assay the activity, calculate in vitro percent bound to red cells with the following formula.

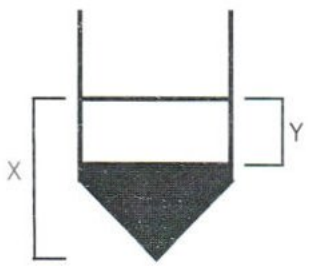

Fig 1. Sedimentation of ^{99m}Tc - RBC in Falcon tube.

$$= \frac{\text{Activity of volume X} - \frac{\text{Volume Y}}{10}\text{ (activity of 10 ml supernatant)}}{\text{Activity of volume X}}$$

The in vitro percent bound of ^{99m}Tc-RBC in 35 patients, were greater than 97%. This indicates that neither washing nor centrifugation is needed in the labeling process in the future for high hematocrit patients.

IN VIVO QUALITY CONTROL FOR ^{99m}Tc-RBC USING INHOUSE Sn-KIT.

To examine in vivo stability of ^{99m}Tc-labeled red cells, the blood activity was followed in four patients at intervals of 10, 20, 30, 60 and 120 minutes after injection of 6 ml (about 100 μCi) of ^{99m}Tc-labeled red blood cells from 2*. 5 ml of postinjection samples of blood were drawn in heparinized syringes from a vein on the opposite limb at intervals of 10, 20, 30, 60 and 120 minutes. The samples were pipetted triplicately and the activity was counted by using scintillation well counter. Red cell volumes at 10, 20, 30, 60 and 120 minutes were calculated.

RESULTS

The labeling efficiency in vitro was found greater than 97%, and in vivo stability of ^{99m}Tc-labeled red blood cells was confirmed by comparing the sequential red cell volume measurement at various times after injection. The results expressed as the percentage change between the values obtained with 10 minute sample. The figures are shown in table 1. The red cell volumes are almost identical for the first hour with slight increase in the second hour sample.

Table 1. Sequential Red Cell mass measurements at various time after injection

		% 10-minute value (ml)				
Subjects	Time (minutes)	1	2	3	4	Mean
	10	100	100	100	100	
	20	100.2	100.1	100.3	100.2	100.2
	30	100.4	100.3	100.4	100.5	100.4
	60	100.3	100.6	100.5	100.6	100.5
	120	102.4	103.3	104.5	101.8	103.0

DISCUSSION

From the study, a new method for labeling red blood cells with pertechnetate ion without using the centrifugation was developed. From this technique more red cells could absorb almost all ^{99m}Tc in order to gain high yield. The results showed that the technique is useful for adult patients with high hematocrit.

REFERENCES

1. Fischer J, Wolf R, Leon A. Technetium-99m as a label for erythrocytes. J Nucl Med 1967;8:229-32.
2. Hauboid U, Pabst HW, Hor G. Scintigraphy of the placenta with ^{99m}Tc labeled erythrocytes. In Symposium on Medical Radioisotope Scintigraphy, Vienna. IAEA, 1969.pp 1-3.

3. Burdine JA, Legfay R. Spleen scans with ^{99m}Tc-labeled heated erythrocytes. Radiology 1968;91:162-4.
4. Weinstein MB, Smoak WM. Techical difficulties in ^{99m}Tc-labeling of erythrocytes. J Nucl Med 1970;11:41-2.
5. Eckelman WC, Reba RC, Albert SN. A rapid simple improved method for the preparation of ^{99m}Tc red blood cells for determination of red cell volume. Am J Roentgenol Radium Ther Nucl Med 1973;118:-861-4.
6. Eckelman W, Richards P, Atkins HL, et al. Visualization of the human spleen with ^{99m}Tc-labeled red blood cells. J Nucl Med 1971;12:310-1.
7. Atkins HL, Eckelman WC, Hauser W, et al. Splenic sequestration of ^{99m}Tc-labeled red blood cells. J Nucl Med 1972;13:811-4
8. Smith PSH : ^{99m}Tc labelled erythrocytes for spleen scanning. Int J Appl Radiat Isot 1974;25:137-9.
9. Atkins Hl, Eckelman WC, Klopper JF, et al. Vascular imaging with ^{99m}Tc-red blood cells. Radiology 1973;106:357-60.

ACCURATE METHOD FOR DETERMINATION OF RED CELL VOLUME IN POLYCYTHEMIA VERA

Nisarut RUKSAWIN M.S.

ABSTRACT

The detailed procedure was performed to determination of blood volume in polycythemia vera. The usual protocol takes 3 hours to run with patients but the new procedure takes only 1.5 hours, 87% of patients who come to section of nuclear medicine, Siriraj Hospital, for blood volume measurement are polycythemia vera. This special development saves 45% of time without using any money because this research comes from routine work. It is an example for young staffs who always complain about lacking of money and time to do research.

INTRODUCTION

A simple hematocrit reading can mislead the doctors in estimation of red cell mass ; for example, if the patient has a low plasma volume the hematocrit will be falsely high. Keith N.M.et al.proposed dilution principle for clinical investigation.[1] Application of techniques in nuclear medicine has improved understanding and knowledge of accurate measurement of the circulation volume. The first Thai originators in using ^{51}Cr in estimation of blood volume and red cell volume are Suwanik Romsai[2] and Intrasupta Somlak.[3] Ruksawin Nisarut[4] used ^{99m}Tc instead of ^{51}Cr after Sukavatsesiri Valeerat[5] proved that no sinificant difference of blood volume value between the use of ^{51}Cr-RBC and ^{99m}Tc- RBC as tracers. The new process described here has developed to the most natural one so the clot or aggregation of RBC should not occured during the process.

MATERIALS

1. Heparin 5000 I U per ml.
2. 5 ml of sterile water for injection in sterile serum vial.
3. Terumo Surflo Int Typr Wing Infusion Set. (21G, 9 cm tubing with releasable injection site)
4. Normal saline
5. Stannous kit[6]
6. Falcon plastic centrifuge tube # 2098
7. ACD solution formula A 2.5 ml ; This amount can be prepared by aseptically transfer 5 ml serum vials and reautoclave. Store at room temperature.
8. ^{99m}Tc pertechnetate 200 μCi ; this amount can be prepared by using $Na^{99m}TcO_4$ 10 mCi/ml 2drops from tuberculin syringe with needle.
9. Analytical balance
10. 100 ml volumetric flask
11. Hematocrit determination set
12. 1 ml automatic pipette with replaceable plastic tip
13. Test tubes
14. Gamma well counter

METHODS

1. No preparation of the patient is required.

Department of Radiology, Faculty of Medicine, Mahidol University, Bangkok 10700

2. Preparation of dilute heparin by adding 0.25 ml of heparin to 5 ml of sterile water for injection.

3. Insert infusion set in the patient's arm vein, 5 ml sample of blood is removed from the patient to establish patient background level.

4. Flush the infusion set with 0.5 ml of dilute heparin to keep it patent.

5. Add 1.5 ml of normal saline to stannous kit, mix the vial and withdraw the solution from the vial then inject to the releasable injection site, flush with normal saline to push all of the stannous solution in the circulation followed by 0.5 ml of dilute heparin.

6. Allow a circulation time of 10 minutes before withdrawing a 12 ml blood sample, put the blood sample in sterile Falcon plastic tube containing 2.5 ml ACD solution. Mix the sample and immediately put 200 mci of Na $^{99m}TcO_4$ and mix well.

7. Incubate(6) for 5 minutes for ^{99m}Tc to tag to red blood cells (^{99m}Tc-RBC). Mix and use syringe to draw 6 ml of ^{99m}Tc-RBC.

8. Weigh(7) by analytical balance Weight of syringe + needle + ^{99m}Tc-RBC = $\mathbf{W_1}$ g

9. Preparation of standard solution by filling 100 ml volumetric flask with 95 ml of tab water. Inject ^{99m}Tc RBC about 0.2 ml into the volumetric flask, make the total volume to 100 ml by adding tab water.

10. After discarding about 0.2 ml of ^{99m}Tc-RBC in (9), the rest of ^{99m}Tc-RBC is weighed again as $\mathbf{W_2}$ g $\mathbf{W_1}$-$\mathbf{W_2}$ is the weight of the amount of ^{99m}Tc-RBC in volumetric flask.

11. Inject normal saline 2 ml via the releasable injection site for checking the patency.

12. Inject ^{99m}Tc-RBC via the releasable injection site, flush with normal saline to push all of ^{99m}Tc-RBC in the 9 cm tube into blood circulation. Remove the infusion set. Weigh the syringe containing residual of ^{99m}Tc-RBC as $\mathbf{W_3}$ g $\mathbf{W_2}$-$\mathbf{W_3}$ will be the exact weight of ^{99m}Tc-RBC injected in the blood circulation of the patient.

13. Allow a circulation time of 10 minutes before withdrawing 5 ml blood sample with heparinized syringe from a vein on the opposite limb in order to avoid contamination.

14. Triplicately pipette (3), (9) and (13) 1 ml of each into 9 test tubes and mark each as to their content. Count each sample in ^{99m}Tc window by autogamma well counter.
Let the average activity from (3) be **Bg** cpm
Let the average activity from (9) be **Std** cpm
Let the average activity from (12) be **Sample** cpm

15. Calculate total activity injected to blood circulation of the patient

$$= (\text{Average } \mathbf{Std} - \text{Average } \mathbf{Bg}) \times 100 \left[\frac{\mathbf{W2 - W3}}{\mathbf{W1 - W2}} \right] = \ldots\ldots\ldots\ldots \text{ cpm}$$

16. Dilution Volume

$$= \frac{\text{Total activity injected to blood circulation of the patient}}{(\text{Average } \mathbf{Sample} - \text{Average } \mathbf{Bg})} = \ldots\ldots\ldots \text{ ml}$$

17. Red Cell Volume = $\frac{\text{Dilution Volume x Hematocrit}}{100}$ = ... ml

RESULTS

The new protocol for measurement of red cell mass in patients with hematocrit higher than 50% was prepared for teaching session on radiopharmaceuticals at division of nuclear medicine, department of radiology, Siriraj Hospital. Excellent result were obtained with a modification of this method for polycythemia vera. The labeling procedure described here is not identical to other procedures because no centrifuge is used. With 5 minute incubation time and no washing of red blood cells saves 45% of time.

DISCUSSION

There are three reasons to discuss about the advantages of the new protocol. First reason , the Surflo Int type Wing Infusion Set was used to reduce three venipunctures to one, it is not only to create the non-invasive investigation but also to establish the most accurate way to put all ^{99m}Tc-RBC in the blood circulation. Second reason, Sn-kit was used instead of MDP-kit, the Sn-kit is cheaper but more powerful in labeling that incubation time could be reduced to 5 minutes. Third reason, thismethod does not use centrifuge to wash the red cells, so it reduces time and mechanical steps.

REFERENCES

1. Keith NM, Rowntree LG and Geraghty JT. A method for the determination of plasma and blood volume. Arch Int Med. 1915;16:-547.
2. Suwanik R, Maharakaka N, Chayasuta S, Pleehachinda R, Intrasupt S, Buranapongse P, Premyodhin M, Healy MJR, Chambers EA, Sukaroj S, Na Songkhla S, Attanatho V, Boonnamsiri V, Phasuk N, Hemindhra P, Satayavannich S, Ruksawin N. Blood volume in Thais, J Med Ass. Thailand 1971;54:920-38.
3. Intrasupta S et al. Red cell volume, its prediction in Thais, Thai Journal of Radiology 1972;9:33-45.
4. Ruksawin N et al. New method for measuring blood volume. Siriraj Hosp Gaz 1985;37:265-70.
5. Sukavatsesiri V. Labeling red blood cells with Technetium - 99m for determination of blood volume. Thesis for master degree of Engineering, Department of Nuclear Technology Graduate School, Chulalongkorn University.
6. Ruksawin N. Evaluation of Technetium-labeled red cells using Sn - kit. The Asean Journal of Radiology 1997;3:3:283-286.

1st INTERNATIONAL POSTGRADUATE COURSE ON ONCOLOGY OF GASTROINTESTINAL DISEASES

JANUARY 14-16 1998 KHON KAEN, THAILAND

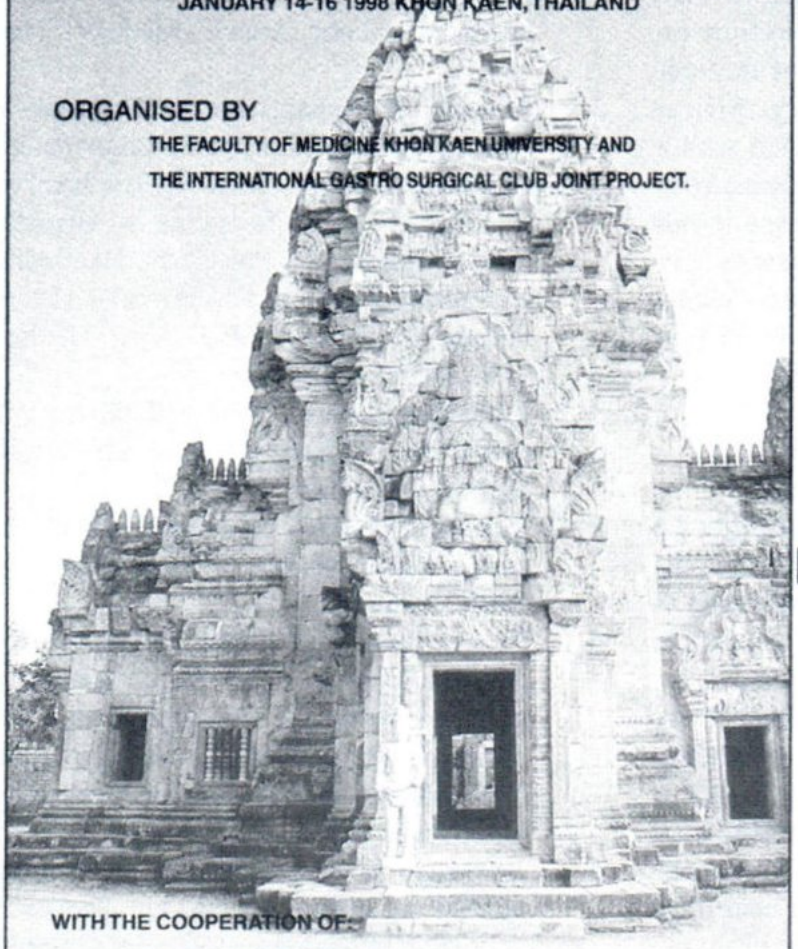

ORGANISED BY

THE FACULTY OF MEDICINE KHON KAEN UNIVERSITY AND

THE INTERNATIONAL GASTRO SURGICAL CLUB JOINT PROJECT.

WITH THE COOPERATION OF:-

MINISTRY OF PUBLIC HEALTH
THE ROYAL COLLEGE OF SURGEONS OF THAILAND
THE SOCIETY OF SURGEONS OF THE NORTHEAST OF THAILAND
THE ROYAL COLLEGE OF PHYSICIANS OF THAILAND
THE ROYAL COLLEGE OF RADIOLOGISTS OF THAILAND
THE ROYAL COLLEGE OF PATHOLOGISTS OF THAILAND
AND THE GASTROENTEROLOGICAL ASSOCIATION OF THAILAND

ADVISORY BOARD

KITISIN, P.
KULLAVANICH, P.
LYGIDAKIS, N.J.
PAUSAWASDI, A.
POTTHNAM, S.
TUNGSUBUTRA, K.
WORA-URAI, N.

SCIENTIFIC PROGRAMME

The Program will consist of three-day scientific sessions concentrated on the oncology of gastrointestinal diseases presented in the form of:

Lecturettes
Video sessions
Symposia
Plenary sessions
Clinical case discussion
Live demonstration

FACULTY MEMBERS

EUROPE :-		
BICHA-CASTELO	H.	PORTUGAL.
JAECK	D.	FRANCE.
LYGIDAKIS	N.J.	GREECE.
RIEMANN	J.E.	GERMANY.
ASIA:		
ABDULMAJID	A.	MALAYA.
BUDHISAWASDI	V.	THAILAND.
KANJANAPITUK	A.	THAILAND.
KARAWADA	Y.	JAPAN.
KITISIN	P.	THAILAND.
KULLAVANICH	P.	THAILAND.
MAIRIANG	P.	THAILAND.
MAKUUCHI	M.	JAPAN.
NAKAO	A.	JAPAN.
NOORI	S.M.	MALAYA.
PAUSAWASADI	A.	THAILAND.
RAU	KB.	INDIA.
SUCHAKUL	V.	THAILAND.
SUKHONTHAMAN	Y.	THAILAND.
SUWANVILAI	C.	THAILAND.
SUPROMAJAKR	V.	THAILAND.
UTTARAVICHIEN	T.	THAILAND.
VAEUSORN	N.	THAILAND.
VATHANOPHAS	V.	THAILAND.
WORA-URAI	N.	THAILAND.

LOCAL ORGANIZING COMMITTEE

CHAIRMAN:	UTTARAVICHIEN, T.
VICE CHAIRMAN:	BUDHISAWASDI, V.
SECRETARY :	MAIRIANG, P.
DEPUTY SECRETARY :	RENTON, E.
TREASURER:	KUPTARNOND, C.
SCIENTIFIC PROGRAMME:	CHATBANCHACHAI, V.
CONGRESS FACILITIES:	MUSIKAPODOK, P.
ACCOMMODATION AND TRANSPORTATION:	CHAU-IN, S.
SOCIAL PROGRAMME:	MAIRIANG, E.
PUBLIC RELATION:	TANTUYASAWASDIKUL, V.
REGISTRATION:	KUPTARNOND, C.
PUBLICATION:	CHOWCHUEN, B.
MEMBERS:	PAIROJKUL, C.
	TUSANAVIWANA, P.
	CHAIYAKUM, J.
	KARUSUN, S.
	SUKEEPAISARNJAROEN, W.

JANUARY 14-16 1998

CHAROEN THANI PRINCESS

OFFICIAL LANGUAGE: *English*

CALL FOR PAPERS:
Oral, Poster, Video Presentations on GI Oncology were invited.

Deadline of the Submission of Abstract is October 15th 1997.
For Further details please contact the Secretary General.

SECRETARIATE OFFICE:

DEPARTMENT OF SURGERY
FACULTY OF MEDICINE
KHON KAEN UNIVERSITY
KHON KAEN, 40002
THAILAND.
TEL.66-43-348393
FAX : 043-243064, 043-348375

ULTRASOUND DIAGNOSIS OF INTUSSUSCEPTION

Thavorn DENDUMRONGSUP, M.D.[1] Paithoon CHONGCHITNANT, M.D.[1]

ABSTRACT

Retrospective study of ultrasound (US) appearance of intussusception was done in 15 patients with clinically suspected of intussusception, 12 pediatric and 3 adult patients. Intussusception was correctly diagnosed and correctly excluded by US in 12 and 3 patients respectively. Most common characteristic US findings are smooth, well defined round or oval mass with multiple concentric rings. Other signs included sandwich sign, donut sign, crescent-in-donut sign, Hayfork sign. Clinical signs and symptoms are often not typical, only 33% of our patients had classic triad. US is useful for screening and diagnosis of intussusception. Unnecessary invasive procedures for diagnosis or treatment could be avoided.

INTRODUCTION

In the past, barium enema was used for the diagnosis of intussusception. Clinical diagnosis is frequently uncertained, leading to unnecessary barium enema. At present role of US in the diagnosis of various gastrointestinal lesions including intussusception is widely accepted. US is an appropriate procedure especially for pediatric patients because it is non - invasive and without radiation. We have performed several cases clinically suspected intussusception with US.We retrosceptively reviewed the US images to define its appearances.

MATERIAL AND METHOD

Retrospective study was done in 15 patients with clinically suspected of intussusception. Ultrasound was performed with realtime, 3.75 MHz machine. The US images were reviewed as well as clinical data, operative and pathological findings from the medical records.

Age of the patients with intussusception is varied from 4 months to 43 years, 5 males and 7 females. Mean age of pediatric patients is 9.7 months. Seven cases were proven by barium enema, one case of ileoileal intussusception by GI-follow through and the other four cases by surgery. Three cases were successfully reduced by hydrostatic barium reduction.

RESULTS

Twelve cases of intussusception were correctly diagnosed by US. There are 3 negative cases who were given conservative treatment and discharged uneventfully. US findings of intussuscepetion are characteristic. Most common findings were well - defined smooth round or oval mass with multiple concentric hypo- and hyperechoic rings (Fig. 1). Other US findings were donut appearance (Fig. 2), sandwich appearance (Fig. 3), triangular hyperechoic band (Fig. 4), crescent-in-donut appearance (Fig.5) and "Hayfork" appearance (Fig. 6)

[1] Department of Radiology, Faculty of Medicine, Prince of Songkhla University, Hatyai, Sonkhla, Thailand.

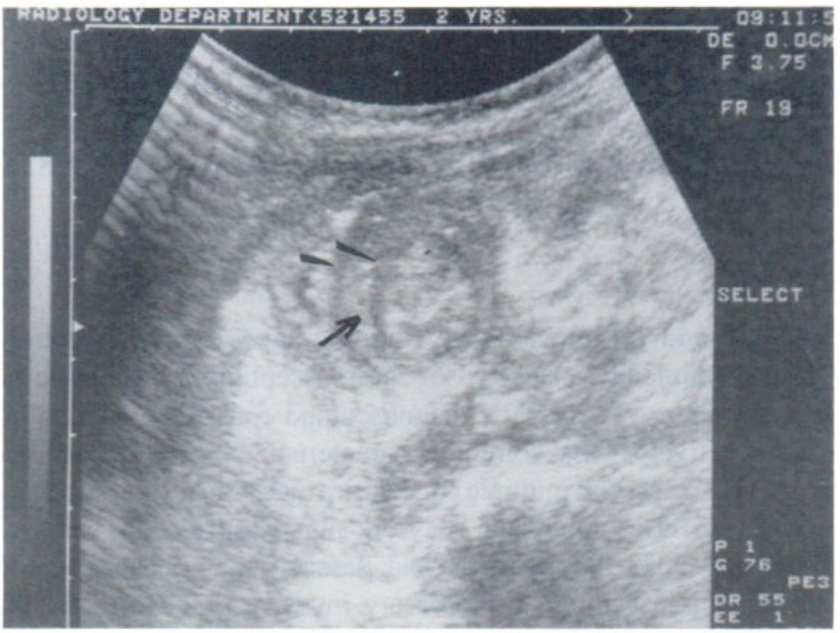

Fig. 1 Transverse image of the intussusception shows well-defined round mass with multiple concentric rings. Hypoechoic (arrowheads) alternates with hyperechoic rings(arrow) are demonstrated.

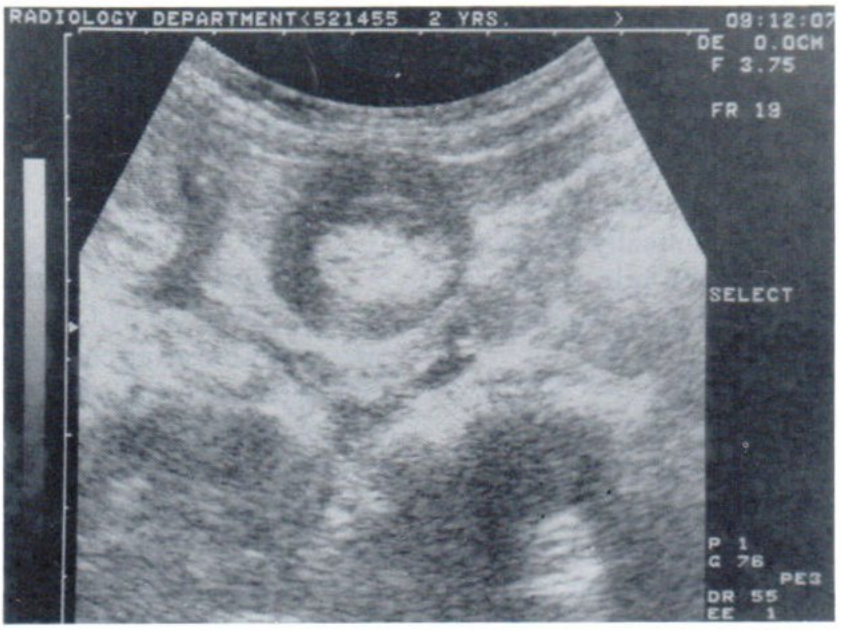

Fig. 2 Transverse image of the intussusception shows a donut sign.A well defined round mass with hyperechoic center surrounded by thick hypoechoic rim of edematous wall.

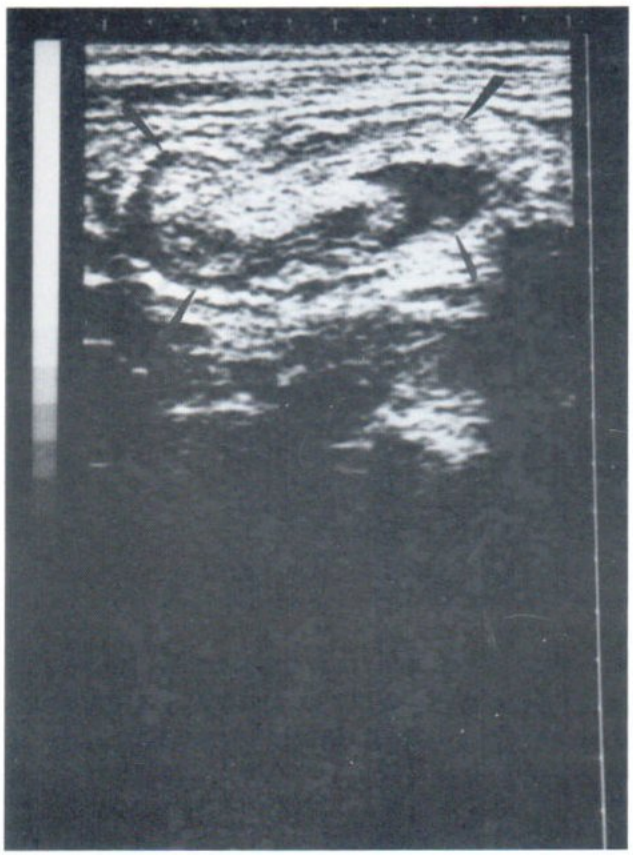

Fig. 3 Longitudinal image of the intussusception reveals an oval mass with multiple hypo-and hyperechoic layers (arrowheads), the sandwich sign.[15]

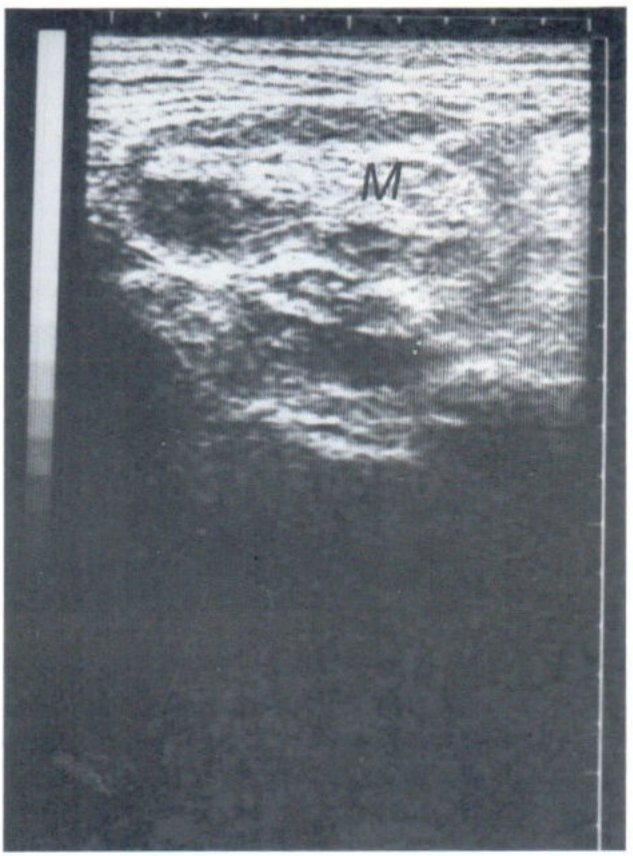

Fig. 4 Longitudinal image shows a triangular hyperechoic area with its apex directed to the apex of intussusception corresponding to mesentery with abundant fat.

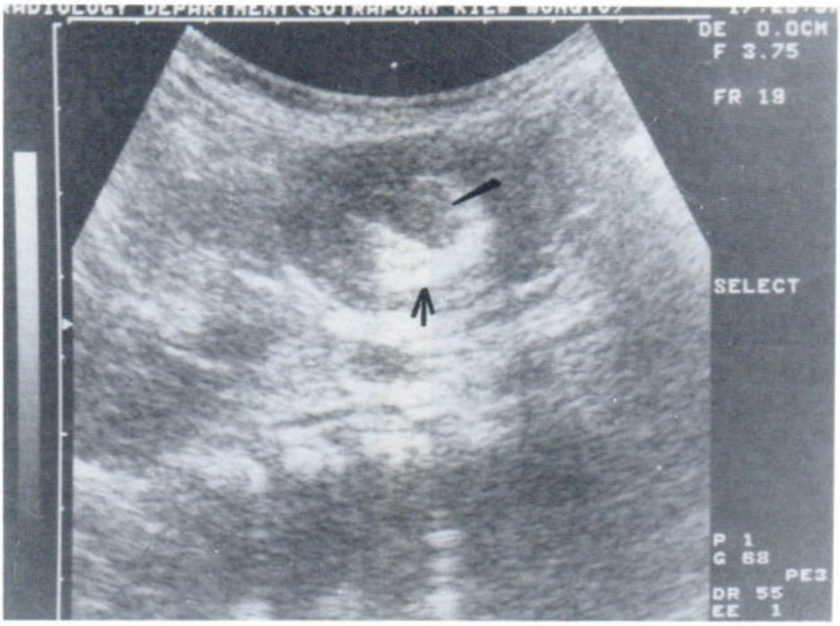

Fig. 5 Transverse image shows the crescent-in-donut sign. Echogenic crescent(arrow) enclosing hypoechoic center(arrowhead) represent mesentery enclosing the entering limb of intussusceptum. The outer hypoechoic ring is formed by the intussuscpiens and returning limb of intussusceptum.

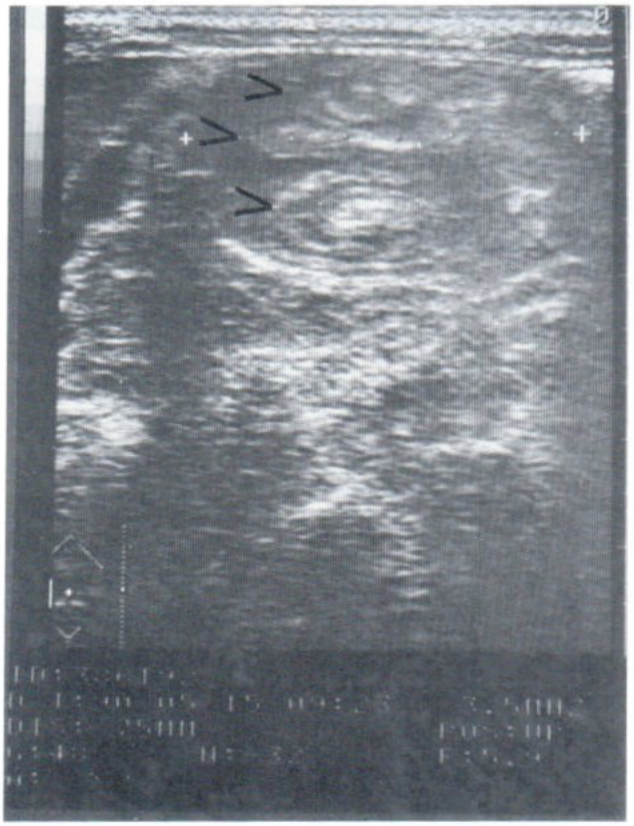

Fig. 6 Longitu dinal image shows the intussusception (between cursors) and the "Hayfork" sign (arrowheads)

Five of the twelve cases had leading points found at surgery. They are Meckel's diverticulum and ectopic pancreas in pediatric patients, lymphoma,lipoma and caseous granuloma in the adults. The types of intussusception and clinical signs are shown in table 1 and 2. There is 1 case of ileocolocolic type which the intussusceptum reached the rectum.

Table 1 : Types of intussusception

Type of intussusception	No.	remarks
Ileocolic	8 (67%)	-
Ileoileal	2 (17%)	Ectopic pancreas, Caseous granuloma
Ileoileocolic	1 (8%)	Meckel's diverticulum
Ileocolocolic	1 (8%)	-
Total	12	

Table 2 : Clinical signs and symptoms

Clinical signs	No.	
Abdominal pain	10	(83%)
Vomitting	9	(75%)
Currant jelly stool	7	(58%)
Palpable abdominal masses	7	(58%)
Questionable abdominal masses	3	(25%)
No palpable mass	2	(16%)
Classic triad	4	(33%)
Classic triad and masses	2	(16%)

DISCUSSION

The US findings of intussusception is characteristic and quite different from that of the other gastrointestinal lesions such as tumour, inflammatory disease and some other lesions. Various US findings of intussusception were described in the literature. The target-like abdominal mass,[1,2,11] hourglass, fused target - like configurations[3] were described in the early reports. Subsequently, dual-pattern images with anatomical explanation was reported by several authors.[4,5,6,7,10] Later US findings that were described were multiple concentric ring sign,[6] Hayfork[13] or trident sign[14] and recently the crescent-in-donut sign.[10]

The various US findings depend on the level and direction of scanning plane[5,10] degree of parietal edema as well as the length of the dragged mesentery.[10] The intussusceptum is telescoped into the intussuscepiens until it cannot go furthur owing to traction of the mesentery which is dragged between the entering and returning limbs of intussusceptum. Venous obstruction occurs with resultant wall edema. The edema is maximal at the apex of intussusceptum.[4] Therefore at or near the apex a target - like or donut pattern was demonstrated. Very thick hypoechoic rim is due to severe edema of the entering and returning limbs of intussusceptum[5] with resultant obliteration of echogenic interface between them and also due to the absence of mesentery.[10] Scanning at the middle or at the base of intussusception may show the crescent - in - donut appearance, of which the echogenic crescent represents mesentery enclosing the entering limb of the intussusceptum.[10] Multiple concentric ring appearance on the transverse plane and the layering tubular mass (sandwich-like) on the longitudinal plane are due to parietal edema of the more proximal intussus-cepted bowel in less severe cases.[5]

In our patients, the most common US finding is the multiple concentric rings. This was a retrospective study so not all signs were expected to be demonstrated on the films. Multiple concentric ring sign is characteristic and easiest to be recognized. There may be no need to try to demonstrate all signs that have been described. In adult patients, one may need to differentiate mass of intussusception from tumour mass. The contour of intussusception is smooth, round or oval shaped with uniform wall thickening. Tumour frequently have irregular lobulated contour with asymmetrical wall thickening.

Prospective studies of the diagnostic value of US in clinically suspected intussusception compared with barium enema showed negative predictive value of 100%, sensitivity of 100% and specificity of 88%-93%.[8,9,12] In our series, only 4 in 12 patients (33%) had clinical triad, abdominal pain, vomitting and currant jelly stool (Table 2). US diagnosed intussusception in the 4 patients with the classic triad as well as the 8 patients without it.

Searching for intussusception is easy to perform because of its relatively large size and characteristic appearances. Its widest diameter is usually 3 cm. or greater.[8] The majority of intussusception (88%) were found in transverse or subhepatic portion of colon.[8] In our patients, most of them are located in the right side of abdomen. Examination should be done throughout the abdomen especially in case without palpable mass.

US can demonstrate intussusception even through it is ileoileal type. But it could be difficult to recognize that it is ileoileal type. This may cause problem when trying to reduce it either by barium, air or saline enema. If barium enema is performed and results in negative study, intussusception should not be excluded yet. GI-follow through or CT scan should be considered.

CONCLUSION

Retrospective study of intussusception was done. Intussusception was correctly diagnosed and correctly excluded by US in all cases. It showed characteristic appearance. Clinical signs are frequently not typical, US screening could prevent unnecessary invasive procedures for diagnosis or treatment.

REFERENCES

1. Daniel L. Weissberg, William Scheible, George R. Leopold. Ultrasonographic Appearance of Adult Intussusception. Radiology 1977;124:791-792.
2. Hugo Uhland, Philip F. Parshley. Obscure Intussusception Diagnosed by Ultrasonography. JAMA, Jan 16, 1978 - Vol. 239, No. 3.
3. Richard A. Bowerman, Terry M. Silver, Mark H. Jaffe. Real-Time Ultrasound Diagnosis of Intussusception in Children. Radiology 1982;143:527-529.
4. Martin E. Morin, Douglas H. Blumenthal, Anton Tan, Yuk P. Li. The Ultrasonic Appearance of Ileocolic Intussusception. J. Clin. Untrasound 1981;9:516-518.
5. G. Montali, F. Croce, L. Defra, L. Solbiati. Intussusception of the bowel : a new sonogrophic pattern. BJR 1983;56:621-623.
6. Holt S., Samuel E. Multiple concentric ring sign in the ultrasonographic diagnosis of intussusception. Gastrointest Radiol 1978;-3:307-309.
7. Swischuk LE, Hayden C.K., Boulden T. Intussusception : Indications for ultrasonography and an explanation of the doughnut and pseudokidney signs. Pediatr Radiol 1985;15:388-391.
8. Paul Verschelden, Denis Filiatrault, Laurent Garel, Andree Grignon, Gilles Perreault, Jacques Boisvert, Josee Dubois. Intussusception in Children : Reliability of US in Diagnosis- A Prospective Study. Radiology 1992 ; 184 : 741-744.
9. Edward Weinberger, William D. Winters. Intussusception in Children : The Role of Sonography. Radiology 1992;184:601-602.
10. Gloria del-Pozo, Jose C. Albillos, Daniel Tejedor. Intussusception : US findings with pathologic correlation : The Crescent-in-Doughnut Sign. Radiology 1996;199:688-692.
11. Joseph R. Fakhry, Robert N. Berk. The "Target" Pattern : Characteristic Sonographic Feature of Stomach and Bowel Abnormalities. AJR 1981;137:969-972.
12. Donna M. Bhisitkul, Listernick R, Shkolnik A, et al. Clinical Application of US in the Diagnosis of Intussusception. J. Pediatr. 1992;121:182-186.
13. Alessi V, Salerno G. The "Hayfork" sign in the ultrasonic diagnosis of intussusception. Gastrointest Radiol 1985;10:177-179.
14. Alfred B. Kurtz, Barry B. Goldberg. Gastrointestinal Ultrasonography. Clinics in diagnostic ultrasound 23. Churchill Livingstone, 1988, P.210-211.
15. Sandra L. Hagen-Ansert. Textbook of Diagnostic Ultrasonography, Mosby-Year Book, Inc., 4th edition, 1995, P.428-431.

Tc-99m MIBI MAMMOSCINTIGRAPHY : A FUNCTIONAL IMAGING FOR BREAST CANCER

Molrudee EKMAHACHAI, M.D.,[1] Nonglak VILASDECHANON, M.Sc.,[1]
Chanpen VONGBOONTAN, Cert. in Rad.Tech.,[1] Sombut BOONYAPRAPA, M.D.[1]

ABSTRACT

Drug resistance of malignant cells is a major cause of failure in cancer chemotherapy. Multidrug resistance (MDR) mediated by the transmembrane pump P-glycoprotein (Pgp) is an important mechanism of tumor resistance against chemotherapy. Recent study by Ciarmiello et al reported that Tc-99m MIBI efflux from the breast cancers with high levels of Pgp was significantly faster than that observed in cancers with low Pgp levels. The purpose of our study was to evaluate the pattern and characteristic of Tc-99m MIBI uptake in the breast cancers.

METHODS

The Tc-99m MIBI mammoscintigraphies were performed in 16 female patients with suspected of breast cancer, age range 32-73 years, mean 52 years. The early and delayed planar images of the breasts were obtained at 20 minutes and 1 hour after injection with 20 millicuries of Tc-99m MIBI intravenously. The Tc-99m MIBI tumor indices were also calculated and analyzed.

RESULTS

All patients had the final diagnosis of infiltrating ductal carcinoma of the breast. Our results revealed two different patterns of Tc-99m MIBI uptake within the breast carcinomas. Of the 16 patients, 15 patients (93.75%) had negative value of the MIBI tumor index (washout pattern) and one patient (6.25%) had the positive value (accumulation pattern).

CONCLUSION

From our study, we found different patterns of Tc-99m MIBI biokinetic changes within the breast cancers. Therefore, we consider that the Tc-99m MIBI mammoscintigraphy may not only be useful for the diagnosis, but also for the prediction of chemotherapeutic response in the patients with breast cancer.

INTRODUCTION

Drug resistance of malignant cells is a major cause of failure in cancer chemotherapy. Multidrug resistance (MDR) mediated by the transmembrane pump P-glycoprotein (Pgp) is an important mechanism of tumor resistance against chemotherapy. Pgp is a 170 kDa membrane transport protein present in many normal tissue and tumors, which appears to function as a cellular efflux pump of a variety of potent chemotherapeutic agents.[1,2]

Technetium-99m Sestamibi (Tc-99m MIBI) is a lipophilic cationic isonitrile analog that has been used for myocardial perfusion imaging as an alternative to Thallium-201 since 1989.[3] Later,

[1] Department of Radiology, Faculty of Medicine, Chiang Mai University, Chiang Mai 50200, THAILAND

Tc-99m MIBI has been accepted as a tumor imaging agent for detection a number of benign and malignant tumors in clinical imagings.[4-7] The use of Tc-99m MIBI as a new agent for mammoscintigraphy was initially reported by Campeau et al in 1992.[8] In the past several years, a number of reports have indicated that Tc-99m MIBI mammoscintigraphy is an effective procedure in the diagnosis of breast carcinomas.[9-15] Recent publications have shown that breast imaging with Tc-99m MIBI has a high sensitivity and improved the specificity of conventional mammography for the diagnosis of breast cancer.[9,12,16,17] It was recently reported that Tc-99m MIBI is a Pgp transport substrate, and thus Tc-99m MIBI scintigraphy may be used as a noninvasive imaging to detect the Pgp expression in human tumors in vivo.[1,18,19] The study by Ballinger et al also supported the potential use of Tc-99m MIBI for functional imaging of Pgp activity in patients undergoing chemotherapy.[2] Interestingly, recent study by Ciarmiello et al which performed the Tc-99m MIBI mammoscintigraphy in patients with breast cancer, showed that Tc-99m MIBI efflux from the breast cancers with high levels of Pgp was significantly faster than that observed in cancers with low Pgp levels.[20]

We proposed Tc-99m MIBI mammoscintigraphy as a functional imaging for breast cancers and the purpose of our study was to evaluate the pattern and characteristic of Tc-99m MIBI uptake within the breast cancers.

MATERIALS AND METHODS

Sixteen female patients with suspected of breast carcinoma aged 32 - 73 years, mean 52 years were referred for the Tc-99m MIBI mammoscintigraphy. All patients had palpable breast masses. The lesion size ranged from 2.0-8.0 cm in diameter (mean 4.2 cm) by mammographic or physical findings. Five of these also had ipsilateral palpable axillary nodes, and one had both ipsilateral axillary and supraclavicular node palpable. All of them underwent surgery and/or fine needle aspiration biopsy of the breasts for the final diagnosis.

The mammoscintigraphy were performed with intravenous injection of 20 mCi of Tc-99m MIBI in the arm contralateral to the abnormal breast. Planar anterior imagings were obtained including both breasts and axillary regions at 20 minutes (early image) and 1 hour (delayed image) after injection, with the patients in supine position, the arms were raised and the hands were placed behind the head. Additional posterior oblique views of the breast were also imaged in the upright position. The Tc-99m MIBI mammoscintigraphies were acquired with a preset time of 2 minutes for each image in 256 x 256 matrix, using a large-field-of-view gamma camera (Apex-SP4 Elscint), equipped with low energy general purpose collimator.

Furthermore, the regions of interest were drawn over areas of increased Tc-99m MIBI uptake in the primary tumors, in order to get the numbers of counts from both early and delayed images in every patient. Then, the Tc-99m MIBI tumor indices were calculated and analyzed by using the following formula.

$$\text{MIBI tumor index} = \frac{\text{(Counts at 1 hour - Counts at 20 min)}}{\text{Counts at 20 min}} \times 100\ \%$$

RESULTS

All patients had the final diagnosis of infiltrating ductal carcinoma of the breast, proven by surgery and/or biopsy.

The early and delayed Tc-99m MIBI mammoscintigraphic results demonstrated focal areas of increased uptake that corresponded to the palpable breast masses in all patients. In addition to the uptake of Tc-99m MIBI in primary breast tumors, 5 of these also revealed other focal areas of increased uptake in the palpable axillary nodes, and one showed positive MIBI uptake in the regional axillary and supraclavicular lymph node metastases. However, the breast cancers in our study were all palpable and rather big in size, with the smallest is 2.0 cm in diameter.

As compared the two interval early and delayed mammoscintigraphic findings in each patient, and also from the analysis of the MIBI tumor indices, we found that there were two types of Tc-99m MIBI uptake within the breast tumors, which were classified as washout and accumulation patterns. Of the 16 patients , 15(93.75%) had negative value of the MIBI tumor index (washout pattern), which ranged from -12.77% to -40.07%, mean -23.56%. The remainder one patient(6.25%) had positive value of the MIBI tumor index (accumulation pattern), which was +1.26%.

DISCUSSION

Tc-99m MIBI is a lipophilic cationic agent, which accumulates within the mitochondria and cytoplasm of cells on the basis of electrical potentials generated across the cell membranes.[3] The exact mechanism of Tc-99m MIBI uptake in tumor cells is not yet clearly understood. However, it is considered to be multifactorial, including regional blood flow, viability, cellularity, metabolic activity, mitochrondrial activity, plasma membrane potentials and Pgp expression in tumor cells.[3,21-23] The Pgp is an energy-dependent transmembrane efflux pump, which decreases the accumulation of a broad spectrum of chemotherapeutic drugs, including anthracyclines, vinca alkaloids, podophylotoxins, actinomycin-D, and mitomycin within the tumor cells.[24] The presence of Pgp overexpression represents an expression of MDR in patients with cancer.[21,25] Previous study from France found that Tc-99m MIBI uptake by cells expressing no immunodetectable levels of Pgp was significantly higher than that by cells expressing high Pgp levels.[19] Ballinger et al from Canada performed Tc-99m Sestamibi imaging study in a rat breast tumor cell line and its doxorubicin-resistant variant, and found that Tc-99m MIBI washed out of the resistant tumors at three times the rate of non-resistant tumors.[2] Therefore, the mammoscintigraphy using Tc-99m MIBI has been proposed as a noninvasive imaging method in demonstrating Pgp expression or MDR tumor in many recent series.[20,25]

Conventional mammography is still the only imaging examination recommended for breast cancer screening. However, Tc-99m MIBI scintigraphy plays an important role as a complementary imaging to mammography especially in patients with dense breast or equivocal mammographic findings.[10] Tc-99m MIBI mammoscintigraphy is well accepted as a sensitive test in detecting primary breast carcinoma, moreover it can detect the axillary lymph node metastases as well.[11,26,27] Like in our study, in addition to uptake in the primary breast tumors, we found Tc-99m MIBI uptake in the axillary node metastases in 5 patients, and in one patient we found Tc-99m MIBI uptake in the primary left breast cancer, left axillary nodes, and also in left supraclavicular node metastases as well.

The MIBI tumor index were derived from percent difference between the early and delayed tumor counts, thus the MIBI tumor index represented the Tc-99m MIBI washout from or accumulation within the tumors. From the

literature review, we found that Tc-99m MIBI uptake related to the Pgp levels within the tumor cells.[2,19,20] Therefore, we consider that the Tc-99m MIBI tumor index, may relate to the difference of Pgp levels within the tumor cells as well. Of the 16 patients, one patient with positive value of MIBI tumor index represented Tc-99m MIBI accumulation within the breast tumor, may probably associate with no Pgp expression of the tumor cells. The remainder 15 patients with varying range of negative MIBI tumor index indicated different rate of washout of Tc-99m MIBI from those breast tumors. In contrast to the former assumption, the washout pattern may probably relate to the different Pgp expression within the tumor cells in those patients.

However, further studies are required to confirm whether theTc-99m MIBI tumor index relates to the difference of Pgp levels within the tumor cells or not, and if so this finding will be very helpful in the prediction of chemotherapeutic response in the patients with breast cancer.

In conclusion, Tc-99m MIBI mammoscintigraphy is a simple, noninvasive and useful imaging in the detection of breast carcinoma. Our results revealed different patterns of Tc-99m MIBI biokinetic changes within the breast cancers. Therefore, we consider that the Tc-99m MIBI mammoscintigraphy may not only be useful for the diagnosis, but also for the prediction of chemotherapeutic response in the patients with carcinoma of the breast.

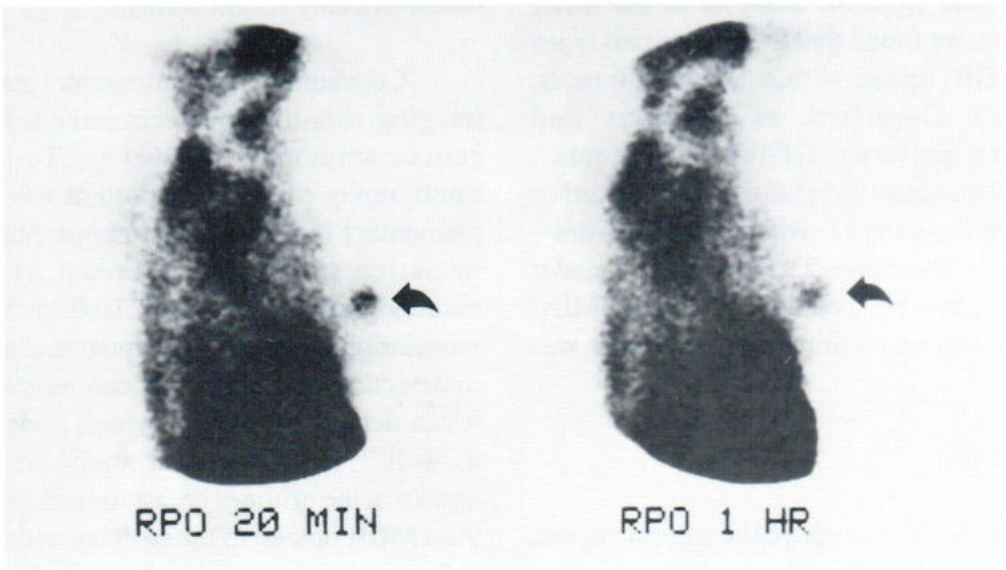

Fig. 1. A 44-year-old woman presented with a palpable right breast mass. Physical examination revealed a 4-cm right breast mass at the upper outer quadrant. Right posterior oblique views of Tc-99m MIBI mammoscintigraphy performed at 20 minutes and 1 hour after injection, show definite focal increased uptake in the right breast tumor (curve arrows). The MIBI tumor index was -20.93%, which represented washout of the Tc-99m MIBI from the breast tumor. Biopsy findings corresponded to infiltrating ductal carcinoma.

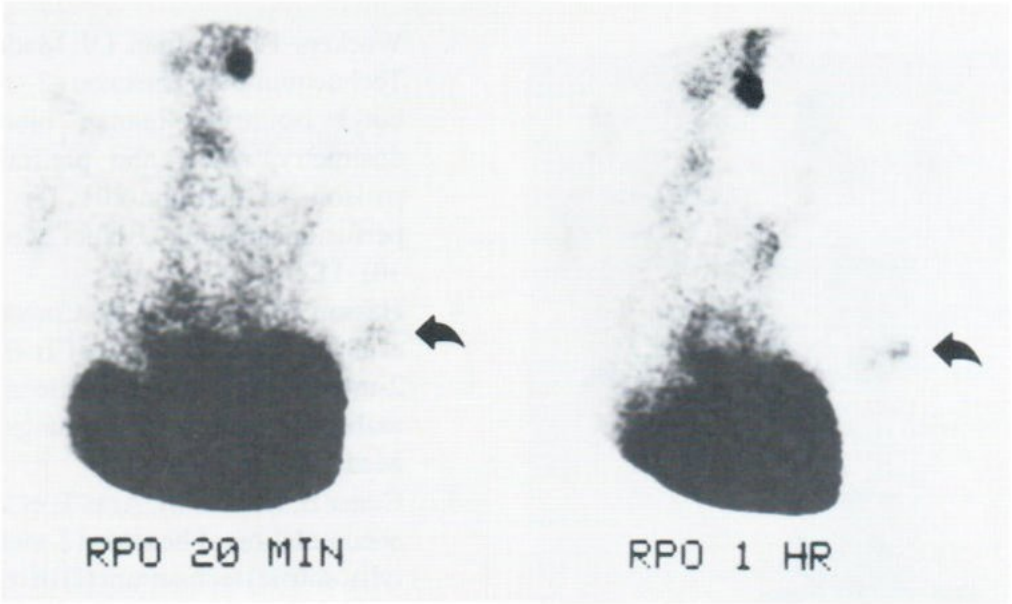

Fig. 2. A 48-year-old woman presented with a palpable right breast mass. Physical examination revealed a 6-cm right breast mass at the central portion. Early and delayed images of Tc-99m MIBI mammoscintigraphy obtained in the right posterior oblique view reveal an area of focal increased uptake in the right breast tumor (curve arrows) that corresponded to the palpable breast mass, with accumulation pattern. The MIBI tumor index was +1.26%. The final diagnosis was infiltrating ductal carcinoma, proven by surgery.

Fig. 3. Anterior view of Tc-99m MIBI mammoscintigraphy performed at 20 minutes after injection, demonstrates definite focal increased uptake in the primary right breast tumor (thick arrow) and ipsilateral axillary lymph node metastases (curve arrow). Moreover, diffuse increased uptake in the soft tissue of right breast surrounding the primary tumor (thin arrow) is also noted, represents skin involvement of the cancer. These scintigraphic findings corresponded to the physical examination. Biopsy of the right breast mass revealed an infiltrating ductal carcinoma.

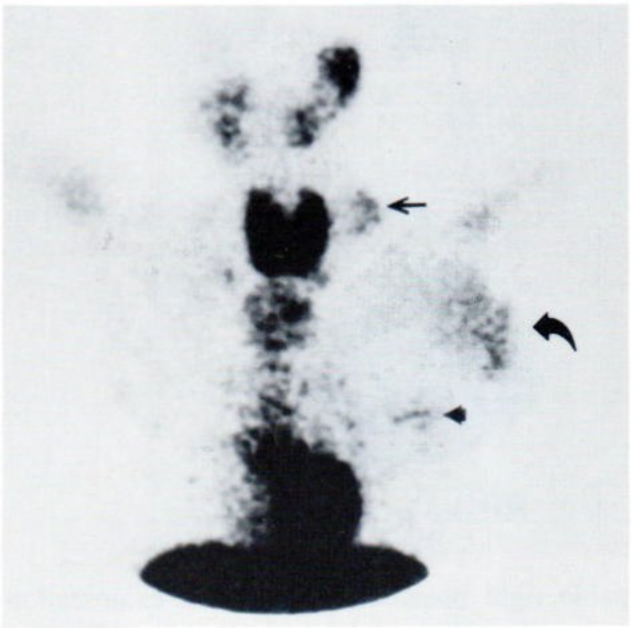

Fig. 4. Early anterior image of Tc-99m MIBI mammoscintigraphy reveals focal areas of increased uptake in the primary left breast tumor (arrow head), ipsilateral axillary node (curve arrow) and supraclavicular lymph node metastases (thin arrow), corresponding with the physical findings. Biopsy of the left breast mass indicated infiltrating ductal carcinoma.

REFERENCES

1. Piwnica-Worms D, Chiu ML, Budding M, et al. Functional imaging of multidrug-resistant P-glycoprotein with an organo-technetium complex. Cancer Res 1993;53:-977-84.
2. Ballinger JR, Hua HA, Berry BW, et al. Tc-99m sestamibi as an agent for imaging P-glycoprotein-mediated multi-drug resistance: In vitro and in vivo studies in a rat breast tumour cell line and its doxorubicin-resistant variant.Nucl Med Commun 1995;-16: 253-7.
3. Wackers FJ, Berman DJ, Maddahi J, et al. Technetium-99m - hexakis - 2 - methoxyisobutyl isonitrile: human biodistribution, dosimetry, safety and preliminary comparison to thallium-201 for myocardial perfusion imaging. J Nucl Med 1989;30:-301-11.
4. Hassan IM, Sahweil A, Constantinides C, et al. Uptake and kinetics of Tc-99m-hexakis 2-methoxy isobutyl isonitrile in benign and malignant lesions of the lungs. Clin Nucl Med 1989; 14: 333-40.
5. Caner B, Kitapci M, Aras T, et al. Increased accumulation of hexakis (2-methoxyisobutylisonitrile) technetium (I) in osteosarcoma and its metastatic lymph nodes. J Nucl Med 1991; 32: 1977-8.
6. Taillefer R, Boucher Y, Potvin C, et al. Detection and localization of parathyroid adenomas in patients with hyperparathyroidism using a single radionuclide imaging procedure with Technetium-99m-Sestamibi (double-phase study). J Nucl Med 1992;33:-1801-7.
7. Bagni B, Pinna L, Tamarozzi R, et al. SPET imaging of intracranial tumours with Tc-99m-sestamibi. Nucl Med Com 1995;16:-258-64.
8. Campeau RJ, Kronemer KA, Sutherland CM. Concordant uptake of Tc-99m Sestamibi and Tl-201 in unsuspected breast tumor. Clin Nucl Med 1992;17:936-7.
9. Khalkhali I, Cutrone JA, Mena IG, et al. Scintimammography: The complementary role of Tc-99m sestamibi prone breast imaging for the diagnosis of breast carcinoma. Radiology 1995;196:421-6.
10. Khalkhali I, Mena I, Diggles L. Review of imaging techniques for the diagnosis of breast cancer: a new role of prone scintimammography using technetium-99m sestamibi. Eur J Nucl Med 1994;21:57-62.

11. Taillefer R, Robidoux A, Lambert R, et al. Technetium-99m-Sestamibi prone scinti-mammography to detect primary breast cancer and axillary lymph node involvement. J Nucl Med 1995;36:1758-65.
12. Khalkhali I, Cutrone J, Mena I, et al. Technetium-99m - Sestamibi scintimammography of breast lesions: Clinical and pathological follow-up. J Nucl Med 1995;-36:1784-9.
13. Palmedo H, Schonburg A, Grunwald F, et al. Technetium-99m MIBI scintimammography for suspicious breast lesions. J Nucl Med 1996;37:626-30.
14. Villanueva-Meyer J, leonard Jr MH, Briscoe E, et al. Mammoscintigraphy with technetium-99m Sestamibi in suspected breast cancer. J Nucl Med 1996;37:926-30.
15. Khalkhali I, Cutrone J, Mena I, et al. Clinical and pathologic follow-up of 100 patients with breast lesions studied with scintimammography [abstract]. J Nucl Med 1994;-35:22P.
16. Waxman A, Nagaraj N, Ashok G, et al. Sensitivity and specificity of Tc-99m methoxy isobutyl isonitrile (MIBI) in the evaluation of primary carcinoma of the breast: comparison of palpable and non-palpable lesions with mammography [abstract]. J Nucl Med 1994;35:22P.
17. Palmedo H, Grunwald F, Bender H, et al. Scintimammography with technetium-99m methoxyisobutylisonitrile: comparison with mammography and magnetic resonance imaging. Eur J Nucl Med 1996;23:940-6.
18. Rao VV, Chiu ML, Kronauge JF, et al. Expression of recombinant human multidrug resistance P-glycoprotein in insect cells confers decreased accumulation of Technetium-99m-Sestamibi. J Nucl Med 1994;35:510-15.
19. Cordobes MD, Starzec A, Delmon-Moingeon L, et al. Technetium-99m Sestamibi uptake by human benign and malignant breast tumor cells: Correlation with mdr gene expression. J Nucl Med 1996;37:286-9.
20. Ciarmiello A, Del Vecchio S, Potena MI, et al. Tc-99m Sestamibi efflux and P-glycoprotein expression in human breast carcinoma [abstract]. J Nucl Med 1995;36:129P.
21. Derebek E, Kirkali Z, Dogan AS, et al. Tc-99m MIBI scintigraphy in metastatic renal cell carcinoma: clinical validation of the relationship between Tc-99m MIBI uptake and P-glycoprotein expression in tumour tissue. Eur J Nucl Med 1996;23:976-9.
22. Crane P, Laliberte R, Heminway S. Effect of mitochondrial viability and metabolism of technetium-99m-sestamibi. Eur J Nucl Med 1993;20:20-25.
23. Piwnica-Worms D, Holman BL. Noncardiac applications of hexakis-(alkylisonitrile) technetium-99m complexes. J Nucl Med 1990;31:1166-7.
24. Lum BL, Fisher GA, Brophy NA. Clinical trials of modulation of multidrug resistance: pharmacokinetic and pharmacodynamic considera-tions. Cancer 1993;72 Suppl:-3502-14.
25. Moretti JL, Azaloux H, Boisseron D, et al. Primary breast cancer imaging with technetium-99m sestamibi and its relation with P-glycoprotein overexpression. Eur J Nucl Med 1996;23:980-6.
26. Kao CH, Wang SJ, Yeh SH. Tc-99m MIBI uptake in breast carcinoma and axillary lymph node metastases. Clin Nucl Med 1994;19:898-900.
27. Lam WWM, Yang WT, Chan YL, et al. Detection of axillary lymph node metastases in breast carcinoma by technetium-99m sestamibi breast scintigraphy, ultrasound and conventional mammography. Eur J Nucl Med 1996;23:498-503.

บริษัท คงศักดิ์เอ็กซเรย์การแพทย์อุตสาหกรรม จำกัด
KONGSAK X-RAY MEDICAL INDUSTRY COMPANY LIMITED
212/1 PHAHONYOTHIN SOI 55 BANGKHEN BANGKOK 10220
TEL. 5213214, 5511794 CABLE: KELEX FAX: 5523744

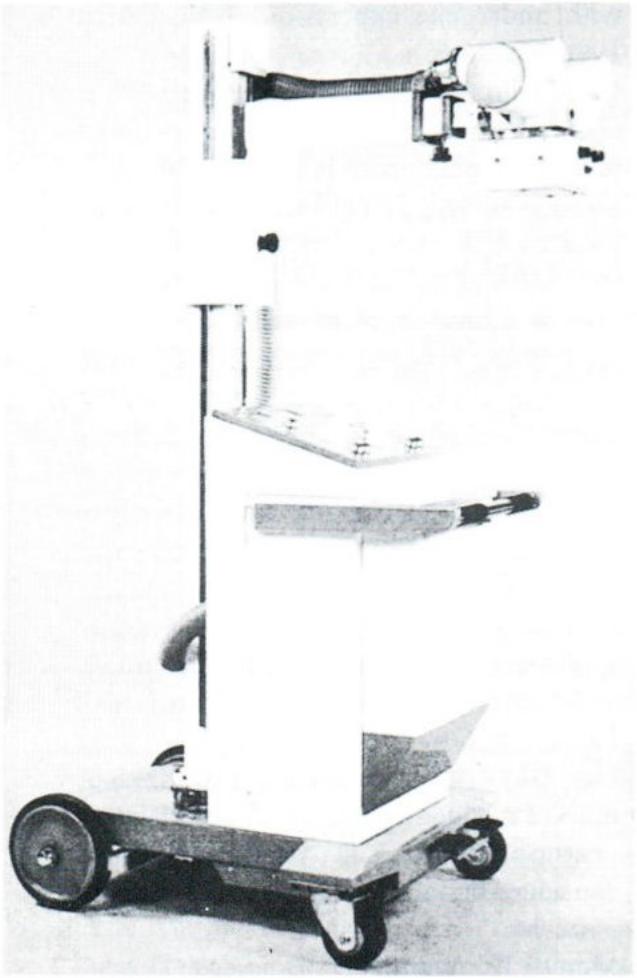

KELEX
50 mA 100 KV MOBILE TYPE DIAGNOSTIC X-RAY UNIT MODEL MD 50-99

- # เหมาะสำหรับคลินิคเอกชนและโรงพยาบาลทั่วไป
- # มีช่างผู้ชำนาญให้การบริการ ตลอดอายุการใช้งาน
- # พร้อมทั้งจำหน่ายอุปกรณ์เอ็กซเรย์

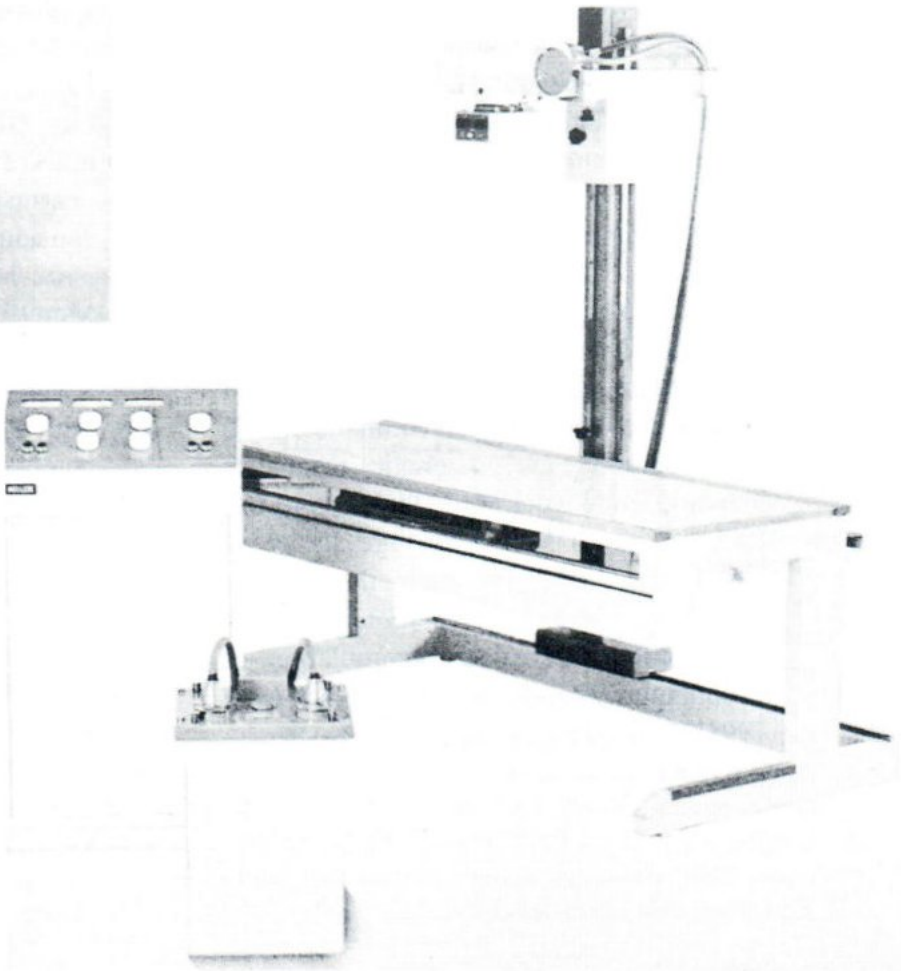

KELEX
MD 100-99 X-RAY SYSTEM
FULL WAVE 100 MA 100 KV

SPINAL CANAL DIAMETERS AND THEIR RELATIONSHIP TO CERVICAL SPINE GLIOSIS IN MAGNETIC RESONANCE IMAGING

Dr Thomas CHEE,[1] Dr FL THOO,[2] Dr CS YU[3]

ABSTRACT

To determine the most frequent levels of atraumatic cervical spine cord gliosis in cervical spondylosis and relationship, if any, between cervical spine gliosis and the degree of adjacent cervical stenosis on Magnetic Resonance Imaging (MRI). Preliminary results of post-surgical outcome was obtained for patients with pre-op cervical cord gliosis.

MATERIAL AND METHODS

89 MRI examinations of the cervical spine performed in a hospital setting over a period of 1 year from June 93 to May 94 were reviewed. Magnetic Resonance Imaging examination showing cord changes consistent with gliosis without a history of trauma were selected for analysis. 13 patients with MRI features of gliosis were studied. MRI features of gliosis include high intensity signals on T2 weighted and proton density sequence which is usually well defined and with no mass effect.

Using the sagittal and axial SE T1W and FSE T2W images acquired on a GE Signa Horizon 1.5 T Echospeed, measurements were made of the relevant spinal canal diameters. The cranio-caudal extent of gliosis of the cervical cord was also recorded.

Additionally, the causes of the spinal canal stenosis were determined and the subsequent treatment including operative findings and followup management were determined from the patient's clinical notes.

At each intervertebral junction from C1-2 to C7-T1 levels, the mid sagittal diameter was measured in the sagittal and axial planes of the MRI examination. At each level, two measurements were taken. The actual diameter (AD) is the actual diameter of the spinal canal and the expected diameter (ED) is measured by extending an imaginary border of the where the canal margins should be, if there was no pathology present (Figure 1a &1b). A ratio of the actual diameter over the expected diameter was then calculated and an attempt was made to correlate these ratios with presence or absence of adjacent gliosis and extent of gliosis.

[1,2] Department of Diagnostic Imaging
[3] Department of Orthopaedic Surgery

CORRESPONDENCE TO : Dr Thomas Chee / Dr FL Thoo, Department of Diagnostic Imaging, Tan Tock Seng Hospital Moulmein Road, Singapore 308099

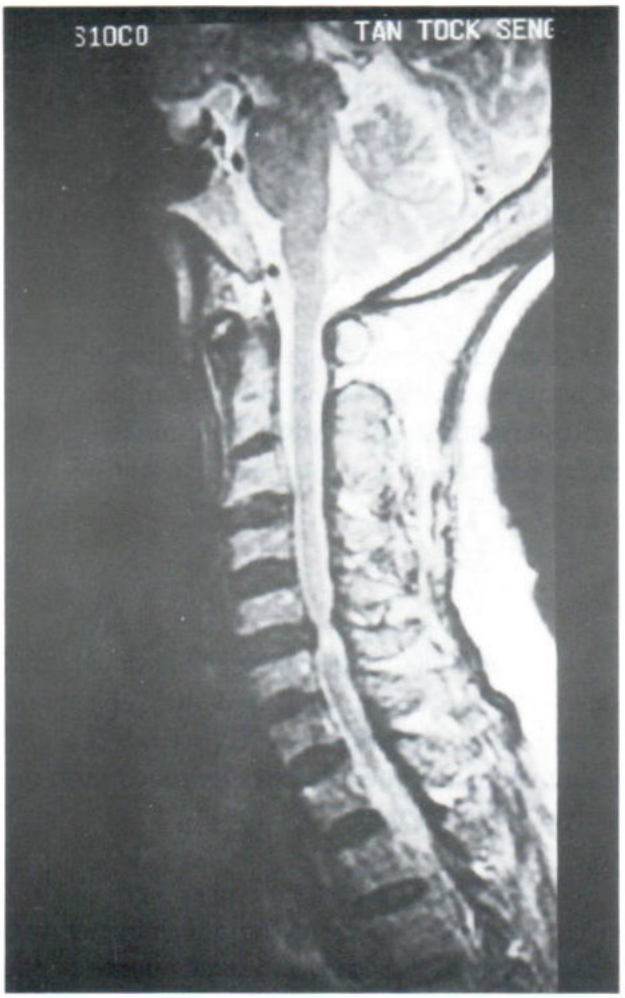

Fig 1a. T2-weighted MR image shows the measurements of the actual diameter, AD (white arrow) and the expected diameter, ED (black arrow) of the spinal canal in the sagittal plane.

RESULTS

There were 13 patients, 10 males and 3 females (12 Chinese and 1 Indian) with cervical cord gliosis. Their ages range from 33 to 82 years with a mean of 56 years. The patients at presentation gave a history of symptoms varying from 3 weeks to several years.

Cervical spine gliosis was seen from C2 to C6 vertebral levels. 10 patients had gliosis involving one intervertebral level and 3 patients had gliosis affecting 2 intervertebral levels. Therefore, a total of 16 intervertebral levels of gliosis were seen in these 13 patients. Analysis of these 16 intervertebral levels showed that the most frequent level of gliosis was at C3-4 (8 cases), followed by C4-5 (4 cases) as illustrated by Fig. 2 below.

The gliosis was most frequently caused by a combination of disc herniation and osteophytes in 9 patients. This is followed by disc herniation by itself in 2 patients and a combination of osteophytes, ligamentum flavum and facet joint hypertrophy in the remainder 2 patients. Cervical cord gliosis is associated with cervical atrophy in 38% of the patients.

Where gliosis was present, the associated sagittal spinal canal stenosis ratio varied widely from 0.25 to 0.88 and the axial spinal canal stenosis ratio varied from 0.43 to 0.9. Where the cord showed no gliosis the associated sagittal spinal canal stenosis ratio ranged from 0.5 to 1 and the axial spinal canal stenosis ratio ranged from 0.55 to 1. No specific relationship was demonstrated between the degree of cervical canal stenosis and the gliosis.

As expected, there is a general trend for the sagittal and axial ratios to be fairly similar in value at intervertebral levels with gliosis as illustrated in (Fig. 3.)

The location of the gliosis in relationship to the causative intervertebral levels was next evaluated. One of the thirteen patients was noted to have a long segment stenosis extending over two vertebral levels. As it was difficult to ascertain whether the site of gliosis occurred at or below the canal stenosis in this patient, he was excluded for this evaluation. Two of the remaining twelve patients were noted to have gliosis involving two intervertebral levels. Therefore, 14 intervertebral levels were evaluated for the site of gliosis in relation to the canal stenosis; this is illustrated in (Fig. 3.) 64% of the gliosis occurred below the site of the canal stenosis as compared to 36% at the level of the canal stenosis. (Fig. 4)

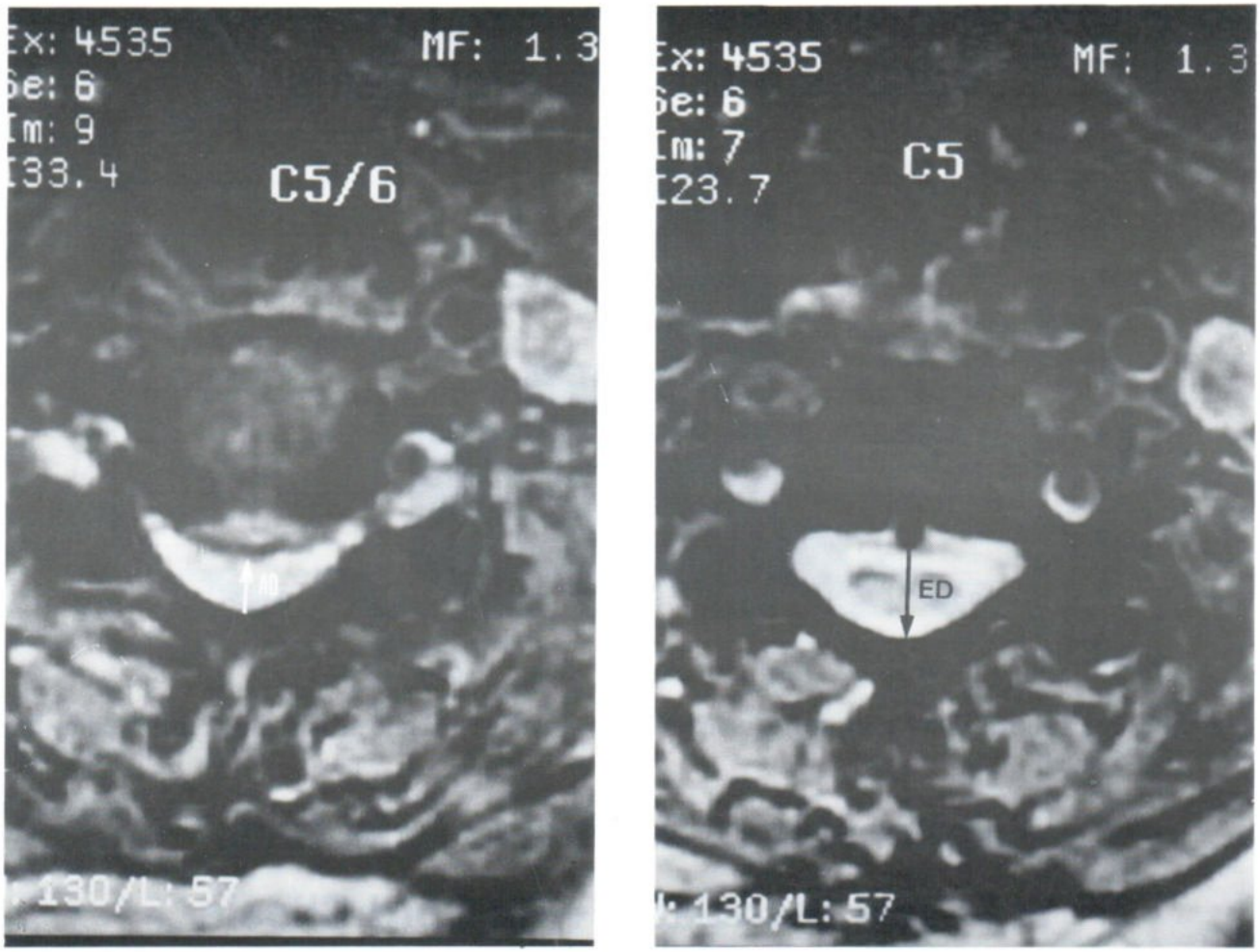

Fig 1b. T2-weighted images show the measurements of the actual diameter, AD (white arrow) and the expected diameter, ED (black arrow) of the spinal canal in the axial planes.

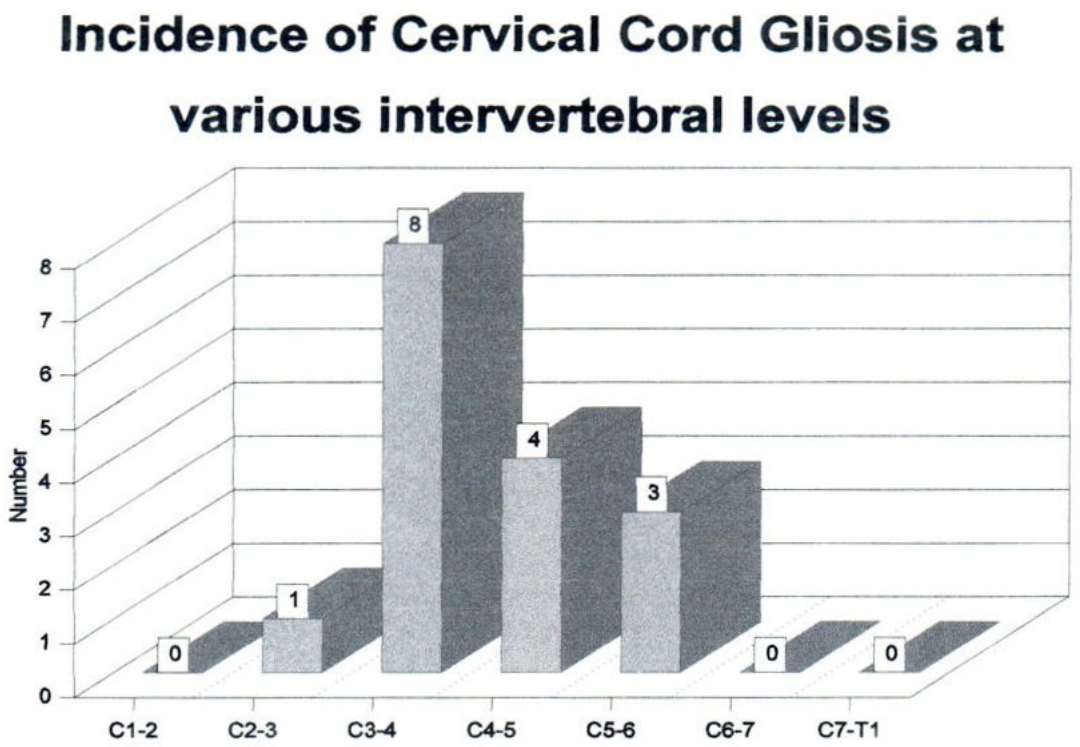

Fig 2. Bar chart shows that the most frequent level for cervical cord gliosis is at C3-4, followed by the C4-5 level.

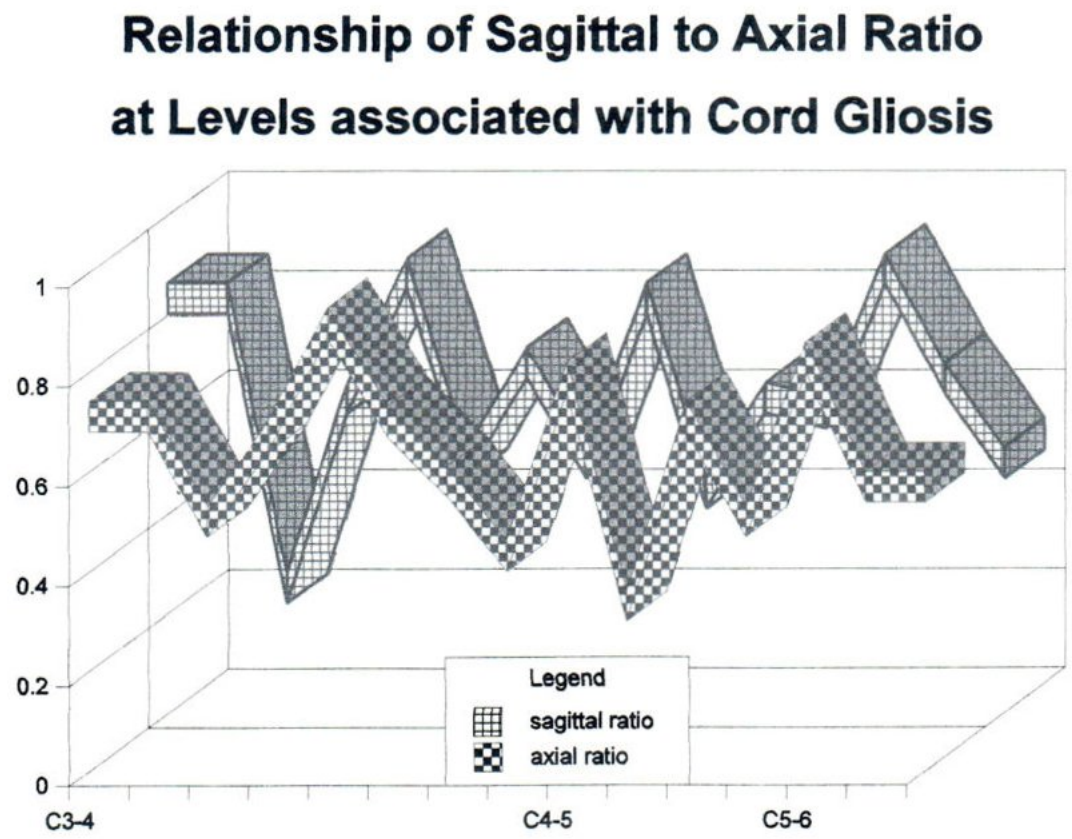

Fig. 3 Illustrates the relationship between the sagittal ratio and the axial ratio of diameters calculated at the various intervertebral levels associated with cervical cord gliosis.

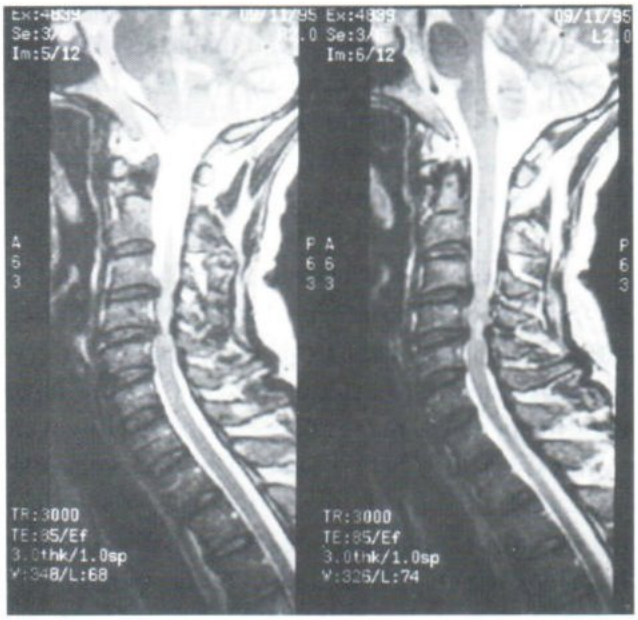

Fig. 4a. T2-weighted sagittal MR image shows gliosis at the level of stenosis.

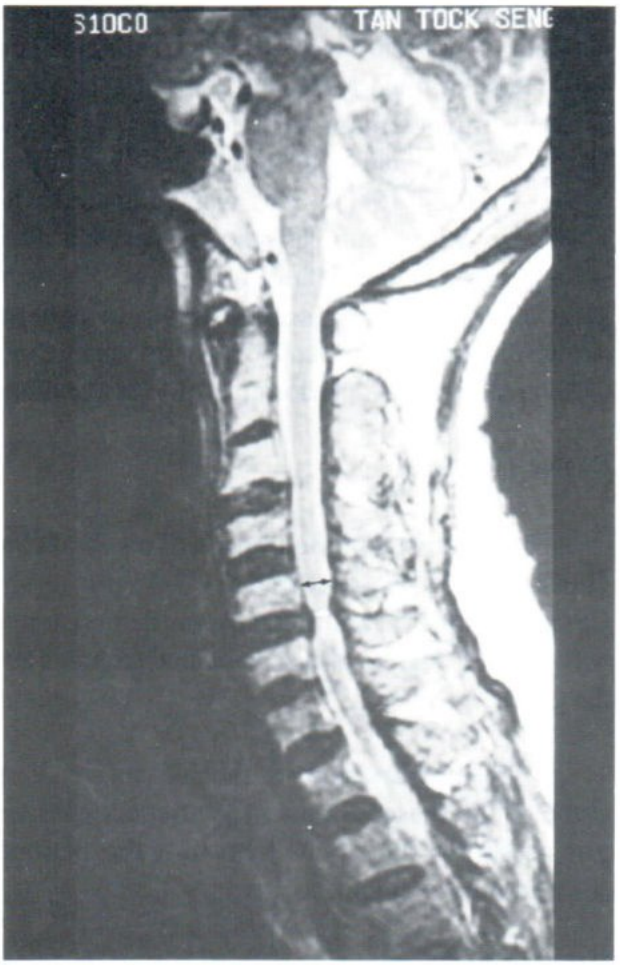

Fig. 4b. T2-weighted sagittal MR image shows gliosis at level caudad to stenosis.

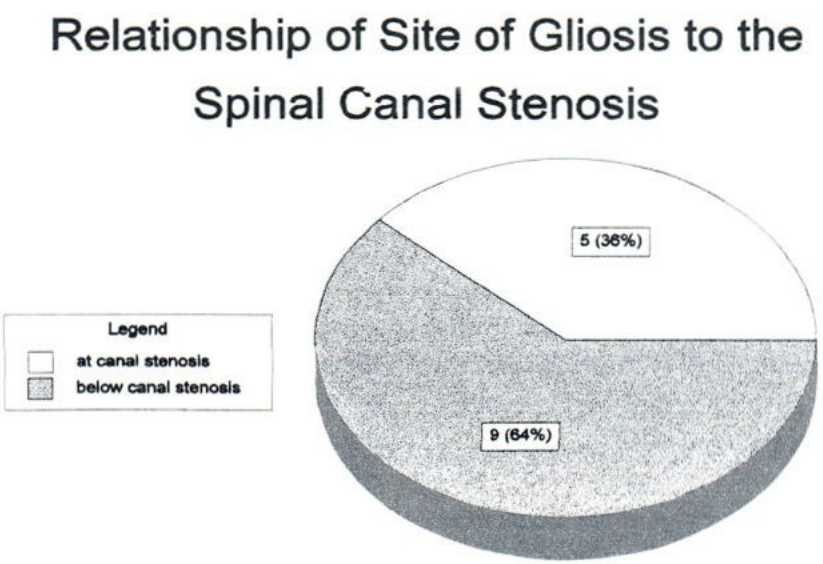

Fig. 5 Illustrates the relationship between the site of gliosis to the spinal canal stenosis in the 13 intervetebral levels evaluation in 11 patients.

On review of the clinical notes of these 13 patients, 11 patients went for cervical spine surgery. Post surgical follow up 6 months to a year showed improvement in 6 patients (55%), no change in 4 patients (36%) and deterioration of gait in 1 patient (9%). This was compared with 12 patients without gliosis who had cervical spine surgery who did not default follow up. Post surgical follow up in the second group of patients showed improvement in 9 (75%), no change in 2 (17%) patients and deterioration in 1 (8%) patient.

CONCLUSION

The most common levels of cervical cord gliosis in this study occurred at C3-4 followed by C5-6. No specific relationship was demonstrated between the degree of cervical canal stenosis and the gliosis.

Preliminary study of the post surgical outcome of the these 13 patients with cervical cord gliosis shows that more than half the patients showed improvement.

DISCUSSION

Innumerable aetiologies are responsible for narrowing the spinal canal. Besides acquired diseases, narrow spinal canal can also be associated with syndromes such as Achondroplasia, hypochondroplasia, pseudohypoparathyroidism and diastrophic dwarfism.[1]

However, the more common causes of spinal block include widespread malignancy, neural tumours and disorders of intervertebral joints. Intervertebral joint pathology is believed to be the third commonest cause of spinal block, responsible for up to 15% of such cases.[2]

Included in this subgroup are degenerate disease,[3] microtrauma or calcification of the posterior longitudinal ligament[4] and disc prolapse.

It has been previously recognised that spinal canal stenosis is most frequent at the C5-6 level. It is estimated that 90% of intervertebral disc herniation occur at the C5-6 and C6-7 levels and most of these herniations are degenerative in origin.[5] At the C5-6 level the spinal cord occupies a spinal canal space usually only 1.8 times as large as the spinal cord and a dural sac about 1.2 times as large as itself.[6]

The arterial supply to the cervical spinal cord is through the anterior spinal artery which is a branch originating from the vertebral arteries prior to their joining the basilar artery. This artery supplies the anterior two thirds to four-fifths aspect of the spinal cord.

The posterior aspect of the spinal cord is supplied by the paired posterior spinal arteries which also originates from the vertebral artery. Notably these two arterial systems do not have significant anastomoses between them. However, at the C3-4 to C7-T1 vertebral body levels (except at the C6-7 level), the vertebral, thyrocervical and costocervical arteries give off radicular branches which anastomose with the spinal arteries. The venous drainage is comparable to this arterial architecture.

The white matter of the central nervous system can be damaged by a variety of causes. Trauma, either chronic or acute, can result in Wallerian degeneration which refers to the antegrade degeneration of axons and their accompanying myelin sheath. It results from injury to the proximal portion of the axon or its cell body.[7]

In spinal cord injury one expects to visualize Wallerian degeneration in the corticospinal tracts below the lesion and in the dorsal columns above the lesion.[8] Several reports of MR Imaging of Wallerian degeneration have been published and even staging of it has been proposed.[9,10]

In the staging proposed for the brain by Kuhn et al,[7] Stage I represents physical degradation of the axon with little biochemical change in

the myelin. No abnormality on MR Imaging is seen in this stage which occurs in the first four weeks.

At four to fourteen weeks, the myelin protein breaks down and the tissues becomes more hydrophobic. This is Stage 2. The high lipid-protein ratio causes the hypointense signal on T2W MRI.

After fourteen weeks, which is termed Stage 3, the tissue becomes more hydrophilic with myelin lipid breakdown and hyperintense signal on T2W images.

The final Stage 4, sees volume loss from atrophy.

These changes in signal intensity would likely be similar to Wallerian degeneration in the spinal cord.[8]

In cord compression, the myelopathy resulting from it produces abnormally high signal intensity within the cord. This is believed to be due to myelomalacic changes.[5]

In the work published by J Becerra et al,[8] Wallerian degeneration in the spine was identified by MR at seven weeks and longer following injury. This corresponded to Stage 2 of Kuhn (4 - 14 weeks) in Wallerian degeneration in the brain.[9] Becerra et al believed their analysis explains abnormal MR signals at sites away from the centre of injury.

In our series 64% of the gliosis occurred below the site of canal stenosis and cord impingement. This possibly implies that in such situations there seems to be a predominance of associated descending degeneration.

This compared with only 36% of gliosis occuring only at the site of the stenosis.

In a study by Bucciero et al,[11] they reviewed 35 cervical spondylotic myelopathy patients showing high signal intensity within the cervical cord on T2 and proton density weighted MR images. They then measured on axial images, the ratio of the anteroposterior diameter to the transverse diameter (anteroposterior compression ratio or APCR at the most compressed segment of the cervical cord and compared this with the patient's neurological status. Their findings revealed patients having a better neurological status if their APCR was 40% or more, and following surgery, patients with preoperative APCR of 15% or more improved after the operation. Those patients who were unchanged postoperatively had pre-operative APCR of 10% or less.

Whilst our study did not primarily attempt to correlate surgical outcome with the degree of canal stenosis, we did discover that 55% of patients with gliotic change of the cevical cord showed improvement post-surgically compared with 75% of patients who did not exhibit gliotic change in the spinal cords on MRI.

We could find no specific correlation between the degree of cervical canal stenosis and the presence or extent of gliosis of the cervical spinal cord.

In concluding, our study showed that the most common level of cervical cord gliosis to be at C3-4 level followed by C5-6 intervertebral level. No specific relationship was found between the degree of cervical canal stenosis and gliosis. Preliminary review of the post-surgical outcome of these 13 patients with cervical cord gliosis shows that more than half the patients showed improvement. This correlates well with an ongoing trial involving the post-surgical outcome of 35 patients with high signal intensity on the T2W sequence prior to surgery.

Further work will be necessry to determine if MRI features of gliosis indeed has any prognostic relationship with post-surgical outcome.

REFERENCES

1. Aids to Radiological Differential Diagnosis, 2nd Edition. Stephen Chapman and Richard Nakielny, Baillere Tindall, pg 68
2. Aids to Radiological Differential Diagnosis, 2nd Edition. Stephen Chapman and Richard Nakielny, Baillere Tindall, pg 70
3. Cervical Stenosis, Spondylosis and Herniated Disc Disease. Jahnke RW and Hart BL, Radiologic Clinics of North America, 29:777-791
4. Spinal Cord Compression due to Ossification of Ligaments. Yamashita Y, Takahashi M, Matsuno Y, et al, MR Imaging, Radiology 175:843-848
5. The Raven MRI Teaching File. MRI of the Spine by Robert B Lufkin, William Bradley Jr, Michael Brant-Zawadzki, Raven Press 1991, pp 188-189
6. Roentgen Diagnosis of the Craniovertebral Region, Springer, Berlin, Heidelberg New York, pp 215-251
7. Wallerian Degeneration after Cerebral Infarction: Evaluation with Sequential MR Imaging by Mathew J Kuhn, David J Mikulis et al, Radiology 1989, 172:179-182
8. MR-Pathologic Comparisons of Wallerian Degeneration in Spinal Cord Injury. Jose L Becerra, Willian R Puckett, Erik D Hiester et al, AJNR 1995 Jan, 16:125-133
9. Wallerian Degeneration: Evaluation with MR Imaging. Kuhn MJ, Johnson KA, Davis KR, Radiology 1988, 168:199-202
10. MR Imaging of Wallerian Degneration in the Brainstem; Temporal Relationships. Inoue Y, Matsumura Y, Fukuda T, et al, AJNR 1989, 152:835-842
11. Cord Diameters and their Significance in Prognostication and Decisions about Management of Cervical Spondylotic Myelopathy. Bucciero A, Visioli L, Tedeschi G, Journal of Neurosurgical Sciences 1993 Dec; 37(4):223-8

MRI OF A CHILD WITH MARFAN SYNDROME

Pannee VISRUTARATNA[1], MD., Rekwan SITTIWANGKUL[2], MD., Ladda CHALOEYKITTI[1], B.Sc.

ABSTRACT

We report an 8-year-old girl with Marfan syndrome who had dilatation of the aortic root and ascending thoracic aorta, seen on MR imaging. Besides these anatomical abnormalities, aortic regurgitation was also seen on MR imaging, which is a good noninvasive method to diagnose aortic abnormalities in children with Marfan syndrome.

INTRODUCTION

Marfan syndrome is a generalized connective tissue disease primarily involving elastic tissue which results in ocular, skeletal, and cardiovascular anomalies. This syndrome is diagnosed more often in adults than children. One reason is that most manifestations of Marfan syndrome become more evident with time.[1] Echocardiography, computed tomography (CT) and magnetic resonance (MR) imaging are noninvasive methods to diagnose thoracic aorta abnormalities in these patients. We present a child with Marfan syndrome whose MR imaging showed not only dilatation of the aortic root and ascending thoracic aortic but also aortic regurgitation.

CASE REPORT

An 8-year-old girl was first evaluated for impaired vision 3 years ago. There was no history of Marfan syndrome in her family. Pertinent results of physical examination included dislocation of the lens of both eyes and signs of moderate to severe aortic regurgitation. Her weight was proper for her height (weight to height ratio = 91%). She had no apparent tall features (height to age ratio = 96%) but had arachnodactyly and a decreased upper to lower trunk ratio. On palpation cardiac examination revealed the apex was downward. Aortic regurgitation murmur was heard at the upper left sternal border. Chest radiographs showed cardiomegaly with an enlarged left ventricle and dilatation of the ascending aorta (Figs. 1 and 2). Echocardiography showed a huge dilated aortic root and moderately severe aortic regurgitation. Cardiac MRI with T1-weighted spin echo technique showed dilatation of the aortic root and ascending aorta and dilatation of the left ventricle (Figs. 3 and 4). A cine phase contrast study showed aortic regurgitation jet extending all the way to the cardiac apex (Fig. 5). She underwent aortic root graft and aortic valve replacement with uneventful recovery.

DISCUSSION

Marfan syndrome is a hereditary disorder of connective tissue, inherited as an autosomal dominant. In approximately 15 per cent of cases no other family member has signs of the syndrome.[2] The clinical expression of this syndrome varies. In its classic form, there are

[1] Department of Radiology and
[2] Department of Pediatrics, Faculty of Medicine, Chiang Mai University, Chiang Mai 50200, Thailand.

abnormalities of the eye (ectopia lentis), aorta (aneurysm of the ascending aorta and aortic regurgitation) and skeleton (limbs disproportionately long compared with the trunk, arachnodactyly, pectus deformity and mild joint laxity). Pyeritz and McKusick[2] have based the diagnosis of this syndrome on the four criteria of characteristic family history and ocular, cardiovascular, and skeletal features. They thought that it was prudent to require at least two of these criteria to make the diagnosis.

In our patient, the diagnosis of Marfan syndrome was made based on 3 criteria: ocular (ectopia lentis), cardiovascular (aortic root dilatation and aortic regurgitation), and mild skeletal signs (arachnodactyly and increased length of the limbs compared with the trunk (decreased upper to lower trunk ratio).

In the past the term "Forme fruste" was used when a person had this syndrome with all the manifestations except tall features.

Phornphutkul et al[3] examined 36 patients younger than 16 years of age and found that mitral regurgitation was the most frequent cardiac lesion (47%). Dilatation of the aortic root was also present in a significant number of children (28%) with Marfan syndrome with no apparent aortic regurgitation. This regurgitation will usually develop later on in life.

Chest radiographs are usually not helpful in detecting enlargement of the aortic root. Since the aortic root is within the cardiac silhouette, dilatation or an aneurysm of it is usually not recognized in chest radiographs unless they are very large.

Both echocardiography and CT have been used to make initial measurements and monitor the diameter of the thoracic aorta. Echocardiography is noninvasive and relatively inexpensive, but without good resolution it may not be able to demonstrate the entire thoracic aorta.[4] CT allows one to diagnose an aortic aneurysm and aortic dissection, which are important causes of death in these patients. Relative disadvantages of CT are exposure of patients to ionizing radiation and the need for contrast media.

MR imaging has been shown to be useful in diagnosing aortic abnormalities in these patients.[4,5] It is a noninvasive method showing anatomical abnormalities, as in our patient. It also shows pathophysiology, such as aortic regurgitation.

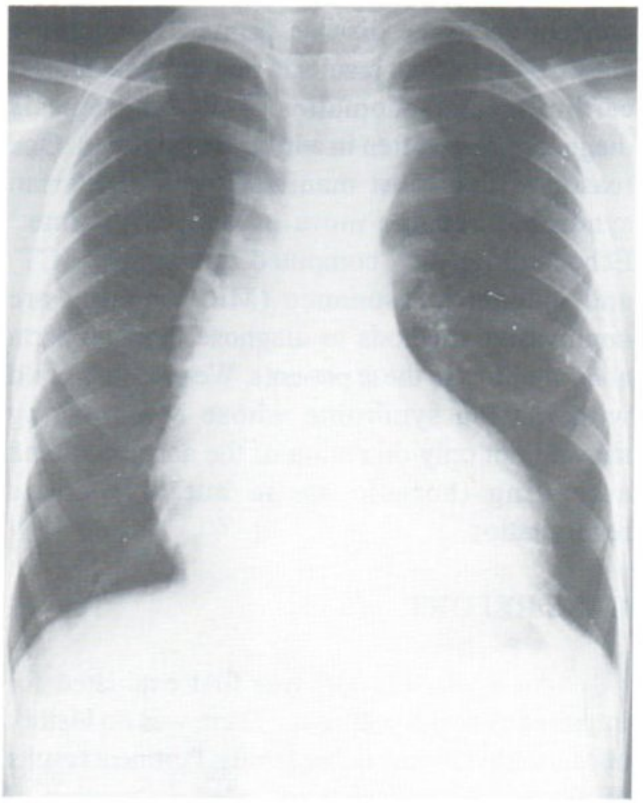

Fig.1 Frontal chest radiograph shows cardiomegaly and dilatation of the ascending thoracic aorta.

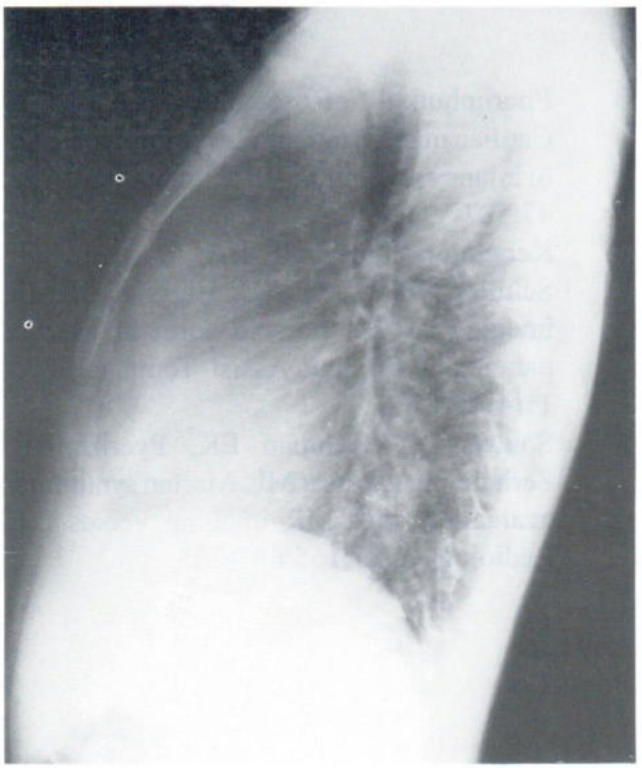

Fig.2 Lateral chest radiograph shows obliteration of the retrosternal clear space by the dilated ascending thoracic aorta.

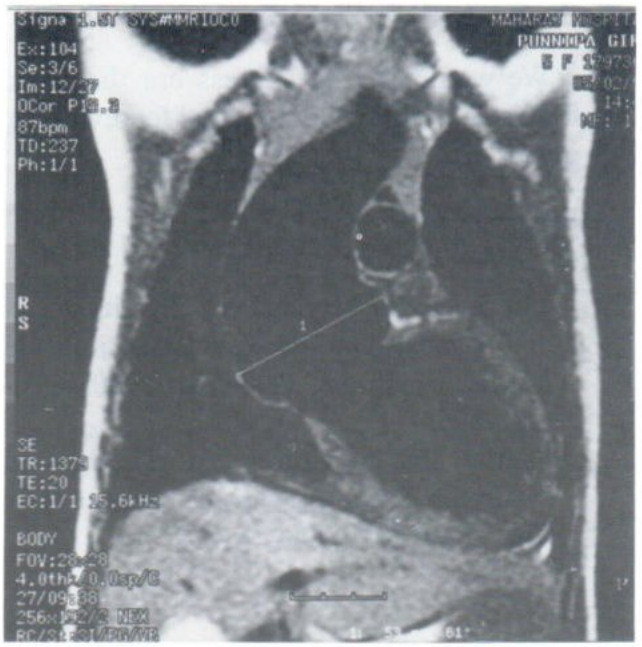

Fig.3 Coronal MR image shows a huge dilatation of the aortic root and the ascending thoracic aorta. Note the dilated left ventricle.

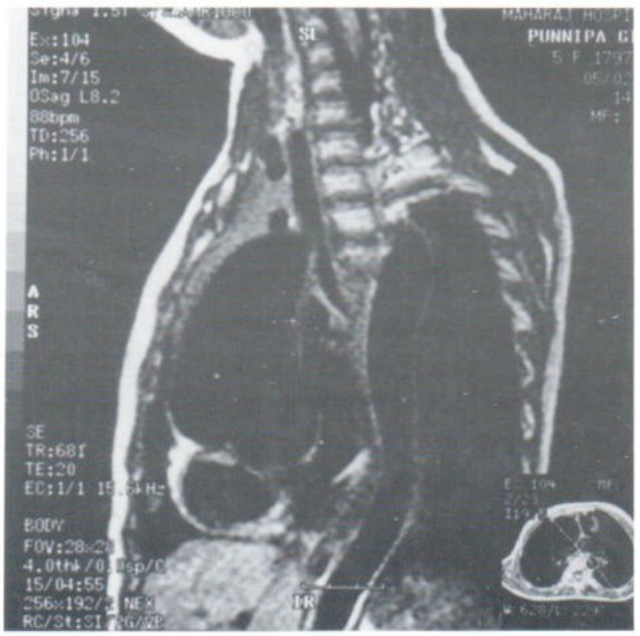

Fig.4 Oblique sagittal MR image shows a huge dilatation of the aortic root and the ascending thoracic aorta.

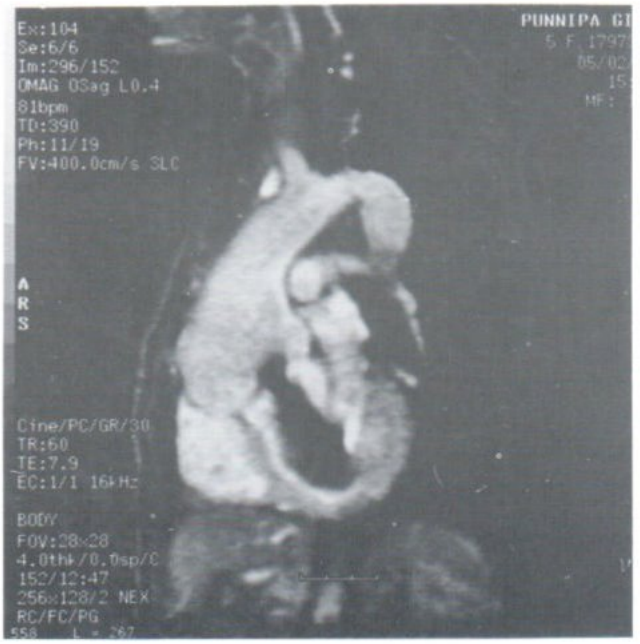

Fig. 5 Phase contrast oblique sagittal MR image shows regurgitation of blood from the aortic root into the left ventricle (signal void in left ventricle).

ACKNOWLEDGMENTS

We would like to express our thanks to Professor Dr. Charlie Phornphutkul for reviewing the manuscript.

REFERENCES

1. Morse RP, Rockenmacher S, Pyeritz RE, et al. Diagnosis and management of infantile Marfan syndrome. Pediatrics 1990;86(6)-:888-895.
2. Pyeritz RE, McKusick VA. The Marfan syndrome: diagnosis and management. New Eng J Med 1979;300(14):772-777.
3. Phornphutkul C, Rosenthal A, Nadas AS. Cardiac manifestations of Marfan syndrome in infancy and childhood. Circulation 1973;-47:587-596.
4. Kersting-Sommerhoff BA, Sechtem UP, Schiller NB, Lipton MJ, Higgins CB. MR imaging of the thoracic aorta in Marfan patients. J Comput Assist Tomogr 1987;-11(4):633-639.
5. Soulen RL, Fishman EK, Pyeritz RE, Zerhouni EA, Pessar ML. Marfan syndrome: evaluation with MR imaging versus CT. Radiology 1987;165:697-701.

MRI OF THE BRAIN IN WILSON'S DISEASE PRESENTING WITH NEUROPSYCHIATRIC MANIFESTATION

M. PUVANESWARY[1], M. PARSONS[2]

ABSTRACT

A 32- year old female patient is described presenting with neuropsychiatric manifestation of wilson's disease which was initally diagnosed on the basis of MR findings. MRI findings are reviewed.

CASE REPORT

A 32 year old woman who emigrated from Bosnia in 1994, first came to medical attention via an antenatal clinic in 1995 where she was noted to have mild thrombocytopenia [107 x10 / L]. This combined with her past obstetric history of three first trimester miscarriages raised the possibility of anti-phospholipid syndrome. On haematology review, an illness said to be haemolytic anemia in Bosnia in1989 was revealed.The illness spontaneously resolved in 2 weeks with no treatment. Further haemotology investigation showed a mild leucopenia [3.9X10 /L] as well as thrombocytopenia. ANA was 1:40. Anticardiolipin antibodies and lupus anticoagulant were negative. In early 1996 she had noted tremulousness, unsteadiness and poor concentration. The only abnormality on examination was a fine action tremor. She was refered to a psychiatrist for depression and was commenced on an selective serotonin reuptake inhibitor. This led to improvement in mood but after being on the drug for a month she developed generalised dystonia and rigidity. This persisted despite cessation of the drug.She had her first MRI which was reported as cerebral atrophy. She subsequently underwent electro-convulsive therapy with marked improvement in her mental state and in the dystonia and rigidity. She remained well for about 6 months but then developed progerssively worsening abnormal movements over the next 3 months. Her mobility was declining to the stage of requiring 2 people to assist her. She was admitted to the neurology unit for investigation.On examination she had fine action tremor of both hands, choreo-athetosis of all limb, and dystonic posturing of the limbs and trunk. There were no Kayser-Fleisher ring on opthalmoscopy. Her general examination finding was normal except for splenomegaly. Laboratory investigations showed persisting mild thrombocytopenia and leucopenia, a mild rise in liver transminase [ALT 36u/L] and ANA 1:160]. An MRI was performed on 1.5 T superconducting system [Siemens : with a 256 x 256 matrix.] Sagital T1 repitition time/ echo time/excitation 462/12/2, axial proton density, 4000/22/2, and axial T2 4000/90/2 and axial T2-weighted inversion recovery 7000/119/1, and inversion time of 2200msec. T2 weighted images showed increased

Department of Medical Imaging1 and Medicine2

CORRESPONDENCE:
M. Puvaneswary, John Hunter Hospital, Locked Bag No.1, Hunter Region Mail Centre, NSW 2310.
Phone: (049) 213-000, Fax: (049) 213-415

signal intensities in the caudate nucleus, putamen particularly the lateral border, globus pallidus, the thalamus, the tegmentum, red nucleus and periaqueductal region of the midbrain and ventral pons, the claustrum, the superior and middle cerebeller peduncle and adjacent white matter and asymetric focal increase signal intensities in centrum semiovale (Fig 1-5) Areas of low signal intensity were peresent within the hyperintense basal ganglia. Inversion recovery sequences showed increased signal intensity in the dentate nucleus, superior cerebeller peduncle and sub-cortical white matter. (Fig 5B)

Serum cerruloplasmin was 77 [range 280-573 mg/L], 24 hour urinary copper was 11.3 [normal less than 1.6 micromol]. Slit- lamp examination did reveal the presence of Kaiser-Fleisher rings. The diagnosis of Wilson's disease was confirmed and penicillamine and zinc were commenced.

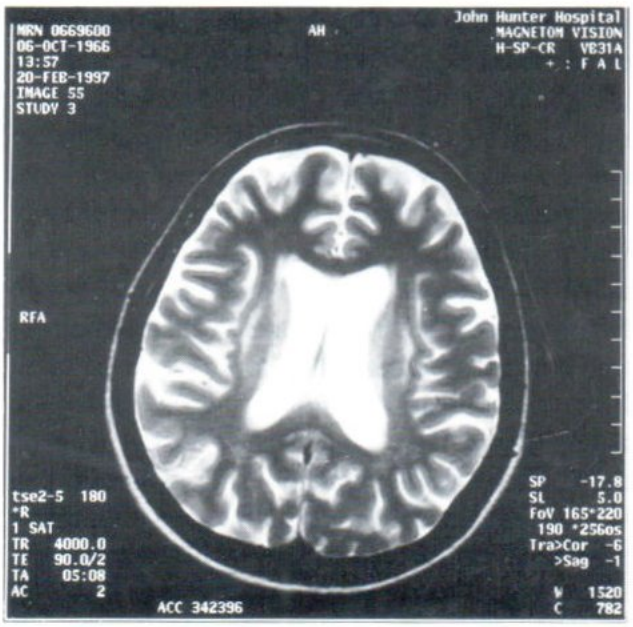

Fig.1 T2 -weighted MR image shows a thick hyperintense claustrum. Both caudate nuclei are hyperintense..

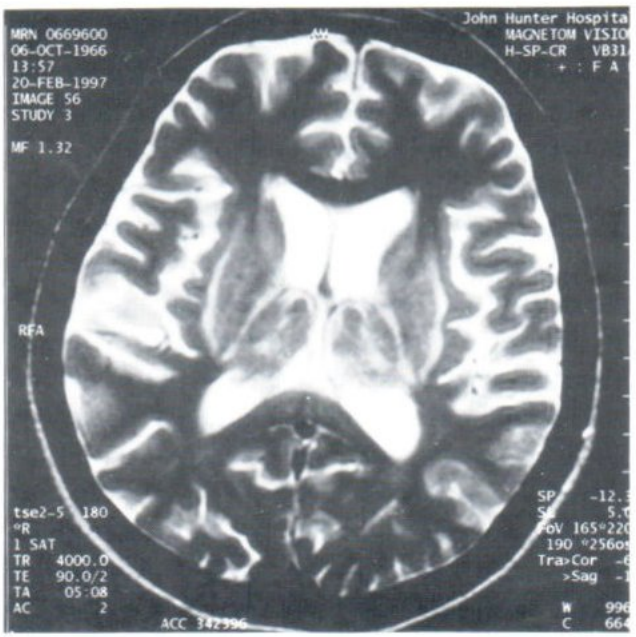

Fig.2 Axial T2-weighted image. High signal intensity in putamen particularly involving the outer rim, caudate nuclei and thalami. Low signal intensity areas are present within the hyperintense basal ganglia.

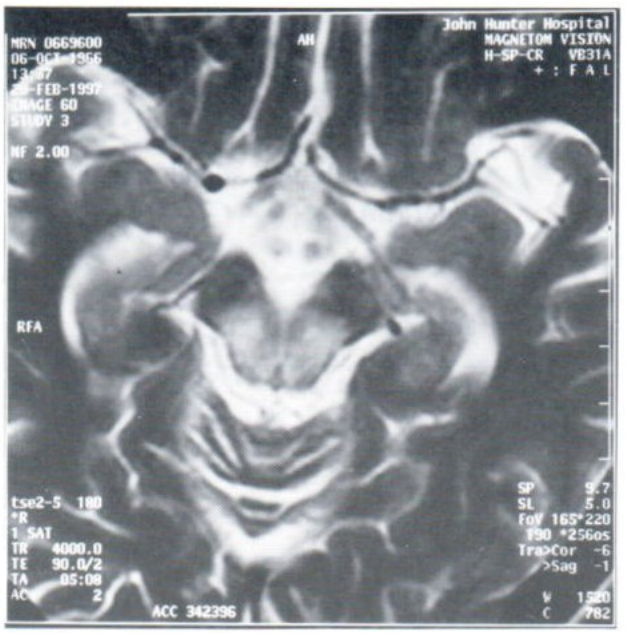

Fig.3 T2-weighted axial MR image through mid-brain shows diffuse increase signal intensity in tegmentum .

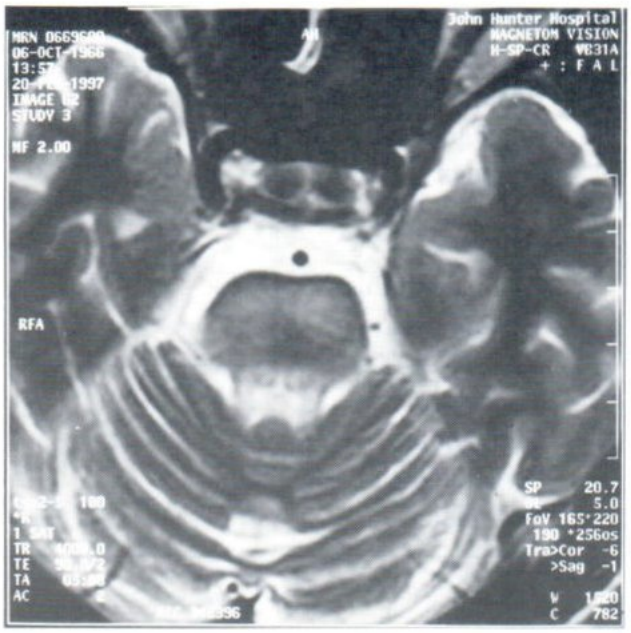

Fig.4 T2-weighted axial MR image through pons reveal increase signal intensity in central pons and superior cerebeller peduncle

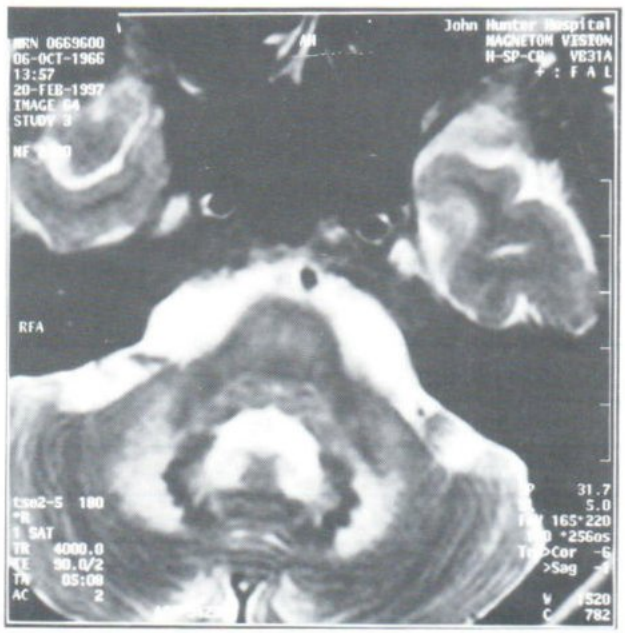

Fig.5 T2-weighted axial MR through cerebellum shows increased signal intensity in middle cerebeller peduncle

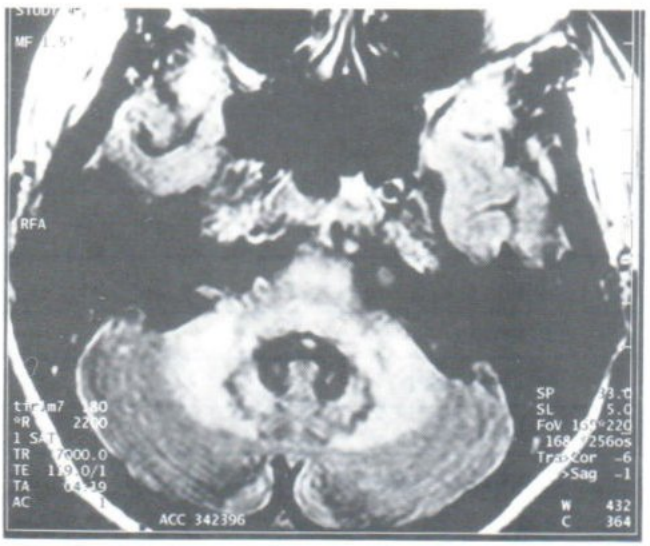

Fig.5 B Inversion recovery sequence demon strate increased signal intensity in cerebellar peduncle and adjacent white matter and dentate nuclei.

SUMMARY OF MRI FINDINGS

Basal ganglia	
Caudate nuclei	Diffuse
Putamen	Diffuse with high signal intensity outer rim
Glubus pallidus	
Thalami	Diffuse
Midbrain	
Tegmentum	
Periaqueductal gray matter	
Red nuclei	
Pon	Ventral
Cerebellum	
Superior peduncle	
Middle peduncle	
Dentate nuclei	
Sub-cortical white matter	Asymmetric
Centum semiovale	Asymmetric

Table 1 Correlation between Neurological signs and brain MRI lesion (REF 6)

Sign	MRI lesion
Dystonia	Putamen
Bradykinesia	Putamen
Dysarthria	Putamen and Caudate
Cerebeller sign and Postural tremor	Dentate nucleus, superior cerebeller peduncle red nucleus
Distractibility of gaze fixation	Frontal lobe

Table 2 Location of MR Abnormalities in Wilsons' Disease (REF 4)

Basal ganglia	Most frequently affected
Putamen	High SI outer rim on T2-W
Globius pallidus	Frequent
Caudate Nucleus	Frequent
Thalamus	Frequent: ventro-lateral aspect
Sub-thalamic region	Rare
Mid brain	Frequent
Tegmentum	
Substantia niagra	
Periaqueductal grey matter	
Red nuclei	
Tectum	
Crura	Rare
Pons	Second most commonly involved
Tegmentum	Frequent
Cerebellum	
Superior cerebeller peduncle	Frequent
Middle cerebeller peduncle	Frequent
Dentate Nucleus	
Vermis	
Medulla	Rare
Subcortical white matter	Asymmetric
	Parietal/Frontal
Claustrum	Frequent
Atrophy	Common
Cerebral	Vary mild to severe
Cerebellum	Mild

DISCUSSION

Wilson's disease is an uncommon autosomally recessive inherited disorder of copper metabolism caused by a deficiency of ceruloplasmin, the serum transport protein for copper. There is excessive deposition of copper in various tissues, especially the liver and brain.

Although it is a rare disease early diagnosis is particularly important as prompt therapy can prevent the irrevisible damage to vital organs such as the liver and the brain and may be reversible if therapy is commenced early. Because it has a variety of clinical manifestation, early diagnosis may be difficult and the first clue to the diagnosis may be made by a radiologist based on MRI findings as was in our patient. Neuropsychiatric manifestation are frequently the first symptoms. Psychiatric symptoms are common and the patient suffers depression, and emotional instability. Neurological symptoms include tremors, dystonia, rigidity, dysarthria, incordination and gait difficulty. There is correlation of dystonia and bradykinesia with lesion of putamen, dysarthria with lesion in putamen and caudate nucleus, cerebeller sign and

postural tremor with dentate nucleus, superior cerebeller peduncle and or red nucleus, distractibility of gaze fixation with frontal lobe involvement.[1,2,3] (Table 1)Patient usually have Kayser-Fleischer ring in the eyes due to deposition of copper in Descement membrane. Biochemical studies will confirm the diagnosis of Wilson's disease.

MR imaging is a sensitive modality for defining the normal anatomy and pathological changes of brain parenchyma and correlates better with clinical symptoms than CT does.

Wilson's disease may have a wide spectrum of abnormality on neuroimaging involving both gray matter and white matter with a predilection for the extrapyramidal system. Lesions have been reported in basal ganglia, thalami, subcortical white matter, mesencephalon, pons, dentate nucleus, vermis and claustrum.

Some of the neuroimaging findings may be related to neurological sign or to the presence of portosystemic shunt. The basal ganglia are the most frequently affected site with the putamen, globus pallidus, caudate nuclei and thalami being involved in up to 50 % of patients.[4] There is bilateral, symmetric involvement in gray matter in contrast to asymmetric white matter disease. The pons is the second most commonly affected structure, with the the pontine tegmentum being the prefered site. Midbrain is frequently abnormal [3,5,6,7] with the tegmentum being the most commonly affected site in the midbrain. Abnormality is present in the substantia nigra, red nucleus, inferior tectum and crura.[4] Thalami are symetrically affected. Maximal involvement is confined to the ventro-lateral nuclei. Minimal abnormal signal intensity was demonstrated in one patient in the subthalamic region.[4] Medulla was rarely involved[8] Half the number of patient had superior cerebeller peduncle and middle cerebeller peduncle involvement. There was symmetric involvement of middle cerebeller peduncle extending into adjacent white matter.[4] There were mild sub-cortical white matter involvement with asymmetrical focal changes or more symmetric diffuse changes in the parietal and frontal lobes.[4] There is relatively high incidence of claustral involvement with thickened and bright signal intensity.[9] Cerebral atrophy was common (Table2)

Histopathological changes in cerebral lesion of Wilson's disease include odema, gliosis, demyelination, neuronal loss and spongiform degeneration and cavitation especially in the putamen. These has been attributed to excessive copper deposition or ischemia or both.

Findings on CT are low density lesion in basal ganglia and widespread brain atrophy. On MRI, the most frequent findings is an increase signal intensity on T2- weighted images and decrease signal intensity on T1-weighted images which reflect underlying odema, gliosis and cavitation. Subtraction techniques enable cavitation to be distinguished from gliosis. The cavities in subtraction images appears as areas of very low signal intensity.[10] High signal intensity of white matter on T2 could be explained by demyelination, spongiformation or cavitation. Hypointensity on T2-weighted images has been reported and has been attributed to the paramagnetic effect of copper deposition.[7,11,12] Another possible cause of decrease T2 signal is iron deposition from previous haemorrhage which may occur in association with basal ganglionic destruction.[7,10,13] Low signal intensity in gray matter nuclei is diffcult to differentiate normal from abnormal low signal intensity as there is a wide variation in signal intensity in normal aging population. There is a physiological and age dependent accumulation of iron in basal ganglia and brain stem nuclei. Occasionally basal ganglia may be normal in signal intensity due to the potential balance effect of gliosis, odema and paramagnetic effect.[14]

Copper deposition in untreated patients had shorten T1 relaxation time that produced diffusely increase signal intensity on T1 weighted images.[4] Hyperintensity on T1 weighted images have been described in globus pallidus in patient with chronic

liver disease [non-Wilson] and has been attributed to accumulation of manganese.[15] High signal intensity on globus pallidus on T1 or high signal intensity in claustrum and frontal white matter on T2 has been associated with severe liver disease in Wilson's.[16] Contrast enhacement of brain lesion on MR images has been reported[17] and has been attributed to hypersensitivty to penicillamine therapy.

There has been conflicting reports ,some authors find good MRI correllation with neurologic examination[10] and other reports found no correlation between MR abnormality and severity of neurological impairment.[4,5,18] King et al[4] noted patient with longer duration of untreated disease had significantly less severe changes in signal intensity on MR images. Clinical response begin three to six months after initiation of therapy and even in the presence of severe neurologic disease a complete recovery may occur.[4,5,10] There were improvement of MR findings on follow up study under therapy.[4,5,10]

REFERENCES

1. Adams RD, Victor M (1985) Tremor, myoclonus, spasms, and tics. In: Adams RD, Victor M (eds) Principles of Neurology, 3rd edn McGraw-Hill, New York, pp 53-89.
2. Lennox G, Jones R (1989). Gaze distract ibility in Wilson's disease. Ann Neurol 25:-415-417.
3. Malgalhaes ACA, Carannelli P, Menezes JR, et al. Wilson's disease: MRI with clinical correlation. Neuroradiology 1994:36:97-100.
4. King AD, Walshe JM, Kendall BE ,Chinn RJS et al. Cranial MR imaging in Wilson 's disease AJR 1996;167:1579-1583.
5. Nazer H, Brismar J, Al-kawi MZ, Gunasekeran TS, Jorulf KH. Magnetic resonance imaging of the brain in Wilson's disease. Neuroradiology 1993;35:130-3.
6. Starosta- Rubenstein S, Young AB, Kliunk et al. Clinical assessment of 31 patients with Wilson's disease: correlations with structural changes on magnetic resonance imaging. Arch Neurol 1987; 44:365-370.
7. Yuh WTC, Fliakinger FW. Unusual MR findings in CNS Wilson's disease AJR 1988; 151:834.
8. Hitoshi S, Iwata M, Yoshikawa K, Mid-brain pathology of Wilson's disease: MRI analysis of three cases. J Neurol Neurosurg Psychiatry 1991; 54:624-626.
9. Sener RN. The Claustrum on MRI: Normal anatomy and the bright clautrum as a new sign in Wilson's disease, Paediatr Radiol 1993: 23:597-596.
10. Thuomas KA, Aquilonius SM, Begstrom K, Westermark K. Magenetic resonance imaging of the brain in Wilson's disease Neuroradiology 1993; 35:134-41.
11. Brugieres P, Combes C, Ricolfi F, Degos JD, Poirie J, Gatson A. Atypical MR presentation of Wilson's disease; a possible consequence of paramagnetic effect of copper? Neuroradiology 1992; 34:222-224.
12. Mironov A. Decreased signal intensity of the putamen and caudate nucleus in Wilson's disease of the brain. Neuroradiology 1993;-35:166.
13. Singcharoen T, Chakkaphak K, Udompanich O, Unusual magnetic resonance findings in Wilson's disease Br J Radiol 1991; 64:752-754.
14. Sener RN, Wilson's disease: MRI demon stration of cavitation in the basal ganglia and thalami. Paediatr Radiol 1993:23:157.
15. Inoue E, Hari S, Narum Y et al. Portal-systemic encephalopathy: presence of basal ganglia lesions with high signal intensity on MR images. Radiology 1991; 179:551-555.
16. Van Wassenaer- van Hall HN, Vanden Heavel AG Hoogenraad T U ,et al . Wilson Disease: Findings at MR imaging and CT of the brain with clinical correlation. Radiology 1996 ;198:531-536.

17. Sener RN. Wilson's disease: Contrast enhancement of cerebral lesions on MR images after penicillamine therapy AJR 1994; 163:228-229.

18. Prayer L, Wimberger D, Kramer J, Grimm G, Oder W, Imhof H. Cranial MRI in Wilson's disease. Neuroradilogy 1990;32:-211-4.

RADIO-OPACITY OF MALAYSIAN FISH BONES- AN *IN VITRO* STUDY

Abdullah BJJ, FRCR., Kaur H, M.Rad. and KH Ng, Ph.D.

ABSTRACT

Foreign body ingestion is a common problem presenting to the Accident Emergency department. The foreign body most commonly ingested being fish bone. A lateral neck radiograph is often requested for making the diagnosis. However, a large proportion of fish bones are not radio-opaque which makes this a difficult diagnostic problem.

OBJECTIVE

The objective of this study was to determine the incidence and types of impacted foreign bodies in the upper gastrointestinal tract in the Malaysian population as well as to assess the radio-opacity of the bones of common Malaysian fish.

METHODS AND MATERIALS

A retrospective study was carried out over a one year period i.e. 1st. Jan - 31st. Dec 1995 at University of Malaya, Medical Center, Kuala Lumpur to note the incidence and type of swallowed foreign body in the Malaysian population. An in-vivo study was done where the dried bones of 18 species of Malaysian fish were radiographed separately as well as in an animal carcass using X-omatic Kodak film with a X-omatic Kodak regular intensifying screen. A Kodak RPX - OMAT processor, model M6B was used.

RESULTS

Foreign body impaction is more common in adults with fish bones being the most common cause (88%). The lateral soft tissue neck was only able to demonstrate 4 out of the 19 patients but those missed were located in the tonsils, valleculae and posterior pharyngeal wall and would be visible on oral examination. In the in vitro study, 89% of the bones were well to moderately visualized in the larynx, 50% moderately to well visualized in the oesophagus but none could be seen in the tonsil or valleculae.

CONCLUSION

The results concur with those of other studies with regards to the age and type of foreign body impaction except that there were no cases of food bolus impaction. Most of the Malaysian species of fish bones were visible in the oesophagus but none placed in the valleculae or tonsil. It would seem that the results are in agreement with those of the retrospective study in that all the impacted foreign bodies located in the oesophagus were visible on the plain radiograph.

Department of Radiology, University of Malaya Medical Center, University of Malaya, 50603 Kuala Lumpur, MALAYSIA

Address correspondence to:
Abdullah BJJ, Department of Radiology, University of Malaya Medical Center, University of Malaya, 50603 Kuala Lumpur, MALAYSIA

INTRODUCTION

Foreign body ingestion is a common problem presenting to the Accident Emergency department. Fortunately of the foreign bodies that reach the gastrointestinal tract, 80-90% will pass spontaneously.[1] However 10-20% will require non-operative intervention and 1% or less will require surgery.[1] Most true foreign bodies especially metallic are radio-opaque and can be identified on plain films of the neck, chest or abdomen. However objects such as fish or chicken bones, wood, plastic, most glass and metal objects are not readily seen.[1] The type of materials that can lodge in the gastrointestinal tract can be classified into 2 groups, one that consists of food bolus impaction while the second consists of true foreign bodies. The latter group consists of blunt (buttons, coins, etc.) and sharp pointed objects (ones, nails, etc.) and the miscellaneous group (disc batteries). The complications that have been noted to arise from swallowed foreign bodies especially sharp foreign bodies are perforation, parapharyngeal abscess, mediastinitis pericarditis, pneumothorax, pneumomediastinum, tracheo-oesophageal fistula and vascular injury.

The majority of swallowed foreign bodies have been noted to be bones. A study done by Sprigg et al[2] looked at the species variation of the radio-opacity of fish-bones in the western context. Of the 14 species of fish radiographed, 64% were moderately to clearly visible in the larynx and oesophagus and 57% being visualised in the valleculae and tonsil. Hence in their study a lateral neck radiograph proved useful in the detection of swallowed fish bones especially when the type of fish ingested is known.

There is no data available on the incidence, types and complications of swallowed foreign bodies at University Hospital, Kuala Lumpur. In addition the radio-opacity of common Malaysian fish bones is also not known.

The objective of this study was to determine the incidence and types of swallowed foreign bodies in the Malaysian population. We also assessed the radio-opacity of the bones of common Malaysian fish on a lateral neck radiograph in an animal carcass and hence the usefulness of a lateral neck radiograph in detection of fish bone impaction.

MATERIALS AND METHODS

A retrospective study covering a one year period from 1st Jan-31st Dec 1995 was carried out to determine the incidence and types of swallowed foreign bodies in the Malaysian population presenting to the University of Malaya Medical Center, Kuala Lumpur. The radiographs and case notes of all the patients who had presented at the Accident and Emergency department for complaints related to foreign body ingestion were reviewed. The case notes were then reviewed to note the age, sex, complaint at presentation, clinical examination findings, findings on endoscopy and any related complications. The radiographs were then reviewed by 2 radiologists and the presence and type of foreign body noted. Results were then tabulated.

The dried clean bones of 18 species of Malaysian fish (Table 1) were radiographed separately to determine the radio-opacity of the bones of common Malaysian fish. This was done by placing different sized bones of all the different species on the same double film-screen combination (as used in the rest of the study) and radiographed. The radio-opacity of the bones was graded as Grade 1- poorly visible, Grade 2- moderately visible and Grade 3- clearly visible.

The fish bones of each species in turn were then placed in the four locations (Figure 1) in the animal carcass and radiographs taken. The locations chosen were the tonsil, valleculae, larynx and oesophagus. The exposure factors used were 48 kVp, 5 mAs , a FFD of 100cm. No grid was

used as the lateral neck radiograph is generally taken without using a grid. The film used was a Kodak X- Omatic while the intensifying screen was a Kodak X- Omatic Regular. The film were processed using a normal processor (KODAK RPX-OMAT processor, model M6B). The radio-opacity of the fish bones was graded by two radiologists by consensus. The radio-opacity of the fish-bones once implanted within the goats neck preparation was as Grade 1- fishbone not seen, Grade 2- fishbone moderately visible and Grade 3- fishbone clearly visible.

The phantom used was an animal carcass consisting of a goat's head and neck. This was chosen as the exposure factors used were comparable to a soft tissue lateral radiograph of the human neck.. There were in addition social and cultural constraints for choosing the goat's preparation. The carcass had been sectioned in the mid-sagittal plane through the oesophagus and trachea allowing easy placement of the fish bones. The carcass was stored in formalin to preserve the soft tissues.

Table I. The Scientific, English and Local names of the 18 species of fish.

Scientific	English	Local
1. Clarius Batrachus	Walking Cat-Fish	Keli Kayu
2. Formio Niger	Black Pomfret	Bawal Hitam
3. Rastrelliger Brachysoma	Short Bodied Mackerel	Pelaling Kembong
4. Megalaspis Cordyla	Hardtail Scad	Cencaru
5. Selaroides Leptolepis	Yellow Banded Scad	Selar Kuning
6. Eleutheronema Tetradactylum	Fourfinger Threadfin	Senangin
7. Hilsa Toli	Tolishad	Terubuk
8. Thunnus Tonggol	Longtail Tuna	Tongkol
9. Chirocentrus Dorab	Dorab Wolf-Herring	Parang
10. Pampus Argenteus	Silver Pomfret	Bawal Puteh
11. Scomberomorus Commerson	Narrow-Barred Spanish Mackerel	Tenggiri Batang
12. Lutjanus Johni	Golden Snapper	Jenahak
13. Lates Calcarifer	Giant Perch	Siakap
14. Leptobarbus Hoevenii	Sultan Fish	Jelawat
15. Epinephelus Sexfasciatus	Six-Banded Grouper	Kerapu
16. Nemipterus Delagoae Smith	Delagoa Threadfish Bream	Kerisi
17. Oreochromis Niloticus	Nile Tilapia	Tilapia
18. Channa Striatus Bloch	Striped Snakehead	Aruan

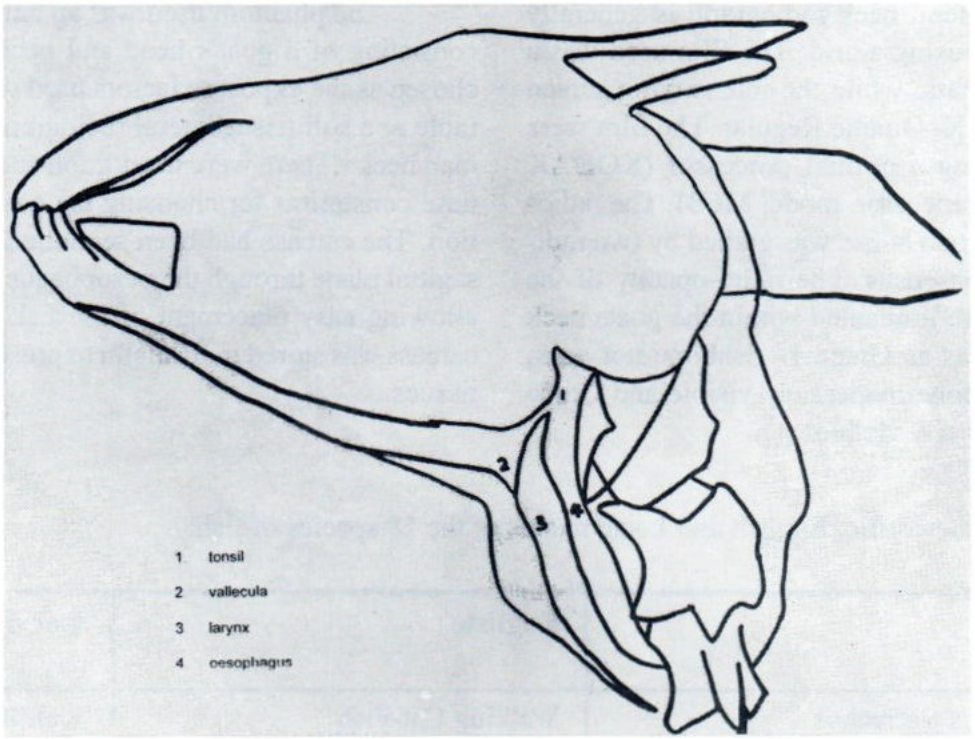

Fig. 1. The line drawing of the goat carcass with the locations of the implanted bones.

RESULTS

The data collected showed that a total of 118 patients (76 adults, 42 children) presented with history of swallowed foreign bodies over the time period evaluated. Swallowed foreign bodies were more common in adults (64.4%), compared to children (35.6%). In adults, swallowed foreign bodies were more common in females (55.3%), compared to males (44.7%), whereas in children the reverse was true i.e. 48% in females and 52% in males (In adults the male: female ratio was 1:1.4 and in children the ratio was 1.1:1). Age ranged from 7mths-73yrs. The mean age was 24yrs while the mode was 32yrs. The most frequently swallowed foreign body noted was due to fishbone, and this being more common in adults. (37 males, 30 females). Coins were noted to be the most commonly swallowed foreign body in children. The other swallowed foreign bodies included pins, bottle stopper, dentures, play-toy, preserved plum seed, metal lid, needle, metal bolt, screw, local kebab stick, wire, chain, nail, ring, gold plated necklace and buttons.

Of the suspected swallowed foreign bodies, bones constituted the largest number i.e. 64.4%, compared to other foreign bodies 35.6%. The commonly swallowed bones were fish bones (88%) followed by chicken bones (10.5%) and duck bones (1.5%). Of the 67 suspected cases of impacted fish bones, 15 patients were not radiographed i.e. just a peroral examination was done and most of the bones were noted to be impacted in the tonsil, followed by posterior pharyngeal wall and valleculae. 52 patients were radiographed and out of these there were 4 which were true positive (confirmed by endoscopy). Of the 48 patients that were radiographed negative, 15 patients were false negative (on examination 8 had bones lodged in their tonsil, 5 in valleculae and 2 in posterior pharyngeal wall). The remaining 33 patients were true negatives. Peroral examination picked-up the 30 patients with impacted fish bones in the oropharynx.

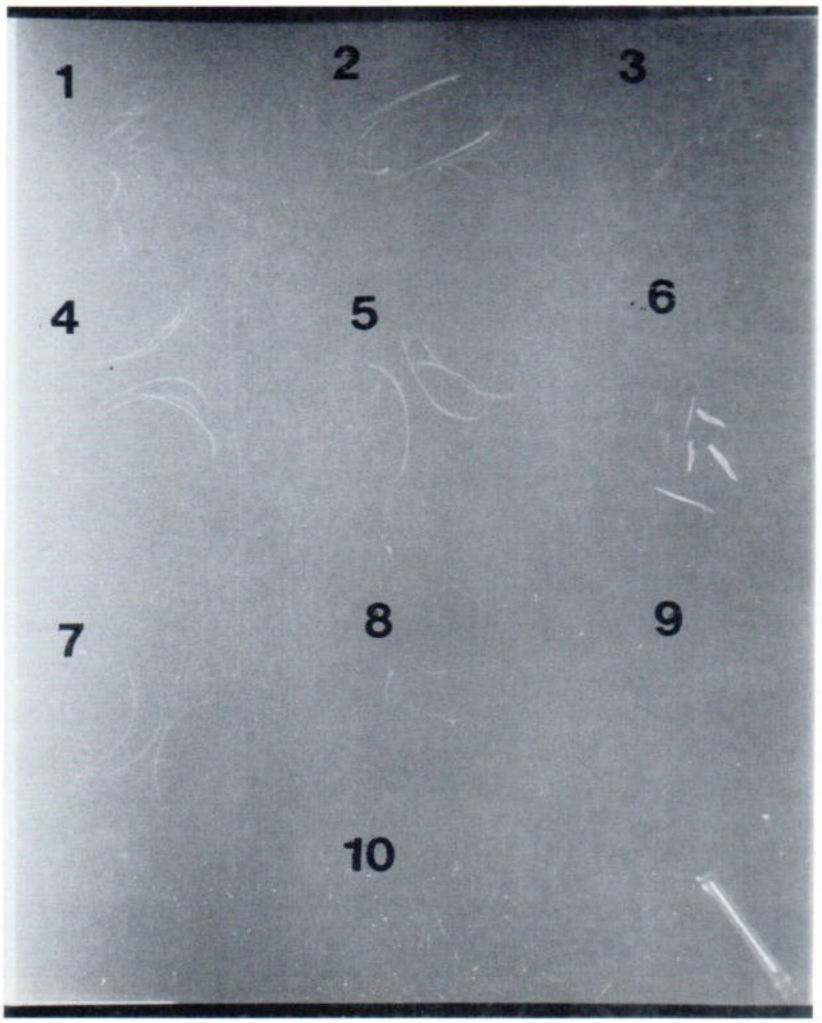

Fig. 2a Radiograph of the dried fish bones prior to implantation labelled as follows

	Scientific	English	Local
1.	Clarius Batrachus	Walking Cat-Fish	Keli Kayu
2.	Formio Niger	Black Pomfret	Bawal Hitam
3.	Rastrelliger Brachysoma	Short Bodied Mackerel	Pelaling Kembong
4.	Megalaspis Cordyla	Hardtail Scad	Cencaru
5.	Selaroides Leptolepis	Yellow Banded Scad	Selar Kuning
6.	Eleutheronema Tetradactylum	Fourfinger Threadfin	Senangin
7.	Hilsa Toli	Tolishad	Terubuk
8.	Thunnus Tonggol	Longtail Tuna	Tongkol
9.	Chirocentrus Dorab	Dorab Wolf-Herring	Parang
10.	Pampus Argenteus	Silver Pomfret	Bawal Puteh

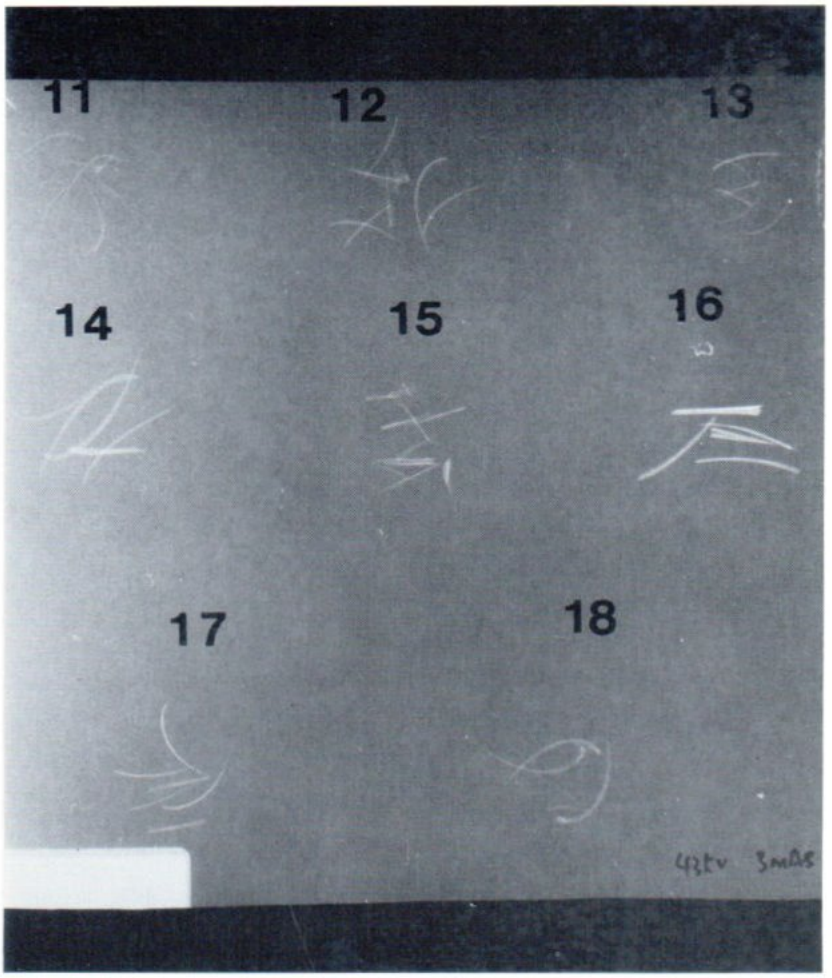

Fig. 2b. Radiograph of the dried fish bones prior to implantation labelled as follows

11.	Scomberomorus Commerson	Narrow-Barred Spanish Mackerel	Tenggiri Batang
12.	Lutjanus Johni	Golden Snapper	Jenahak
13.	Lates Calcarifer	Giant Perch	Siakap
14.	Leptobarbus Hoevenii	Sultan Fish	Jelawat
15.	Epinephelus Sexfasciatus	Six-Banded Grouper	Kerapu
16.	Nemipterus Delagoae Smith	Delagoa Threadfish Bream	Kerisi
17.	Oreochromis Niloticus	Nile Tilapia	Tilapia
18.	Channa Striatus Bloch	Striped Snakehead	Aruan

Of the 42 other swallowed foreign bodies, 36 had x-rays taken. Chest x-ray was diagnostic in 5 patients for coins[4] and dentures.[1] Abdominal x-ray was positive in 16 patients for coins,[9] chain,[2] metallic toy,[1] stopper,[1] pin,[1] screw,[1] button.[1] None suffered complications. Cervical spine x-ray was positive far one patient (coin).No foreign body was detected in the remaining 21 patients.

Most of the swallowed foreign bodies (76/118) are noted to pass through the GIT without complications. Of foreign bodies which commonly impact (mainly fish-bones) 28 were removed by peroral examination and 4 by endoscopy. None of these patients had associated complications. Studies performed revealed a low rate of complications. The common complaints were foreign body sensation in the throat, dysphagia, odynophagia, blood stained sputum and vomiting.

The visibility of the dry bones is as shown in (Table II.) It is noticed that most of the dry bones when radiographed separately are well visualised, except for bones of parang. The bones of bawal puteh were only moderately visible.

Results of the Radiographic Visibility of the 18 species of fish using X-omatic film-screen combination when implanted in the goat carcass are shown in (Table III.) Most of the bones were moderately to well visualised in the larynx (i.e. 89%) except for bones of Walking Cat-fish and Sultan fish. 50% of the bones were moderately to well visualised in the oesophagus i.e. those of Hardtail Scad, Fourfinger Threadfin, Narrow-Barred Spanish Mackerel, Golden Snapper, Giant Perch, Six-Banded Grouper, Delagoa Threadfish Bream, Nile Tilapia and Striped Snakehead. None of the bones were seen in the valleculae or tonsil.

Table II. The radiographic visibility of dry bones of 18 species of fish. The radio-opacity of the dried bones was graded as Grade 1-poorly visible, Grade 2- moderately visible and Grade 3- clearly visible.

NAMES OF FISHES	GRADING
Walking Cat-Fish	3
Black Pomfret	3
Short Bodied Mackerel	3
Hardtail Scad	3
Yellow Banded Scad	3
Fourfinger Threadfin	3
Tolishad	3
Longtail Tuna	3
Dorab Wolf-Herring	1
Silver Pomfret	2
Narrow-Barred Spanish Mackerel	3
Golden Snapper	3
Giant Perch	3
Sultan Fish	3
Six-Banded Grouper	3
Delagoa Threadfish Bream	3
Nile Tilapia	3
Striped Snakehead	3

Table III. Radiographic visibility of bones of 18 species at four different sites in the goat neck preparation. The visibility was graded as 1- not visible, 2- moderately visible and 3- well visualised.

NO	NAMES OF FISHES	LARYNX	VALLECULAE	TONSIL	OESOPHAGUS
1.	Walking Cat-Fish	1	1	1	1
2.	Black Pomfret	2	1	1	1
3.	Short Bodied Mackerel	2	1	1	1
4.	Hardtail Scad	3	1	1	3
5.	Yellow Banded Scad	2	1	1	1
6.	Fourfinger Threadfin	3	1	1	3
7.	Tolishad	2	1	1	1
8.	Longtail Tuna	3	1	1	1
9.	Dorab Wolf-Herring	2	1	1	1
10.	Silver Pomfret	2	1	1	1
11.	Narrow-Barred Spanish Mackerel	2	1	1	2
12.	Golden Snapper	3	1	1	3
13.	Giant Perch	3	1	1	3
14.	Sultan Fish	1	1	1	1
15.	Six-Banded Grouper	3	1	1	3
16.	Delagoa Threadfish Bream	3	1	1	2
17.	Nile Tilapia	3	1	1	2
18.	Striped Snakehead	3	1	1	2

DISCUSSION

Of all patients ingesting foreign bodies, studies performed showed adults to represent 17-85% of cases which is similar to our study where adults constitute 64.4 % of the population. Patients younger than 40 years have the highest incidence of (nonfood) foreign bodies (94%), whereas in patients greater than 60 years, food bolus predominates (72%).[1] It was also found that in the 60 years old group, 72% were found to have associated diseases and as many as 75% had dental appliances. In our study there were no patients older than 40 years. The associated disorders reported for adult patients ingesting foreign bodies have included prisoners, presence of dentures, past history of suicidal attempts, psychiatric histories[1] and alteration in the normal protection mechanism secondary to alcohol or cerebrovascular accidents. Except for the 3 patients who allegedly swallowed dentures none of our patients had any of these associated diseases. This is similar to study by Phillipps and Patel[3] who also found no predisposing factors towards swallowed foreign bodies. The main reasons for people ingesting a foreign body is either sheer misfortune or sheer carelessness

through people "gulping" their food down. Pediatric patients have been cited to comprise 14-83% of patients ingesting foreign bodies. Most occurred in the 3 mth-12 year age group with the incidence being equal in males and females.[1]

Fish bones are the most commonly encountered (50-71.6%) ingested foreign body , followed by meat bones (15%), unknown and coins (26%) and food bolus (10%).[1,3,4] Impaction of food bolus is due to the presence of underlying esophageal disease and poor sensitivity from dental prostheses.[1] Surprisingly in our study there were no cases of food bolus impaction and this is probably related to the younger population as well as the difference of diet which is a more Asian diet with less ingestion of steak.

Most foreign bodies pass through the gastrointestinal tract without major complications. Only 10-20% will lodge and require surgical removal with less than 1% presenting with perforation. The most common site of impaction are in the oral cavity and oropharynx[1,4] which is also the finding in our study (30 out of 34 cases). This is usually due to the smaller sized fish bones whereas the larger fish bones impact in the upper thoracic esophagus (17%) and lower esophagus (6%).[1] Complications of penetration or perforation of the esophagus reported have included include paraesophageal abscess, mediastinitis, pericarditis, pneumothorax, pneumomediastinum, tracheo-oesophageal fistula vascular injury and esophageal diverticulum.[6] However suprisingly in our study none of these complications were reported. This may be related to the early presentation to the Accident & Emergency department and the liberal use of flexible endoscopy. Interestingly, mortality due to perforation was found to be higher with those foreign bodies situated intraluminally and lower with those where the object had migrated out of the lumen.[7] This mortality was highest for dental appliances which had eroded the mucosa particularly when the appliance had lodged in the lower thoracic oesophagus.[7] Infection and vascular complications are the usual cause of death.[7]

Plain radiography is highly specific for fishbone lodgment when the radiograph is positive though however its sensitivity is low.[4,5] This is in contrast to our study where the lateral soft tissue was able to demonstrate all 4 fish bones impacted in the oesophagus but none in the oropharynx. This concurs with the in-vitro study where none of the bones placed in the tonsil or valleculae were seen. The failure to visualize bones impacted in the tonsil or vallecula is not really a problem since an oral examination or indirect laryngoscopy would be able to visualize these impacted fish bones.[4] It has been suggested that patients complaining of ingestion of fish bones, should have an oral examination performed first to detect the fish bone, regardless of symptoms and radiographic findings.[4]

There is uncertainty about the role of the lateral soft tissue neck radiographs in the management of impacted fish bones. Like several authors,[3,12] we feel that plain films (a good quality lateral of the neck and sometimes with a chest radiograph) have been found to be an excellent method of detecting or excluding the presence of most foreign bodies and is basic to the investigation of foreign body ingestion. The presence of an impacted foreign body would allow a definitive diagnosis though the radiographic absence should not obviate the need of endoscopy in the appropriate clinical setting. In dealing with radio-opaque foreign bodies, it will show whether the foreign body is present or not or has passed into the stomach. In addition it is able to demonstrate the presence of complications e.g. subcutaneous emphysema, abscesses etc.. It will also give information on the state of the spine if subsequent general anaesthesia becomes necessary. However several authors[5,3-15] have called into question the value of these radiographs. These radiographs resulted in a change of management in only 1.4% but resulted in a 2% risk of unnecessary endoscopy.[13] Further, there may be an unnecessary delay in definitive management[5] and therefore they suggested that patients with a strong history of complaints of fish bone ingestion i.e. 48 hours or less should first be

evaluated with oral and endoscopic examination.

Calcification of normal laryngeal cartilage especially the vertical plate of the cricoid can make the recognition of a foreign body e.g. fish bone lodged in the pharynx difficult. Misinterpretation of soft tissues and calcified laryngeal appearance as foreign bodies occurred in 18/54 positive radiographs.[4] As fish bones have been found to be commonly swallowed foreign bodies it is helpful to know the exact type of fish that was eaten. Radiodensity is dependent on the type of fish. Shallow water fish have denser bones. Deep water sea fish have reduced ossification. Size wise, bones of larger fish have denser bones.

In practice, when plain films have been obtained and no direct signs (bone) or indirect signs (swelling or gas in soft tissue) are detected then it is important to maintain a low threshold for proceeding to endoscopy, which is both diagnostic and therapeutic. Patients on clinical grounds who are well enough to be sent home after normal plain films should be told to re-attend the next day if symptoms persist so that an ENT specialist can reassess the patient. In addition to localization of radio-opaque objects, presence of free mediastinal or peritoneal air should be assessed.

A study on the radio-opacity of fish bones species variation was done by Ell and Sprigg.[2] They used the clean dry bones implanted in the reconstituted pig offal. Their results showed that most (64%), of the bones were moderately to clearly visible in the larynx and oesophagus (being better visualized in the larynx), and 57% being visualised in the valleculae and tonsil. In our study only 50% were visible in the oesophagus (9 species of fish). Thus in patients ingesting the other 9 species (Walking Cat-fish, Black Pomfret, Short Bodied Mackerel, Yellow Banded Scad, Tolishad, Longtail Tuna, Silver Pomfret, and Sultan Fish) a negative radiograph is going to be the norm and therefore in these species the radiographs may not be used to determine the presence. However for the 9 species that are visible the absence may be good evidence of true negative especially if not symptomatic. 89% were clearly seen in the larynx (16 species of fish, except Walking Cat-Fish and Sultan Fish) but none seen in the tonsil or vallecula.

The differences in the radio-opacity of fish from Malaysia and British Isles may be related to the greater inherent density of the fish of the British Isles though these differences may be due to the different phantom used which may not be truly representative of the actual situation. This may also account for the higher visibility of the bones in the tonsil and vallecula since the identification of the position of the bones. We reckon that our phantom simulates closely the true situation since the goat's head and neck was sectioned through the midsagittal plane without disrupting the anatomy. Ell and Sprigg[2] inferred that a lateral neck radiograph was useful in the further detection of swallowed fish bones especially when the type of fish ingested is known. An earlier study was done by them using chicken legs as the site of implantation[15] but this was certainly not representative of the true situation.

Dense bones (e.g. Hardtail Scad, Fourfinger Threadfin, Narrow-Barred Spanish Mackerel, Golden Snapper, Giant Perch, Six-Banded Grouper, Delogoa Threadfish Bream, Nile Tilapia and Striped Snakehead) will be clearly seen anywhere compared to the poorly opaque bones (e.g. Walking Cat-fish, Black Pomfret, Short Bodied Mackerel, Yellow Banded Scad, Tolishad, Longtail Tuna, Silver Pomfret, and Sultan Fish) which will only be visible when viewed against bone. Long bones will also be better seen than the shorter bones. The density of fish bones can be inferred from its functional design and habitat.[2] In our study the fresh water fish appear to have denser bones compared to the sea dwellers. This has been attributed to dwelling in shallower waters. Other factors which have been suggested as affecting the density of bones include the size (the weight/length to surface area), the speed of swimming and the presence of oils within the fish.[16-18]

There is little role for any contrast studies in the diagnosis of impacted fish bone except the use of cotton wool soaked in barium, but this is no longer a common practice. However contrast studies may have a role in the diagnosis of perforations. Water soluble contrast media (Gastrografin) or even better non-ionic water soluble contrast medium would be used in cases of[1] suspected esophageal perforation to minimize complications (chemical pneumonitis) from leakage of the agent into the mediastinum or pleural space. If no perforation is noted, the examination is completed with inert barium sulfate since it has minimum reactivity in the lungs and is used if aspiration is a concern. Contrast examination should not be performed if high grade acute esophageal obstruction is suspected. For localizing small/low contrast objects, thick barium paste may be used.

Computed tomography (CT scan) reviewed at soft tissue and bone windows has been at times used to detect foreign bodies in the cervical esophagus[9] where there are associated complications, to look for foreign bodies that are seen on radiographs but not on endoscopy, and when there is no plain film evidence of foreign body but on endoscopy mucosal tears are noted suggestive of foreign body impaction.[9] However it is not a good mode of screening. It demonstrates and localizes small calcified esophageal foreign bodies as well as any associated complications. There is better detection of thin, small, minimally calcified foreign bodies which are often obscured by overlying tissues in the usual x-ray studies. Spiral or helical computed tomography, which permits images to be reconstructed at variable positions without additional scanner time or radiation exposure may have a role in the management of impacted fish-bones but this has not been determined.

Impacted foreign bodies require surgical referral. More than 80% of ingested foreign bodies passing the oesophagus will be spontaneously eliminated without complication and therefore expectant observation is indicated in this group of patients. For those that impact in the oesophagus numerous methods of treating these have been described. These involve both pharmacologic and mechanical methods. Rational treatment must be based on symptoms, type and size of foreign body, location of impaction, duration of symptoms and the possibility of underlying pathology. Endoscopy remains the treatment of choice for foreign body extraction by those trained in their use. It is the only non-surgical method of removing impacted sharp foreign bodies. Benefits include direct visualisation of the foreign body, ability to evaluate associated oesophageal pathology and maintain airway control. There are however complications to this procedure and mortality is a recognised complication. Further it requires a general anaesthetic.

CONCLUSION

As compared to studies done elsewhere, the commonest swallowed foreign body in the Malaysian population was noted to be fish-bones in adults and coins in children. The incidence was also higher in adults. The visibility of a fishbone depends on its inherent radio-density and the relative density between it and the tissue in which it is embedded. Based on the results of the radioopacity of the bones of the 18 species of fish on the lateral neck radiograph, it is concluded that most bones were generally moderately to well visualised in the larynx, most of the bones were not visualised in the oesophagus and were never detected in the valleculae or tonsil. Hence as swallowed fish bones generally impact in the valleculae and tonsil for which a peroral examination suffices, a lateral neck radiograph though can be used as a mode of investigation for fish bone impaction in the oesophagus, however it cannot be used to exclude the presence of a foreign body. If clinically suspicious an endoscopy is warranted to minimise the risk of complications.

REFERENCES

1. Taylor R.B. Esophageal foreign bodies. Emergency Medicine Clinics of North America.1987: 5;301-311.
2. Ell SR and Sprigg A The radio-opacity of fish-bones- species variation. Clinical Radiology 1991; 44: 104-107.
3. Phillipps JJ and Patel P Swallowed foreign bodies. Journal Laryngology and Otology. 1988;102: 235- 241.
4. Ngan JHK, Fok PJ, Lai ECS et al. A prospective study on fish bone ingestion. Ann Surg. 1990; : 459-462.
5. Sundgren PC, Burnett A, Maly PV. Value of radiography in the management of possible fishbone ingestion. Ann Otol Rhinol Laryngol 1994; 103: 628- 631.
6. Brady PG Esophageal foreign bodies. Gastroenteerology Clinics of North America. 1991;20: 691-700.
7. Remedios D, Charlesworth C, DeLacey G Imaging of foreign bodies. Imaging 1993;-15:171-179.
8. Mahadevan J, Abdullah B.J. , Abu Kasim N.H., Yunus N. Comparison of dimensions of dental prosthesis on radiographs: relative and true. Malaysian Radiological Society, Annual General/ Scientific Meeting. 16-18th. August 1996, Langkawi.
9. Braverman I, Gomori JM, Polv O et al. The role of CT imaging in the evaluation of cervical esophageal foreign bodies. Journal Otolaryngology 1993;22:311-314.
10. Ginsberg G.G. Management of ingested foreign objects and food bolus impactions. Gastrointestinal Endoscopy 1995;41:33-37.
11. Waggener R.G.,Kereiakes.J.G. and Shalek R.J. Handbook of medical physics Vol. II. CRC press. Pg. 468-506.
12. McGill TJ & Olhms L Foreign bodies of the upper aerodigestive tract. In Otolaryngology-Head and Neck Surgery. 2nd Edition Vol. 3 (Cummings CW, Frederickson JM, Marker LA et al eds) Mosby Year Book, St. Louis pp2396-2400
13. Jones NS, Lanningan FJ & Salaama NY Foreign bodies in the throat: a prospective study of 388 cases. J of Laryngology & Otology 1991:105;104-108
14. Marais J, Mitchell R & Wightmen AJA The value of radiographic assessment of oropharyngeal foreign bodies. J of Laryngology & Otology 1995:109;452-454
15. Ell SR Radiopacity of fish bones. J of Laryngology & Otology 1989:103;1224-1226
16. Mc Farland WN, Plough FH, Cade TJ et al. Vertebrate Life Collier Macmillan, London, 1979 pp210-214
17. Alexander RMcN Functional Design in Fishes Hutchinson, London, 1967 pp194-196
18. Romer AS & Parsons TS. The Vertebrate Body Saunders, Phildelphia 1986 pp328-330

SUPERIOR MESENTERIC ARTERY SYNDROME : A CASE REPORT IN SRISAKET HOSPITAL

SUTHATHIP JAROENPRASERT M.D., Diplomate of Thai Board of Diagnostic Radiology*

ABSTRACT

Superior Mesenteic Artery Syndrome (SMAS) is a rare condition. The case is often undiagnosed because of the unawareness and the roentgenographic or endoscopic examinations are often negative. It should be considered in patients with long standing abdominal complaints and do not respond to the standard medical regimens.

A case of Superior Mesenteric Artery Syndrome, diagnosed by roentgenographic examination of the upper gastrointestinal tract and treated by surgical intervention in Srisaket Hospital after having been treated by medical conservative treatment without improvement, was reported and the literatures had been reviewed.

Key words : Superior Mesenteric Artery Syndrome (SMAS), Chronic abdominal complaints, Partial duodenal obstruction, Roentgenographic findings.

INTRODUCTION

Superior Mesenteric Artery Syndrome (SMAS) is a rare condition of duodenal obstruction. Its symptoms may mimic closely with a variety of upper gastrointestinal disorders, such as peptic ulcers, gall stones, pancreatitis, etc. Even more, the SMAS may associated with each of the aforementioned diseases. It occurs in any age group but more common in young adults. Females are more than males and most commonly found in asthenic habitus. The pathogenesis of this disorder is reported to be anatomically related - the narrowed arteriomesenteric angle. The most helpful diagnosis is roentgenographic examination of the upper gastrointestinal tract with careful fluoroscopic examination. The characteristic findings are a straight cut-off line at the third part of the duodenum and proximal duodenal dilatation with delayed transit time. Strong churning peristalsis may be observed on fluoroscopy. The treatment of choice is medical and conservative treatment which is aimed to increase the patient's calories, therefore increasing the retroperitoneal mesenteric fat. This is reported to result in decreasing the chance of the duodenal obstruction by the superior mesenteric artery. Surgical treatment is indicated when medical treatment is failed. The procedure of choice is duodenojejunostomy. Because of the high morbidity in the patients with SMAS who were not diagnosed and treated properly, the clinicians should keep the SMAS in mind for every patient who suffers from upper abdominal symptoms and does not respond to the medical regimens.

* Srisaket Hospital, Radiology Department. Kasikam Road, Tambon Muangtai, Ampur Muang, Srisaket Province, 33000, Thailand.

CASE REPORT

A 18 years old female presented with a history of prolonged abdominal pain, nausea and vomiting with chronic weight loss for 1 month. Her menstruation history was normal. No pertinent past history was relevant. (Fig. 1)

On examination, the patient looked cachetic and asthenic with scaphoid abdomen. Neither pale nor jaundice was detectable. The body weight was 35 Kg, blood pressure 80/50 mm.Hg. No fever or enlargement of any lymph node was detectable. The abdomen was soft without guarding, rigidity or tenderness. The liver and spleen was not palpable. No abnormality was detectable in the heart, lungs and extremities. The relevant laboratory investigation results were unremarkable.

" Peptic ulcer " was diagnosed at the emergency room and medical treatment was then given. She was observed in the observation room without clinical improvement so she was admitted and roentgenographic examination was performed. The Upper G.I. study showed dilatation of the second part and proximal third part of the duodenum. The stomach was dilated. Churning peristalsis at the dilated segment on careful fluoroscopic examination and delayed transit time were observed. An abrupt linear extrinsic compression band at the third part of the duodenum at the right side of the lumbar spine with proximal dilatation was detected. The duodenal mucosa was intact. The impression was a partial duodenal obstruction from external compression at the third part duodenum. Superior Mesenteric Artery Syndrome was considered. (Fig. 2)

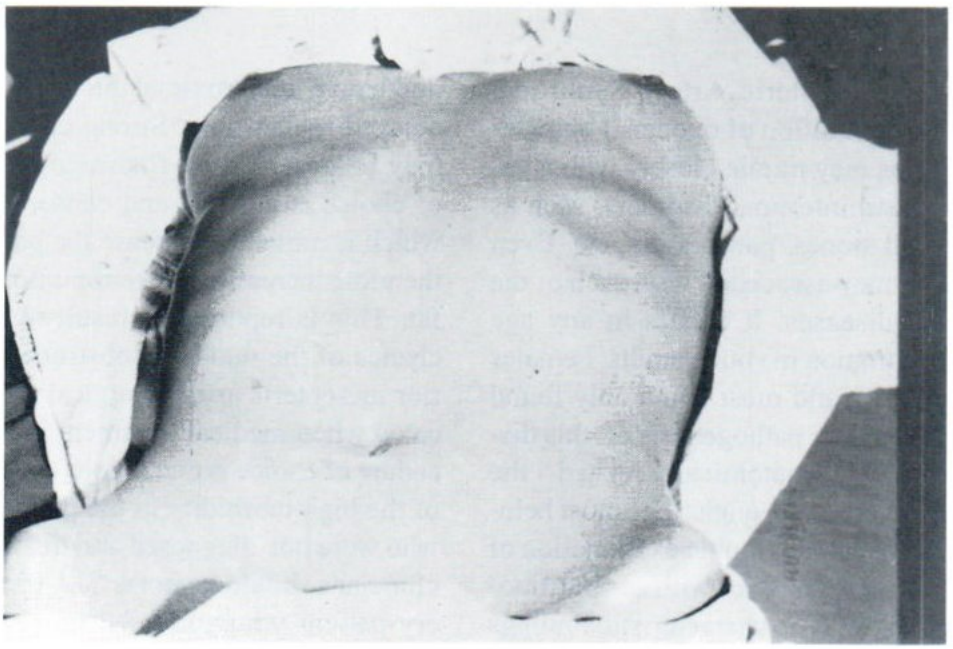

Fig. 1 A female 18-year-old woman with asthenic habitus and scaphoid abdomen.

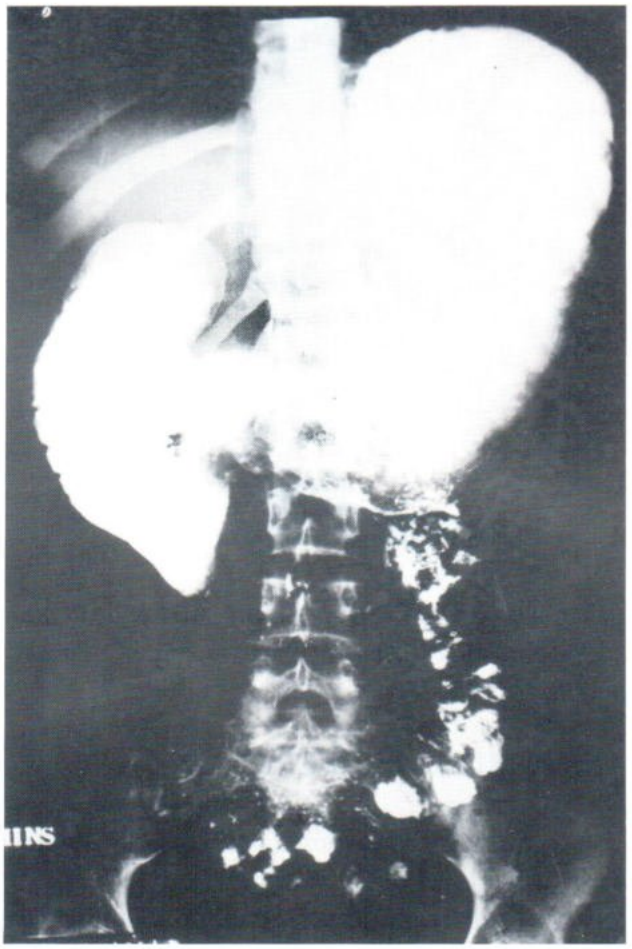

Fig. 2 Upper gastrointestinal study reveals dilatation of the stomach and second part of the duodenum. A straight cut-off line at the third part of duodenum.

TREATMENT

Conservative medical treatment was given without clinical improvement. Surgical treatment was then performed. The operative findings were: The second part of duodenum appeared dilated. The third part of duodenum was compressed by superior mesenteric artery at its anterior aspect with an abrupt change of the caliber of the duodenum at the point of obstruction. There was no evidence of mass or mucosal destruction detectable. Duodenojejunostomy was performed. (Fig 3).

POST OPERATIVE FOLLOW UP

There were no clinical symptoms of gastrointestinal obstruction persisting postoperatively. The patient gained more than ten kilograms of body weight in two months on follow up examination.

REVISION OF THE LITERATURES

Superior Mesenteric Artery Syndrome (SMAS) was first described by Rokitanski[30] in 1842 and was later analysed by Wilkies, Barner and Sherman[30] in 1963. This condition has many synonyms such as; Vascular compression of the duodenum,[11] Wilkies ' syndrome,[11] Chronic intermittent arterio- mesenteric occlusion of the duodenum,[4] Chronic duodenal ileus,[2] Arterio-mesenteric artery syndrome,[6] Superior mesenteric artery syndrome[25], Duodenal regurgitation,[4] duodenal stasis,[4] Arteriomesenteric ileus,[7] Cast Syndrome.[3]

Fig. 3 Surgical findings reveals marked dilatation of th second part of the duodenum (Arrow head and dots). The dilated portion of duodenum is endedd at the site of the superior mesenteric artery (Arrowheads). Distal from this line the duodenum was collapse.

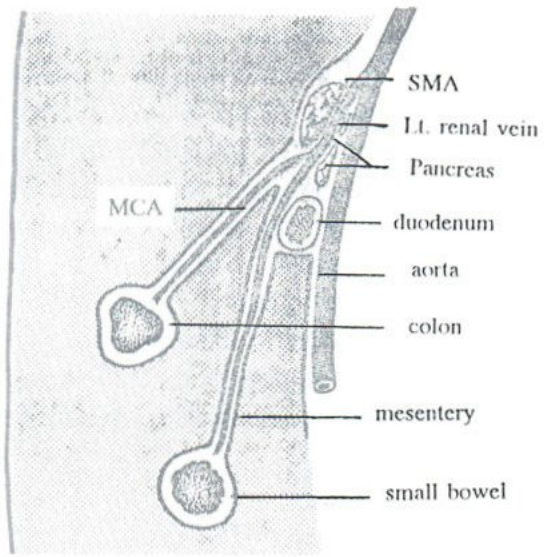

Fig. 4 The third portion of duodenum is trapped in the arteriomesenteric angle which is formed by the Superior mesenteric artery (SMA) and the aorta like a nut in between a "nutcracker" or "scissors"

MCA = Middle Colic Artery

ANATOMIC CONSIDERATION

Superior mesenteric artery arises from the aorta at the level of L1 vertebral body. It runs inferiorly to the right lower quadrant of the abdomen and forming an angle of 45-60^0 to it. The duodenum usually crosses the vertebral column at the level of the thrid lumbar vertebra. In average-sized person this distance is about 5 inches. The thrid part of the duodenum is trapped in the space like a nut in between a **"nutcracker"** or **"scissors".**[21] (Figure 4).

The ascending and the transverse segments of the duodenum is the most fixed portion of the alimentary tract and were in retroperitoneal space. It is limitted in its distal part by the ligament of Treitz and is bounded posteriorly by the vertebral body, the abdominal aorta and the neurovascular bundle of the superior mesenteric artery.

Marchant EA., et al, analysed 11 patients of Superior Mesenteric Artery Syndrome angiographically and found that the arteriomesenteric angle is between 6-15^0 and is in a range of 25-60^0 in normal population.[12]

Retroperitoneal mesenteric fat plays a significant role in Superior Mesenteric Artery Syndrome. It maintains arteriomesenteric angle and keeps the aorta and the root of the mesentery away from the abdominal aorta. Perinephric and retroperitoneal fat help pushing the second part of the duodenum anteriorly and so decrease the chance of duodenal obstruction by the superior mesenteric artery.

In acute weight loss the duodenum is prone to be compressed because of the loss of the retroperitoneal mesenteric fat, but not in every cases. Many other anatomic factors also play some role such as follow : Tight ligament of Treitz, Abnormally high position of the third part of duodenum, Unusual take off superior mesenteric artery from the aorta, Increased lumbar lordosis especially in women,[19] Short mesentery, redundant relaxed abdominal wall increased the dragging effect of the mesenteric root and consequently narrow the space anteriorly,[1] Immobilization in the supine position may cause the superior mesenteric artery to compress the third portion of the duodenum by gravity. The symptoms of Superior Mesenteric Artery Syndrome can be relieved by knee-to-chest or prone position. Because they increased the arteriomesenteric angle,[2] Middle colic artery, a brach of the superior mesenteric artery also crosses the third part of the duodenum and causes Superior Mesenteric Artery Syndrome in some patients.

AGE AND SEX

All age groups can be affected but more often in young adults. It is much more common in females than in males.[4] Seventy five percents of the patients are between 10 and 39 years.[23]

SYMPTOMS

Characteristically, the symptoms are of a recurrent, intermittent nature and partial or complete relief is often obtained in the knee-chest or recumbent position. The chief complaints are vomiting and epigastric pain after meals. Vomiting usually produces immediate relief. The patients usually suffer from the symptoms for a long duration. The abdominal symptoms are vague and often cannot be differentiated from those caused by other more common upper abdominal diseases such as peptic ulcer diseases, gall stones, chronic pancreatitis and cholelithiasis.[4]

The frequent association with other diseases which cause similar symptoms including peptic ulcer disease, bile reflux gastritis,[19] cholelithiasis, cholycystitis, pancreatitis, duodenitis, irritable colon[11] were reported.

The clinical symptoms enlisted in the literatures are post-prandial epigastric pain, fullness, nausea , bile stained vomiting, weight loss, partial or complete relief when the patient adopts the knee-elbow, knee-chest, left lateral or recumbent positions.[25]

DIAGNOSIS

Physical examination often reveals the presence of gastric dilatation. The most helpful diagnostic evaluation of the patients with superior mesenteric artery syndrome is roentgenographic examination of the upper gastrointestinal tract (UGI).[33]

Hayes described "pressure paradox" (Hayes' maneuver)[11] in which pressure is made by the hand placed below the umbilicus in a backward and upward direction for 30 seconds to undo the duodenojejunal kink. This manipulation was claimed to be valuable in the diagnostic relief of the vascular duodenal obstruction.[11]

RADIOLOGICAL FEATURES

The pertinent findings are as follow[5] : 1) Dilatation of the first and second portions of the duodenum with or without gastric dilatation.[31] 2) To-and-fro peristalsis of second and third part of duodenum during fluoroscopy. 3) Abrupt but in-

complete hold up of barium in the third part and dilatation proximal to the point of hold up (along lateral border of right psoas shadow). 4) Vertical cut-off compression at the third part duodenum when the patient is in the left anterior oblique position. 5) Delay in transit of 4 to 6 hours through the gastroduodenal region.[31] 6) Relief of obstruction is obtained when the patient is placed in a position that diminishes the drag of the small bowel mesentery (the left lateral decubitus, prone position, knee-chest position).[31] The patients should be examined in prone or left lateral decubitus to evaluate the degree of obstruction. If the obstruction is decreased, operation may not be nescessary.

Similar roentgenographic findings of dilatation of proximal duodenum can be found in patients with progressive systemic sclerosis or pancreatitis whose compression defect of the duodenum is different from that caused by superior mesenteric artery.[24]

TREATMENT

Medical treatment should be considered first. Surgical treatment is indicated only when the medical therapy is failed.[15,16]

The medical treatment consists of total parenteral nutrition, nasogastric suction and electrolyte correction. Medical treatment should aim to increase the patients' calories and then to increase the body fat , especially the mesenteric fat. This helps to increase the arteriomesenteric angle and decreases the chance of duodenal obstruction.

Positional treatment by simple gravitational maneuvers after meals can relieve the symptoms in some cases. The patient was lied on the side or prone or knee-chest position.

Surgical management : Operation should be performed when the medical treatment is failed.

The criterias for operative intervention are[28]: 1) Confirmation of diagnosis. 2) Radiographic or endoscopic or psychologic evaluation to rule out other causes. 3) Failure of a strict medical regime. 4) The present of associated disease such as peptic ulcer , pancreatitis, etc. 5) Severe cachectic and difficult to gain body weight. 6) Preference of the patient for surgical correction rather than prolonged conservative management.

Surgical treatment of choice is duodenojejunostomy.[7,8,16] Devision of the duodenum with reanastomosis anterior to the superior mesenteric artery is an alternative.

Many surgical techniques were performed such as : lysis of the Ligament of Treitz,[9] mobilization of the entire duodenum, freeing up of the retroperitoneal attachments of the mesentery, positioning the duodenum and most of the small bowel in the right side of the abdomen. Other alternative surgical procedures are gastrojejunostomy, duodenoduodenostomy and inferior displacement of the duodenal junction.

DISCUSSION

Superior mesenteric artery syndrome is an uncommon condition found in young persons especially in women. Narrowing of the arteriomesenteric angle which is formed between the aorta and the superior mesenteric artery is reported to be the predisposing factor. Other anatomical factors also play the role such as high position and tight ligament of Treitz.[23] The duodenum is hung superiorly in the arteriomesenteic angle and the chance for vascular duodenal obstruction is increased. Acute weight loss from any causes that decreased the mesenteric fat such as in anorexia nervosa,[27] prolonged supine position as in burned patient, cancer, head trauma, debilitated state,[20] various generalized systemic diseases, body cast - increased lumbar lordotic curve,[26,29,32] postoperative state[17] especially abdominal surgery, loss of muscle tone of the abdominal wall leading to visceroptosis.[10]

There are two forms of Superior Mesenteric Artery Syndrome - intermittent and chronic.[4] The degree of severity depends on the arteriomesenteric angle. This condition should be considered in the differential diagnosis of upper abdominal symptoms and signs of intestinal obstruction, especially when the symptoms are not relieved by the more common disease regimens.

The most helpful diagnosis is roentgenographic examination of the upper gastrointestional tract. The most important diagnostic criteria is obstruction at the third portion of the duodenum with a straight cut-off line and proximal duodenal dilataion.[28] The examination should be performed during attacks for proper diagnosis. However, negative UGI study does not exclude it. It should be remembered that this condition is intermittent in nature. The diagnosis can be made during careful fluoroscopic examination especially in erect position to accentuate the condition- decreases the arteriomesenteric angle. In prone position, the duodenal retention is usually disappeared more or less completely-as compared to the knee-chest position. The dilated portion of the duodenum exhibits strong churning peristalsis. Reverse peristalsis is quite prominent but this is not a pathognomonic sign[4] since it is observed under various conditions.

Basic principles of therapy of this disorder are important. Medical and postural treatment will relieve and cure a considerable number of patients[2] Surgery is indicated only in cases of failure of medical and conservative treatment. The operation of choice is duodenojejunostomy.

Because of the high morbidity in the patients with Superior Mesenteric Artery Syndrome who were not diagnosed and properly treated, the clinicians should keep in mind, the Superior Mesenteric Artery Syndrome in every patient who suffers from upper abdominal symptoms and does not respond to the medical regimens.

ACKNOWLEDGEMENT

The auther would like to thank Dr. Chit Jaroenprasert, the surgeon who offered the photographs of this patient and Dr. Chutiwan Viwatthanasittipong for her kind assistance in preparing this manuscript.

REFERENCES

1. Kellogg E.L and Kellogg WA. Chronic duodenal obstruction with duodenojejunostomy as a method of treatment. Ann Surg 1921;73:578-608.
2. Wilkie D.P.D. Chronic duodenal ileus. Am J Med Sci 1927; 173: 643 - 649.
3. Dorph M.H. The cast syndrome . N Engl J Med 1950;243: 440.
4. Goin LS. Intermittent Arteriomesenteric occlusion of the duodenum. Radiology 1956;67:729-737.
5. Bitner WP. Arterio-mesenteric occlusion of the duodenum. Am J Roentgenol 1958; 79: 807-814.
6. Strong EK. Mechanics of arteriomesenteric duodenal obstruction and direct sur gery attack upon etiology. Ann.Surg 1958; 148:725-730.
7. Jones SA, Carter R, Smith LL, et al. Arteriomesenteric compression. Am J Surg 1960;100:262.
8. Kaiser GC, Makain JM, Shumacher HB. The superior mesenteric artery syndrome. Surg Gynecol & Obstet 1960; 110: 133.
9. Martorell R, Guest M . Operative treatment of the superior mesenteric artery syndrome. Am Surg 1961; 27, 681.
10. Siman M and Lerner M. Duodenal compression of the mesenteric root in acute pancreatitis and inflammatory conditions of the bowel. Radiology 1962 ;79: 75.
11. Barner HB and Sherman CD. Collective review - Vascular compression of the duodenum. International Abstracts of surgery 1963; 117: 103-118.

12. Marnsberger AR , Hearn JB , Byers RM et al. Vascular compression of the duode num. Emphasis on the accurate diagnosis. Am J Surg1968;115: 89-96.
13. Bunch W, Delaney J. Scoliosis and acute vascular compression of the duodenum. Surgery 1970; 67: 901-906.
14. Wallace RG and Howard WB. Acute superior mesenteric artery syndrome in severely burned patient . Radiology 1970;94: 307-310.
15. Berk RN, Coulson DB.The body cast syn drome. Radiology1971; 93: 303-305.
16. Wayne ER, Miller RE, Eiseman B. Duodenal obstruction by the superior mesenteric artery in bedridden combat casualties. Ann Sury 1971;174:339.
17. Ogbuokiri CG, Law EJ, MacMillan BG. Superior mesenteric artery syndrome in burned children. Am J Surg 1972;124:75-79.
18. Altman DH, Puranik SR. Superior me senteric artery syndrome in children. Am J Roentgenol 1973;118:104-108.
19. Anderson WCI, Vivit R, Kirsh IE et al. Arteriomesenteric duodenal compression syndrome. Its association with peptic ulcer. Am J Surg1973;125:681-9.
20. Akin JT, JR. The anatomic basis of vascular compression of the duodenum. Surg Clin North Am 1974;64:1361-1368.
21. Burrington JD. and Wayne ER. Obstruction of the duodenum by the Superior Mesenteric Artery. Does it exist in children ? J of Pediat Surg 1974;9:733-740.
22. Bisla RS , Louis HJ. Acute vascular compression of the duodenum following cast application. Surg Gynecol & Obstet 1975;140:563-566.
23. Akin JT, Gray SW, et al. Vascular com pression of the duodenum: Presentation of ten cases and review of the literature. Surgery 1976;79:515-522.
24. Gondos B. Duodenal compression defect and the 'superior mesenteric artery syndrome'. Radiology 1977; 123: 575-580.
25. Martinez, N.S., et al. Arterio-mesenteric duodenal compression syndrome: a study of 24 cases. Vascular Surgery 1979;13:1-10.
26. Lundell L and Anders T. Wilkie's syndrome- a rarity? Br J Surg 1980;67:604-606.
27. Pentlow BD and Dent RG. Acute vascular compression of the duodenum in anorexia nervosa .Br J Surg 1981;68:665-666.
28. Jones PA and Wastell C. Superior mesenteric artery syndrome. Postgrad Med J 1983;59:376-379 .
29. Walker C and Kahanovitz N. Recurrent superior mesenteric artery syndrome complicating staged reconstructive spinal surgery: alternative methods of conservative treatment. J Pediatric Ortho 1983; 3 :77-80.
30. Gustafasson L, Falk A, Lukest PJ and Gamklou R.. Diagnosis and treatment of superior mesenteric artery syndrome. Br J Surg 1984; 71: 499-501.
31. Hines JR, Gore RM, Ballantyne GH. Superior mesenteric artery syndrome Diagnostic criteria and Therapeutic Approaches. Am J Surg 1984;148:630-2.
32. Munns SW. Hyperalimentation for superior mesenteric artery (cast) syndrome following collection of spinal deformity. J Bone Joint Surg1984;66:1175-1177.
33. Marchant EA, Alvear DT, and Fagelman KM. True clinical Entity of vascular compression of the duodenum in adolescence,Surg Gynecol & Obstet 1989;168:-381-386.

Message from

Prof.Dr. Kawee Tungsubutra

Editor-in-Chief, The Asean Journal of Radiology.

This is the third issue of the Asean journal of Radiology for the third year which has been kindly supported by the educational grant from Bracco International.

I would like to encourage writers from all the member countries especially Philippines and Indonesia.

We welcome writers from all over the world. At the moment we have papers constantly from Thailand, Singapore, Malaysia and Australia.

Thank you again for the writers and the supporters.

Kawee Tungsubutra.

Kawee Tungsubutra
November, 1997

AMBER

... In the tradition of the old masters

Oldelft, leading the way in Chest Imaging

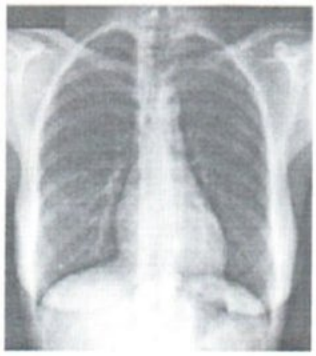

AMBER

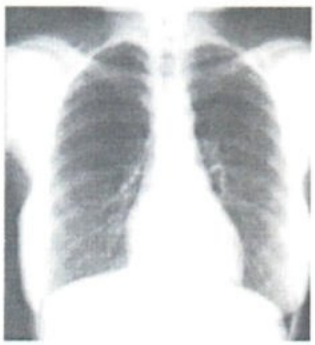

Conventional

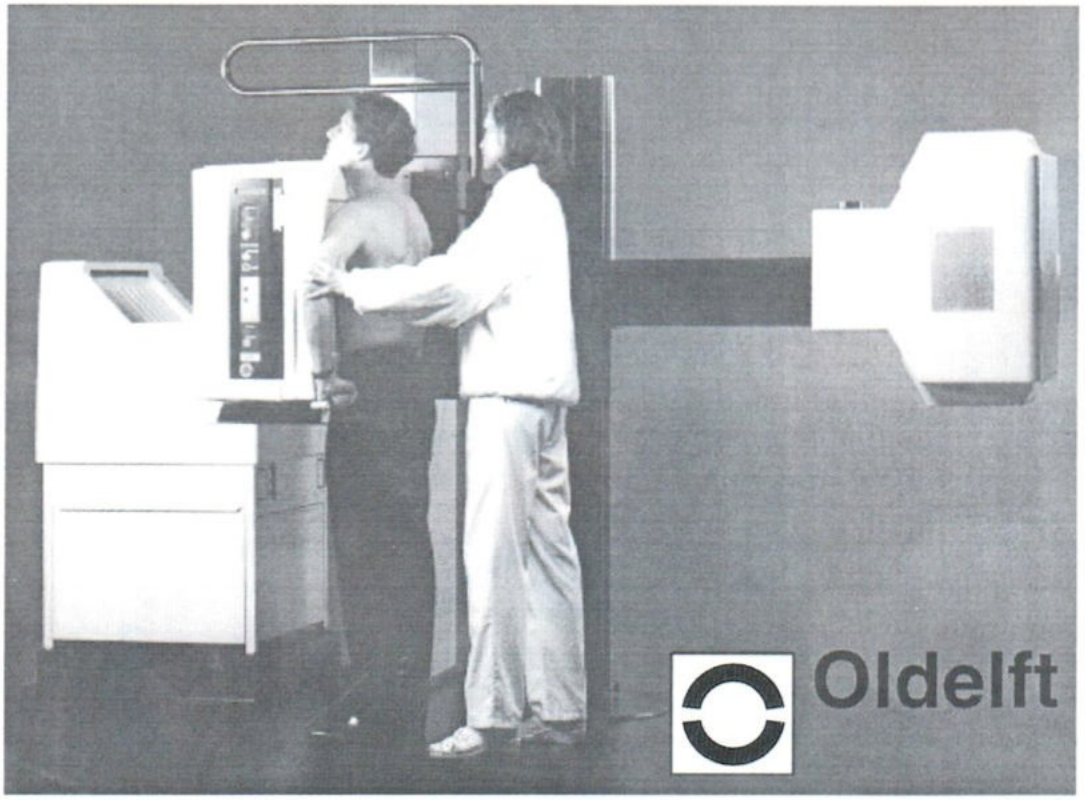

Giotto

The importance of visualizing up to 2 cms. more of breast tissue.

COMFORTABLE, FAST AND PRECISE

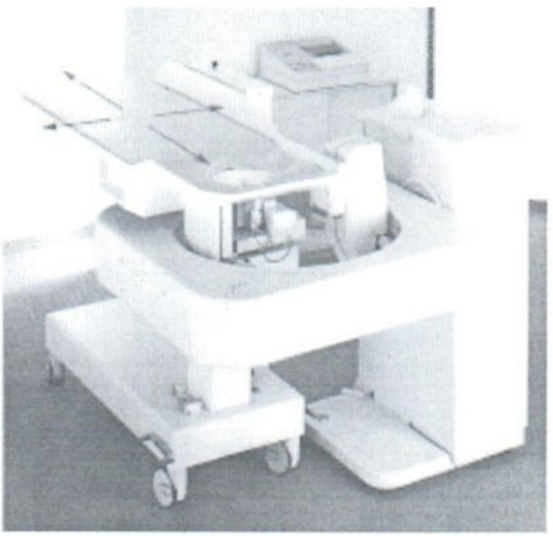

MAMMO-BED AND BIOPSY-M:
FUNCTIONALIITY AND ACCURACY

IMS **INTERNAZIONALE MEDICO SCIENTIFICA S.r.l.**

UNITED

บริษัท ยูนิเตด 4 จำกัด
UNITED 4 CO.,LTD.
43/1085 รามอินทรา 1 ถนนรามอินทรา บางเขน กรุงเทพ 10220
43/1085 RAMINTHRA 1, RAMINTHRA RD., BANGKHEN BANG KOK 10220
TEL. 970-7034, 970-7037, 9707039 FAX : 552-7840 E-MAIL : united4@loxinfo.co.th

FOR MORE INFORMATION PLEASE CONTACT
PHILIPS MEDICAL SYSTEMS
- TEL. 745-4090 Ext. 3332
- FAX. 398-0792

Philips Electronics (Thailand) Ltd.
209/2 Sanpavuth Road, Prakanong, Bangkok 10260

Let's make things better.

PHILIPS

One cost-effective source for a variety of medical imaging solutions

You have many options when it comes to buying medical imaging systems.

As medical imaging technology becomes more complex and more integrated, you need more than a place to buy equipment and services.

You need a solutions provider with a clear vision of the future. One that knows how to integrate the seemingly incompatible myriad of products, systems and technologies. One that understands how to make this new digital world effctive and affordable for your facility.

You need Imation.

We offer the products and technologies you need to acquire, view, print and store medical images.

But more important, we know how to make those solutions work for you, given your needs, your plans and your budget.

Imation DryView Laser Imaging Systems deliver lower operating costs, less waste

Medical Imaging Systems

The medical imaging world is going dry.

Traditional "wet" laser imaging simply costs too much- and it poses too many environmental hazards.

Hospitals around the world are abandoning the hassle and expense of this older technology in favor of 3M™ DryView Laser Imaging Systems by Imation™.

Imation DryView systems deliver superb, diagnostic-quality images-without the added expense of wet chemistry, wet film processors, darkrooms, special plumbing and wet chemistry disposal.

Plus, they can be located virtually anywhere-which makes them a better fit for your evolving medical imaging environment.

In addition to dry laser imaging, we offer a wide range of conventional imaging products and a full line of film systems-including the 3M™ Chest System by Imation™.

Network Solutions

PACS, teleradiology and network printing bring a new immediacy and a new freedom to medical imaging. Instead of waiting for film to be located, dispatched and delivered, images can be acquired, viewed, printed or transmitted with ease.

This powerful, new imaging environment isn't difficult to create-it you choose the right solutions provider.

We offer a full range of network solutions-including PACS, teleradiology and network printing-through a cooperative relationship with Cemax-Icon.

We integrate our strengths to bring you solutions that meet your current requirements-*and* provide expandability and scalability to meet your changing needs.

Count on us for everything from initial consultation through service and support.

Innovation

The strength of two innovative companies with one customer-focused purpose

Digital Image Storage

A full line of reliable, affordable products to meet your data storage needs

As you migrate toward a more digital medical imaging environment, digital storage will become a critical issue for your facility.

Capacity, compatibility, quick access, reliability and cost will drive your decisions regarding digital image archiving.

Rely on us for the right solutions.

We're the leading supplier of the branded diskettes you use in your computer every day. We introduced the first commercial CD-ROM. And today, because our data storage expertise is so strong, drive manufacturers collaborate with us to develop worldwide data storage standards.

Look to us for all your digital storage needs-including optical disks, tape cartridges, reel-to-reel tapes and diskettes.

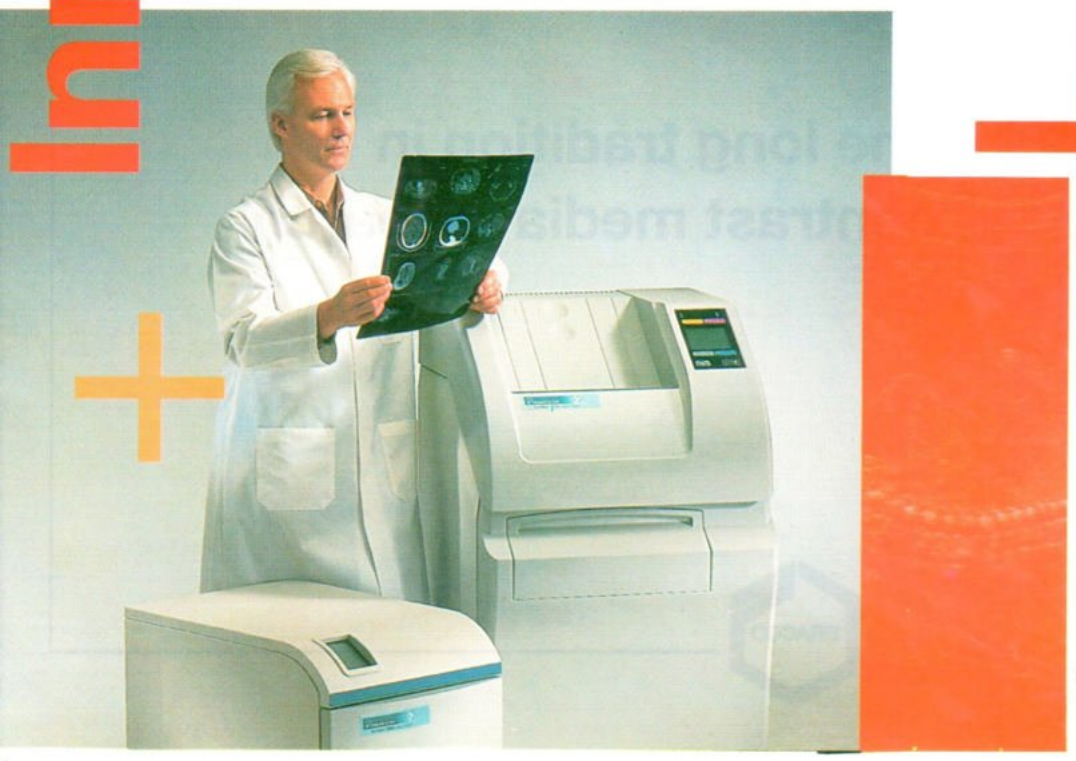

Imation-Borne of 3M innovation.

Imation promises a customer-first focus. We've combined our core technologies-imaging and information-with our core values-innovation and imagination-to create solutions tailored to your needs. Imation products carry with them all of the innovation, quality and service you've come to expect from 3M.

IMATION
Borne of 3M Innovation

Imation (Thailand) Ltd.
9th Floor Na-Nakorn Building,
99/349 Chengwatana Rd., Donmuang,
Bangkok 10210
Tel. (662) 576 0064, 576 0067-9
Fax. (662) 576 0065

1927-1997 **Bracco 70th Anniversary.**

The long tradition in contrast media research.

BRACCO

SIEMENS

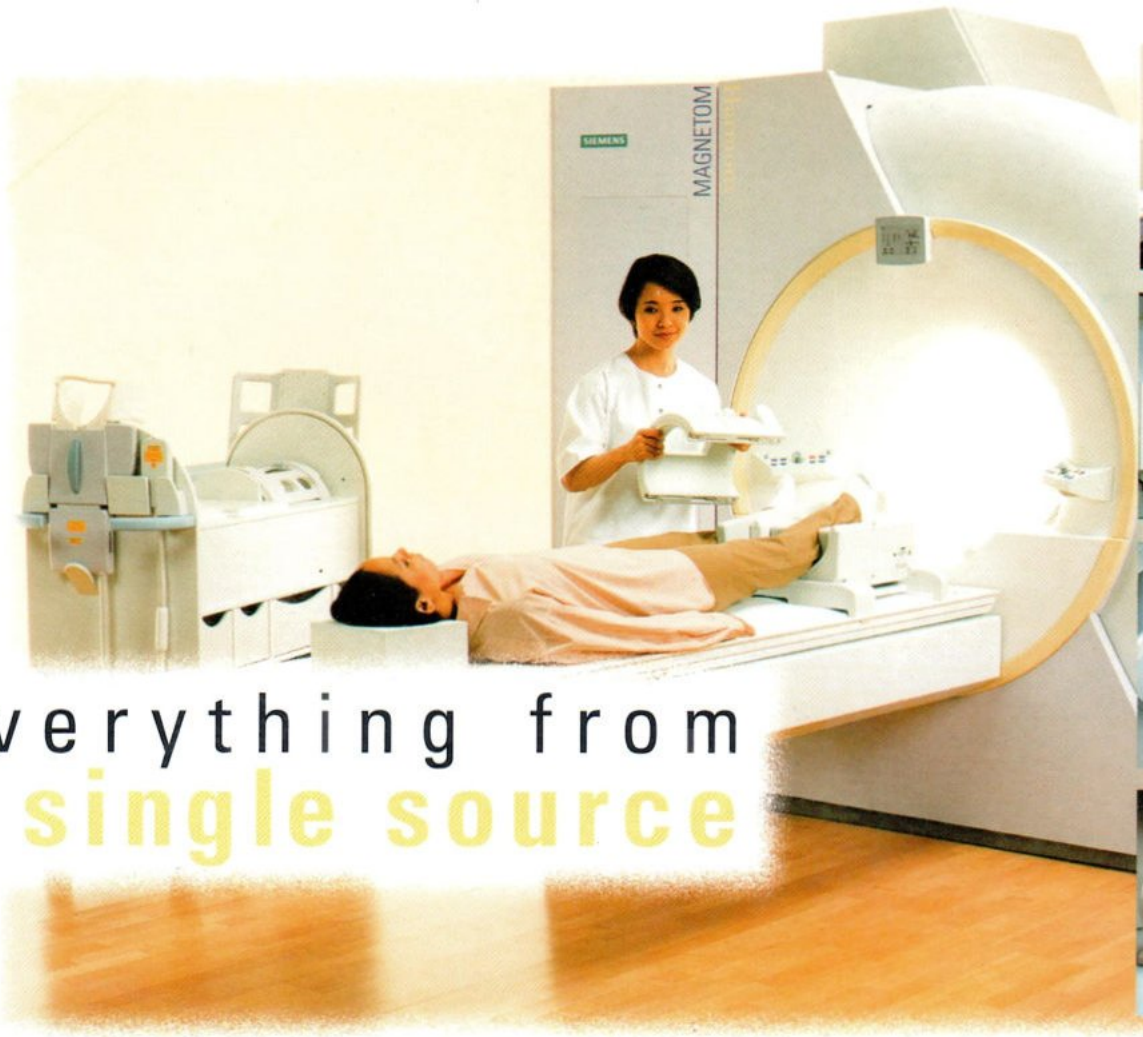

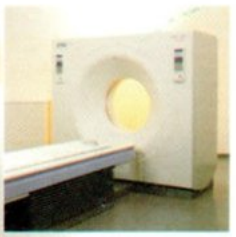

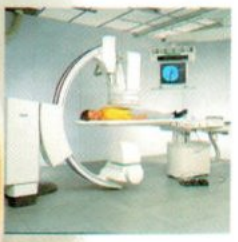

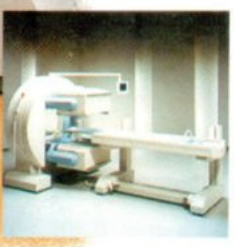

Everything from a single source

Siemens offers the broadest product range worldwide.

But we offer you not only a versatile range of equipment. We advise you, elaborate proposals for you, deliver the medical engineering equipment and familiarize you with the operation and handling of the units and systems.

And if you need our technical service : We are there.

Consulting and project design, installation and service - so that you receive everything from a single source.

Why not talk to Siemens?

For more information, please contact : Siemens Limited, Medical Engineering
Charn Issara Tower II, 25th Floor, 2922/283 New Petchburi Road, Bangkapi, Huaykwang, Bangkok 10320
Tel. : (662) 716-4000 Fax. : (662) 716-4008 or visit us on the Internet, http://www.siemens.de/med

Siemens **medical Solutions** that help